UNIVERSITY OF BELGRADE
FACULTY OF TECHNOLOGY AND METALLURGY
DEPARTMENT OF PHYSICAL METALLURGY

M. Sc. Thesis

SOME ASPECTS OF STATIC RECRYSTALLIZATION IN MICROALLOYED STEELS ON HIGH TEMPERATURES

By

ABDULNNASER. H. A. FADEL

BELGRADE, 2003

1

1

SOME ASPECTS OF STATIC RECRYSTALLIZATION IN MICROALLOYED STEELS ON HIGH TEMPERATURES

By

ABDULNNASER. H. A. FADEL

M. Sc. Thesis

Department of Physical Metallurgy

Submitted to the Faculty of Technology and Metallurgy

UNIVERSITY OF BELGRADE

September 2003

Approved :   Dr. Nenad A. Radovic, Assistant Professor
                  Supervisor

                  Dr. Karlo T. Raic, Professor
                  Committee member

                  Dr. Milan T. Jovanovic, Scientific Advisor
                  Committee member

Date:_____

Acknowledgments

I would like to express my great thanks and appreciation to Dr Nenad A. Radovic for his supervision and guidance during my work in this M.S. Thesis.

My appreciation is extended to the whole staff members of Physical Metallurgy department for their expert teaching and a nice time we spend in the faculty of Technology and Metallurgy.

TO … MY PARENTS, MY WIFE, AND ALL MY FAMILY

ABSTRACT

Data required for calculation the static re-crystallization kinetics have been evaluated from laboratory simulations. In this work series of two hit isothermal tests were conducted for low carbon Nb/Ti microalloyed steel containing (0.074 wt.% C, 1.15 wt.% Mn, 0.035 wt.% Nb and 0.016 wt.% Ti) on high temperature torsion machine. These tests were conducted on four different temperatures and using inter-pass times between 0.5 and 5s with aim to investigate the influence of thermal activation on static re-crystallization. All tests were conducted on temperatures over Tnr temperature, i.e. in temperature range in which all niobium is present only in solid solution. Method of evaluation of recrystallized fraction was mechanical metallography, i.e. evaluation based on shape of each stress-strain curve. Results have provided following solutions:

- On all temperatures, X vs. time dependences have "S" shape, confirming nucleation and growth mechanism of static recrystallization

- Increase of test temperature shortens time required for full recrystallization, confirming thermal activation of static recrystallization

- Activation energy for static recrystallization estimated in this work of 281kJ/mol is in excellent agreement with previously reported data (both experimental and modeled) and indicates that diffusion of Nb in austenite is most probably the rate controlling process;

- Value of Avrami exponent estimated in this work, n=1, implies that static recrystallization occurs at interfaces, i.e. on grain boundaries, twins, deformation bands.

- Full description of Avrami type kinetics of static recrystallization is estimated, the results obtained will be used for optimization of present model for prediction of roll forces for Hot Strip Mill in SARTID Company for Steel Manufacturing.

Key words: Micro-alloyed steels, Static Re-Crystallization, Fractional Softening, Activation Energy.

Scientific field: Technical sciences

Scientific subfield: Metallurgy

CONTENT

INTRODUCTION

High strength low carbon steels containing niobium, vanadium and titanium in total amount of 0.15%, are usually identified as microalloyed steels. These elements share the common feature of precipitation of carbonitrides and/or carbides/nitrides on temperatures of hot working. They are produced as hot-rolled products, usually by utilisation of technology known as "controlled rolling". Roughing stage should be performed in temperature region in which full recrystallization takes place, and finish rolling should be performed in temperature region in which static recrystallization should be inhibited or suppressed. In the case of reverse finish rolling (long interpass times), the recrystallization suppression is due to precipitation of carbonitrides, i.e. precipitates block the grain boundaries, not allowing its motion. In the case of finish train (short interpass times), the recrystallization suppression is due to presence of microalloying elements in solid solution, i.e. soluted atoms decrease the grain boundary mobility. High strength of microalloyed steels is based on very fine ferritic grain, and additionally some very fine precipitation strengthening. After finish rolling, microstructure consists of non-recrystallized austenite grains, with increased dislocation density, deformation bands etc. Following ferrite nucleation can occur on considerably larger number of places, resulting in very fine grain structure. Therefore, knowledge of recrystallization and its possible interaction with precipitation is of great importance.

In recent times, it has been shown that during finish rolling of hot rolled strip, temperature of no-recrystallization can be identified on basis of rolling forces. Also, it has been showed that for good quality of hot-rolled strip, some critical amount of deformation must be provided below Tnr temperature. This amount is in the scope of the research in numerous institutions. Also, it is expected that this amount will depend on austenitic grain size on temperatures just above Tnr temperature.

Modeling of hot rolling requires reliable prediction of rolling forces. Rolling forces depend on microstructure, i.e. of the fractions of recrystallized and non-recrystallized structure. At the moment, several different models for calculation static recrystallization kinetics are present. Their structures are various, from simple models based on linear regressions, models that are physically based to certain extent and fully physically based models coupled with advanced numerical methods. For all of them, common feature is the reliability margin. Therefore, an improvement of existing model for prediction of properties of micro alloyed strip, in area of static recrystallization kinetics sub model is a continuous effort.

Data required for calculation the static recrystallization kinetics will be evaluated from laboratory simulations. Tests will be conducted on high temperature torsion machine, machine which great advantage is in possibility of achieving a large strain, what is a characteristic of rolling. Results of series of two pass (two-hit; double–hit) and multistage (multi pass) tests, data for calculation of static recrystallization kinetics will be evaluated. Method of evaluation of recrystallized fraction will be mechanical metallography, i.e. evaluation based on shape of each stress-strain curve. These tests will be conducted on series of different temperatures with aim to investigate the influence of thermal activation on static recrystallization. Final result should provide a quantification of kinetics of static recrystallization.

Finally, the aim of this work is to quantify recrystallization kinetics, with recommendation for hot-rolling practice.

2. PREVIOUS WORK

2.1 Restoration in deformed materials

The strengthening effect of defects introduced by deformation has been used as a mean of raising the strength level in metals and alloys particularly by cold–working techniques [1]. More recently attention has been given to the increase in strength through a retention of a substructure in hot–worked materials. For example, the extension of a controlled rolling schedule to lower temperatures, in the case of micro alloyed steels (grain, sub grains, dislocations, and precipitates were the most important microstructural features observed in the controlled–rolled steel). This is usually brought about by rolling in the two–phase ($\gamma + \alpha$) region or, at still lower temperatures, in single–phase ferrite. The resultant structure is largely determined by the difficulty of recovery and recrystallization processes [1] . In comparison to undeformed metal, dislocations are distributed both within the grains and in sub grains boundaries. Development of new internal surfaces is increasing the internal energy of metal. Figure (1) shows the relationship between the stored energy and the amount of deformation. Stored energy increases with increasing deformation, so that the fraction of the total energy stored decreases with increasing deformation. The latter effect is shown by a second curve plotted in figure (1). The driving force for generation nuclei is the stored energy, which increases with increasing strain rate and decreasing deformation temperature [2,3]. Since the highest dislocation density is preferentially at the grain boundaries, the nucleation is preferred also with decreasing grain size. The smaller austenite grain after soaking owing to titanium and/or niobium microalloying is one step to prepare a finer recrystallized austenite grain [3]. The increase of strain rate increases the flow stress at any particular strain. Increasing flow stress would be expected to increase the random dislocation density and decrease the sub grain size and hence increase the stored energy (the sub grain boundaries provide the largest contribution to the stored energy) i.e. the driving force for recrystallization will increase [4].
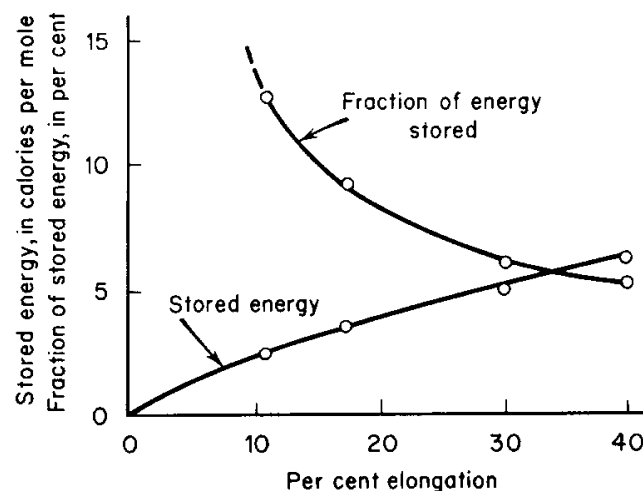
Figure (1) Stored energy of cold work and fraction of the total work of deformation remaining as stored energy for high purity copper plotted as function of tensile elongation [2]

During deformation, all metals undergo a work hardening and dynamic recovery and some may also undergo dynamic recrystallization. The microstructures produced by these processes are unstable and, on holding at temperature after the end of deformation, further structural changes occur by static recovery, recrystallization, and grain growth [5].

During the deformation process, e.g. rolling pass, work hardening takes place but is balanced by the dynamic softening processes of recovery and recrystallization. These processes, which are thermally activated, lead to a flow stress that depends on strain rate and temperature as well as on strain [4].

The structural changes taking place within the material result in an increased dislocation density up to a critical strain (ε_c). If ε_c is reached the stored energy is sufficiently high to cause dynamic recrystallization. For Nb–steels, the critical strain (ε_c) for dynamic recrystallization is related to the initial γ grain size (d_0) and the Zener–Hollomon parameter (Z) as described in chapter 2.2, the statically recrystallized γ grain size (d_{rex}) is related to d_0 and ε. The important feature of (d_{rex}) in Nb steels is that it does not depend on temperature [6]. These dynamic structural changes leave the metal in an unstable state and provide the driving force for static recovery and static recrystallization. The latter may be followed by grain growth if the temperature is sufficiently high.[4], as shown in figure (2) (before ε_c no recrystallization takes place) .
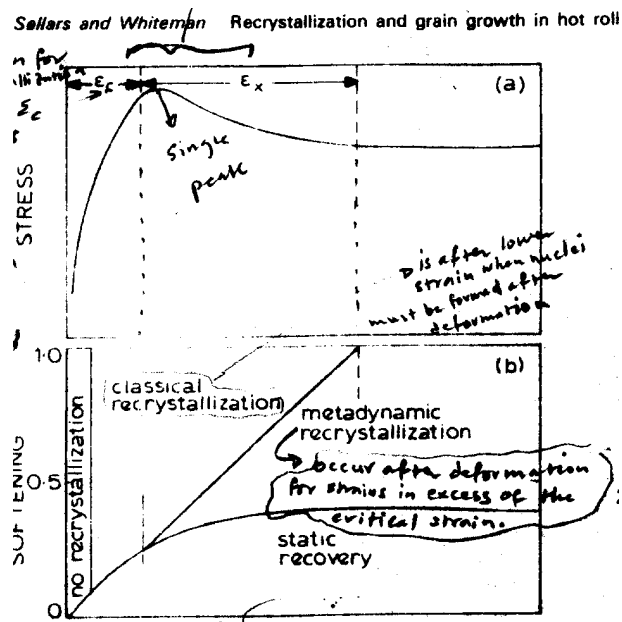

Fig. (2) Schematic representation of (a) relationship between stress/strain behavior during deformation, and (b) mechanisms of static softening that take place after deformation [5] .

The cold working of metal results in an increase in strength or hardness and decrease in ductility [7]. The strain hardening (also referred to as work hardening or cold working) results from a dramatic increase in the number of dislocation interactions and reduces dislocation mobility. It is interesting to note that the strength of a metal approaches extremely high levels when there are either no dislocations present or when the number of dislocations is extremely high ($\geq 10^{10}$/cm^2), low strength levels correspond to the presence of moderate numbers of dislocations ($\approx 10^3 - 10^5$/cm^2) as shown in figure (3) [8]
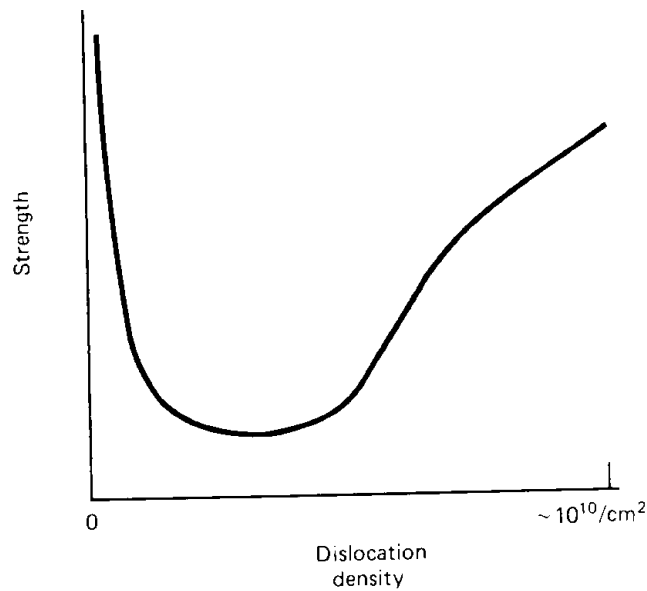
Fig. (3) Strength of metal crystals as function of dislocation density [8]

When cold working is extensive the metal fracture will occur before reaching the desired size and shape. Therefore, in order to avoid such difficulties cold working operations are usually carried out in several steps, with intermediate annealing operation to soften the cold worked metal and restore the ductility. This sequence of repeated cold working and annealing is frequently called cold work annealing cycle.[7] .

Since full annealing restores the material to a strain free lattice structure, it is essentially a softening process. Property changes produced by plastic deformation are removed, and the material returns very nearly to its original properties. Therefore, during annealing, the hardness and strength decrease, whereas the ductility increases. The change in properties is shown schematically in fig (4)[9]
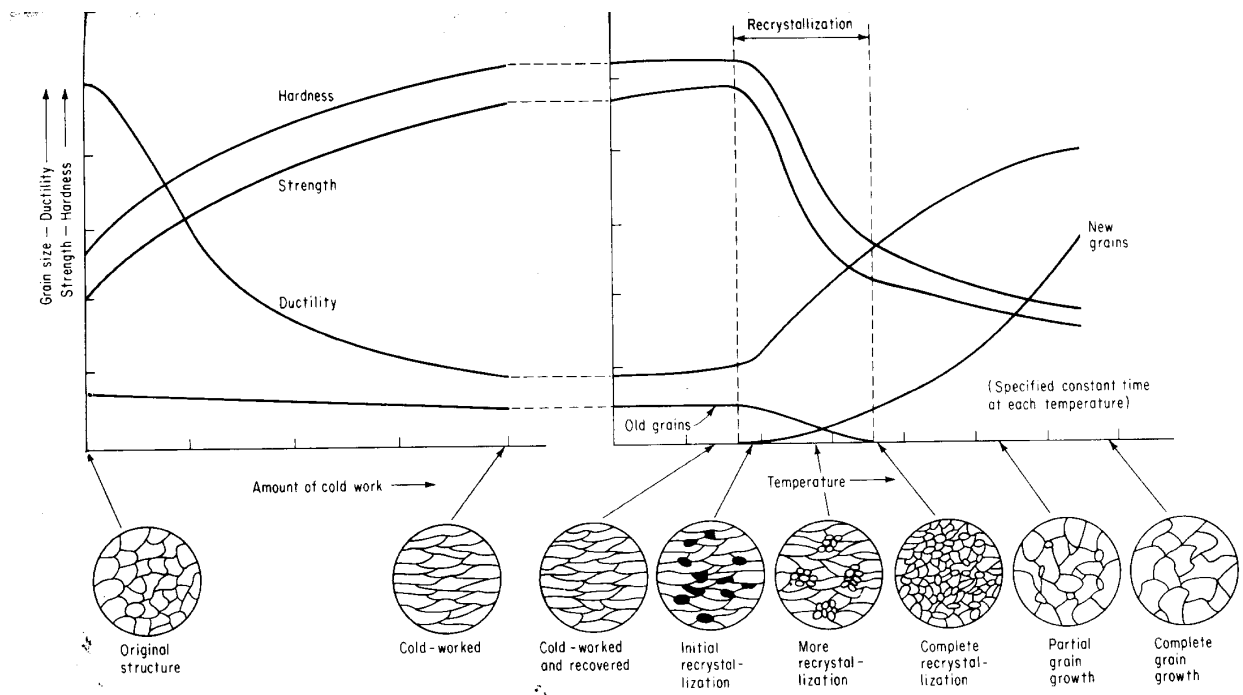

Fig. (4) Schematic representation of the cold work anneal cycle showing the effects on properties [9]

12

The treatment given to the metal to bring about a decrease of the hardness and an increase in ductility is known as restoration. It is conducted by annealing. This usually means keeping the deformed metal for certain time at temperature higher than about one third absolute melting point

$(T > 1/3 T_M)$ [10]. The cold working produces an increase in dislocation density, $10^{10} - 10^{12}$ lines m^{-2} for annealed state to $10^{12} - 10^{13}$ after a few percent deformation, and to $10^{15}-10^{16}$ lines / m^2 in heavily deformed state. Such as array of dislocation gives rise to substantial strain energy stored in the lattice. This means that cold worked condition is thermodynamically unstable in comparison to the undeformed one. Consequently, the deformed metal will try to return to a state of lower free energy i.e. more stable state. In general, this returns to a more stable structure, and cannot occur spontaneously but only at elevated temperature where thermally activated processes such as diffusion, cross slip and dislocation climb take place [10]. The removal of the cold worked condition occurs by a combination of three processes, namely :–
(1) Recovery.
(2) Recrystallization.
(3) Grain growth.

2.1.1 Recovery

The term recovery may be defined as the restoration of the physical properties of cold worked metal without any observable change in microstructure. The properties that are most affected by are those which are sensitive to point defects [7]

The properties which are controlled by dislocation density like strength, hardness is not changed during recovery process as shown in figure (4). Since the mechanical properties of the metal are essentially unchanged during recovery processes for this reason we consider this process as stress relief, as we know when metal or alloy is cold worked this lead to increase the internal energy (higher internal energy) when compared with undeformed alloy.

The principal application of heating in recovery range is stress relieving of cold worked alloys to prevent stress corrosion crack or to minimize the distortion produced by residual stresses. Commercially this low temperature treatment in the recovery range is known as stress relief annealing [7].

The cold worked metal structure consists of high density of dislocation. The main purpose of the recovery processes is to rearrangement of these dislocations and to decrease the energy within the lattice. One, of the most important recovery processes which lead to a resultant lowering of the lattice strain energy is rearrangement of the dislocation into cell walls. This rearrangement of the dislocation is assisted by thermal activation as shown in figure (5) [10] .

The removal of vacancies from the lattice, together with the reduced strain energy of dislocation which result in large change in both electrical resistivity and stored energy observed during this stage, while the change in hardness can be attributed to the rearrangement of dislocations and to the reduction in the density of dislocations.

Polygonization. The term polygonization was used originally to describe the situation that occur when single crystal is bent to a relatively small radius of curvature and then annealed. Bending results in the introduction of an excess number of dislocations of one sign. Dislocations are distributed along the bent–angle planes as shown in fig (5) a.

When the crystal is heated, the dislocations group themselves into the low–energy configuration of a low–angle boundary by dislocation climb. The resulting structure is a polygon like network of low–angle grain boundary fig (5) b [7]
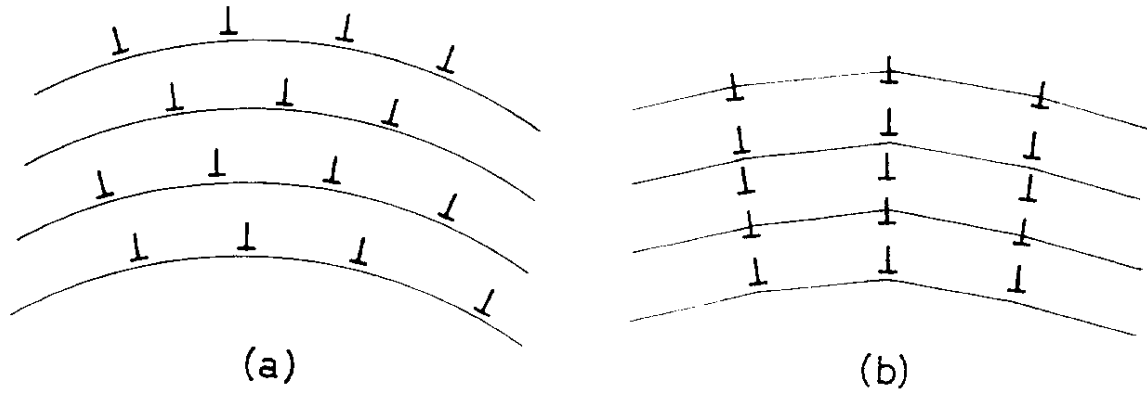
Fig. 5 (a) Random arrangement of excess edge dislocation; (b) Alignment into dislocation walls[10]
.

The most general method of producing a substructure network (i.e. sub grains) is by introducing a small amount of deformation (from about 1% to 10% pre strain) and sub sequent annealing treatment. The amount of deformation and temperature must be low enough to prevent the formation of recrystallization nuclei. This, process has been called polygonization [7]

2.1.2 Recrystallization

The most significant change in the structure properties occur during the primary recrystallization stage. In this stage the deformed lattice is completely replaced by new unstrained one by means of nucleation and growth process, in which practically stress–free grains grow from nuclei formed in the deformed matrix [10]

The recrystallization is a replacement of the cold worked structure by new set of strain free grain [7] . Recrystallization is readily detected by metallographic methods and evidenced by decrease in hardness or strength and an increase in ductility. The density of dislocation decreases considerably on recrystallization and all effect of strain hardening are eliminated [7] .

The driving force for recrystallization is the difference in volume strain energy (i.e. dislocation density) between adjacent austenite sub grains. The austenite grains of low dislocation density will bulge into grains of high dislocation density. The driving force for recrystallization (F_{RXN}) can be described by [11]:

$$F_{RXN} = \mu\, b^2\, \Delta\rho\, / \, 2 \qquad\qquad (1)$$

Where μ is the shear modulus of austenite, b is the burgers vector and $\Delta\rho$ is the change in dislocation density [11] .

As we see from equation (1), there is no direct temperature dependence, but F_{RXN} will decrease with increasing the temperature due to $\Delta\rho$ become smaller i.e. (increasing number of operative slip systems)

The austenite recrystallization will be suppressed by micro alloy precipitates when ($F_{PIN} > F_{REX}$) where F_{PIN} is the total pinning force [11] .

$$F_{PIN} = 4\, r\, \sigma\, Ns \qquad\qquad (2)$$

Where r is the particle radius, σ is the interfacial energy per unit area of boundary, Ns is the number of particles per unit area exert on a migrating boundary.

The sub–grain formation is a necessary preliminary stage to recrystallization; the recrystallization nuclei are formed on heating only from strongly curved regions of the lattice where sub grains can readily form. as sub grains form i.e. it grows to size that the angles between them become of the order of few degrees, so that the boundary mobility begins to increase with increasing angle, the nuclei are formed preferentially in places of high lattice distortion such as near grain boundaries, deformation bands or inclusions [10] .

The microscopic examination reveals that favored sites for recrystallization nuclei include grain boundaries, phase interfaces, twin boundaries, deformation bands and the surface of the material [11] .

The driving force for recrystallization comes from the stored energy of cold work [2] .
The recrystallization process occurs first by nucleation and then growth. These processes depend on six main variables :–
(1) Temperature.
(2) Time.
(3) The effect of prior deformation
(4) Initial grain size.
(5) Amount of recovery or polygonization prior to the start of recrystallization.
(6) Effect of prior strain rate.

2.1.2.1 Influence of time and temperature

Influence of time and temperature is shown in figure (6); the higher the temperature (the grain boundary mobility increases), the shorter the time needed to finish the recrystallization. The S –shaped curves of figure (6) are typical of nucleation and growth processes. The intersection of this line with each of the isothermal recrystallization curves gives the time at a given temperature required to recrystallize half of the structure (t $_{0.5}$)[2] .
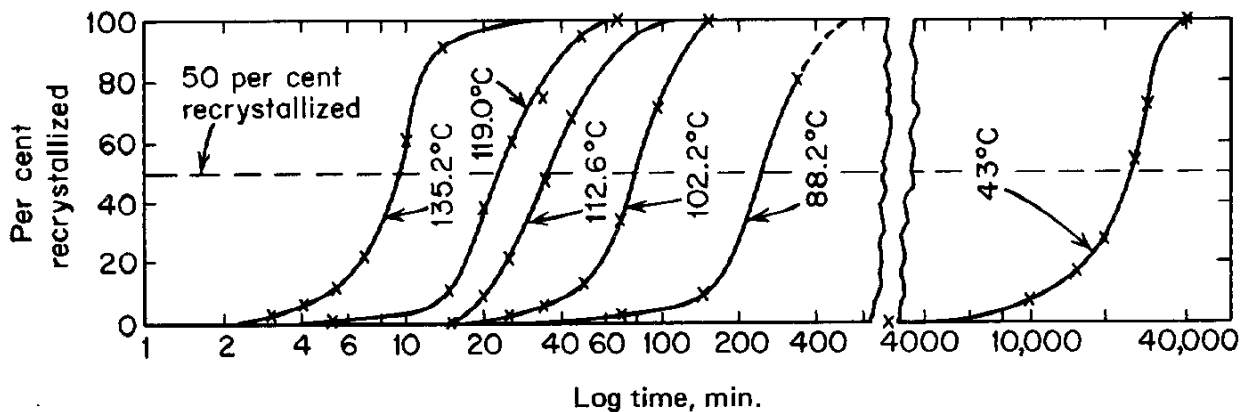
Figure (6) Isothermal transformation (recrystallization) curves for pure copper (99.999 %Cu) cold rolled 98 % [2] .

As shown in figure (6) the time to attain full recrystallization increase with decrease the temperature due to effect of nucleation, as we know within recrystallization stage, the deformed lattice is replaced by a new unstrained one by means of a nucleation and growth process. i.e. stress– free grains grow from nuclei formed in the deformed matrix [10] The rate of nucleation (N) and growth (G) vary as function of temperature as shown in figure (7), both N and G depend on temperature.

Fig. (7) variation of N and G with temperature in an, eutectoid steel [2] .
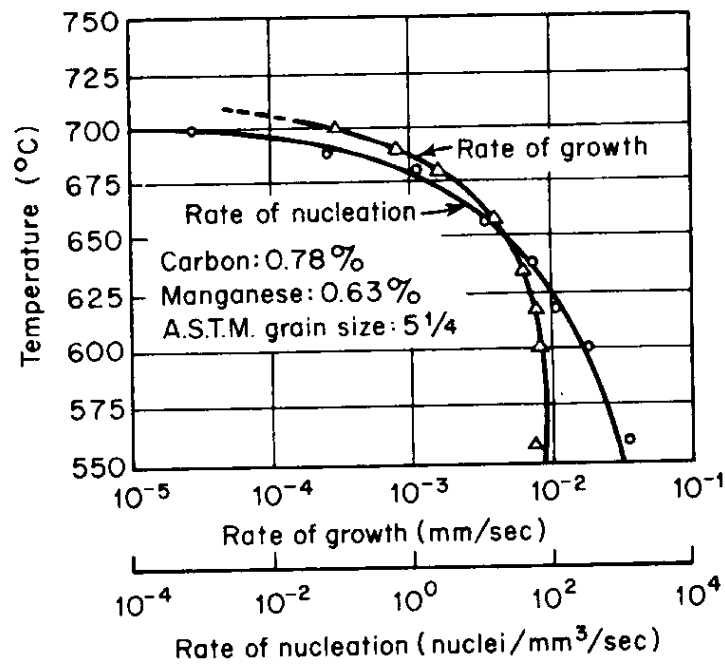
2.1.2.2 Influence of prior deformation

The strain has an effect on recrystallization, as shown in figure (8) The two curves clearly show that recrystallization is promoted by increasing amounts of cold work, when annealed at the same temperature. The metal with the larger amount of cold work recrystallizes much faster than that with lesser reduction and will control the extent to which a grain of the lattice will be curved. The larger the deformation the more severely will the lattice be curved and, consequently shorter time is necessary at any given temperature for the sub – grain to become an active nucleus. In some instances, heavily cold worked metals recrystallize without any significant recovery owing to the formation of strain – free cells during deformation [10]. Also Fig. (9) shows more clearly the influence of pre strain on the kinetics of recrystallization. The time t $_{0.5}$ for softening A (%) = 50 decreases as pre strain (N_1) in torsion test increases from 1 to 6 revolutions[13] .
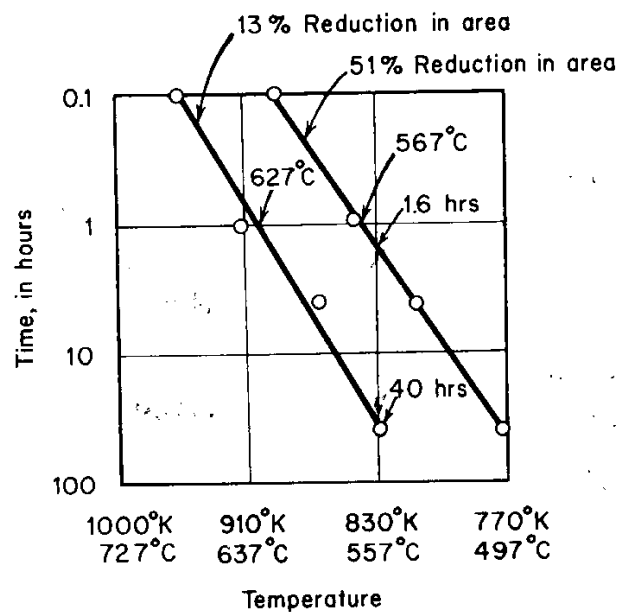

Figure (8) Temperature – time relationships for recrystallization of zirconium (iodide)
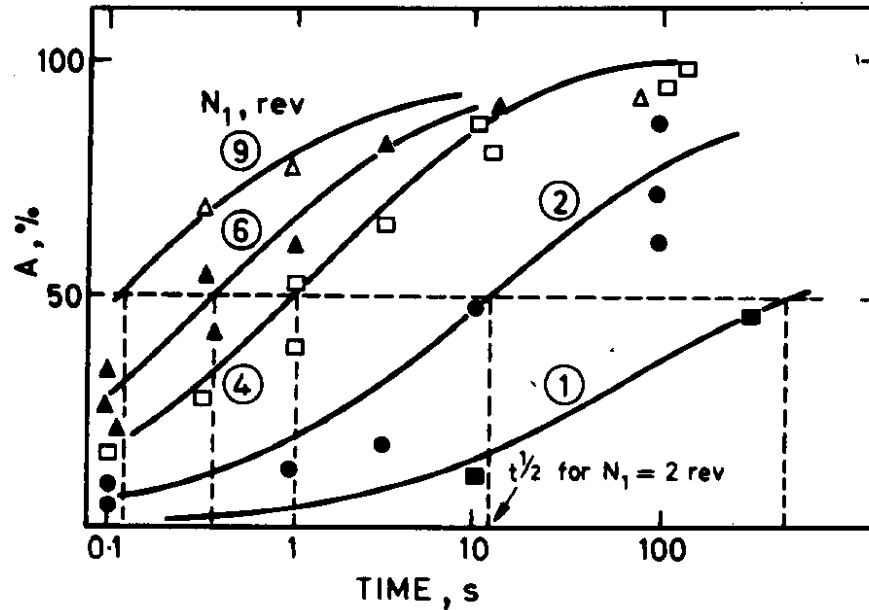Corresponding to two different amounts of prior cold work [2]

16

Fig. (9) Influence of pre strain, N_1, on kinetics of softening[13] .

2.1.2.3 Influence of initial grain size

The lattice adjacent to the grain boundaries is more distorted than in the center of the grains. Decreasing the grain size increases the grain boundary area. The different initial γ grains sizes were obtained by varying the reheating temperature [6] . This effect rises the driving force and the number of possible sites of nucleation and, therefore, the smaller the grains of the metal before cold work, the greater will be the rate of nucleation and smaller the recrystallized grain size for a given degree of deformation.[2] . The effect is similar to influence of prior deformation.

2.1.2.4 Influence of prior strain rate.

During hot torsion testing, at a given deformation the torque increase with the strain rate, so recrystallization rate would be expected to be slower when the strain rate is smaller [13] .The higher prior strain rate, the lower the density of dynamic recrystallization nuclei, and therefore the more rapid the subsequent meta dynamic recrystallization. In addition, the velocity of grain boundary migration will increase as the driving force increases with the dislocation density difference across the grain boundaries [14]. Finally, increase in strain rate will increase the dislocation density as well as driving force for recrystallization.

2.1.2.5 Influence of prior recovery

Recovery decreases driving force for recrystallization, and can significantly lead to decrease in recrystallization rate.

2.1.3. Recrystallization Kinetics

The progress of an isothermal phase transformation can be conveniently represented by Avrami equation :

$$X_{SRX} = 1 - \exp\left(k \cdot t^{n_{SRX}}\right) \tag{3}$$

where:

X_{SRX} – fraction of recrystallized structure

t – time for X_{SRX}

n_{SRX} - Avrami exponent

k – constant

Increase of recrystallized fraction (f) with time elapsing, t, during isothermal transformation of temperature T, can be illustrated on TTT diagram. One example of TTT diagram is shown on figure (10) [12]. In the case of static recrystallization, (transformation α→β), f is the volume fraction of β phase in any moment. Therefore, values of are limited to range between 0 and 1.

Factors affecting relation f (t, T) are: nucleation rate, growth rate and distribution of preferential places for nucleation, overlapping of neighboring diffusion fields of new grains, impeachment of new grains etc.

Regarding recrystallization, type of transformation α→β, transformation is finished at the moment when complete fraction of α phase is transformed. During recrystallization, growth rate of recrystallized grains can be treated as constant, implying that transformation will be finished not because of the decrease in grain growth rate, but because of impeachment of recrystallized grains.

During α→β transformation, nuclei of β are formed continuously during transformation, with constant rate N. Assuming that newly formed nuclei grow in sphere shape manner, with radii r, with growth rate v, the volume of all nuclei formed in starting time (boundary condition when t=0), can be described with following equation:

$$V = \frac{4}{3}\pi r^3 = \frac{4}{3}\pi(vt)^3 \tag{4}$$

Total volume of all nuclei formed up to time τ can be described with next equation:

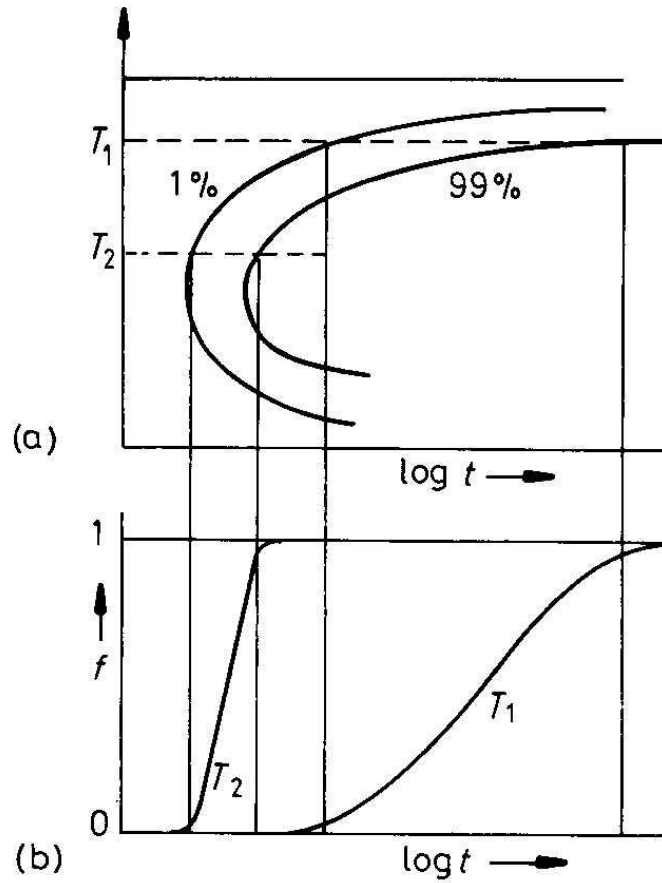$$V = \frac{4}{3}\pi v(t - \tau)^3 \tag{5}$$

Figure (10) Diagram of isothermal decomposition [12]

Number of nuclei formed during increment of time $d\tau$ is equal to $Nd\tau$, per unit volume of starting (non-transformed) phase α. Assuming that grains will not get in contact up to the end of transformation, for unit volume, fraction transformed f, can be calculated as:

$$f = \Sigma V' = \frac{4}{3}\pi N v^3 \int_0^t (t-\tau)^3 d\tau \tag{6}$$

i.e.

$$f = \frac{4}{3}\pi N v^3 t^4 \tag{7}$$

This equation is valid only in the case when f«1. With time elapsing the probability for contact between β (recrystallized) grains increases, leading to decrease in recrystallization rate. Taking into account random distribution of nucleation sites, both for short and long times, recrystallization kinetics can be described with following equation:

$$f = 1 - \exp\left(-\frac{4}{3}\pi N v^3 t^4\right) \tag{8}$$

For short times, this equation is equal to equation (7) because $1-\exp(-z) \approx z$. Also, in the case of long time, $(t\rightarrow\infty)$; $f\rightarrow 1$.

Using replacement,

$$k = \left(\frac{4}{3}\pi N v^3\right) \tag{9}$$

Equation (9) is equal to (3). Equation (3) is known as JMAK (**J**ohnson-**M**ehl-**A**vrami-**K**olmogorov), or more often *Avrami equation*.

After double ln of eqation (3):

$$\ln \ln \frac{1}{1-f} = \ln k + n_{SRX} \cdot \ln t \qquad (10)$$

Avrami exponent n_{SRX}, is derived as slope from equation (10). Theoretically, values of n_{SRX} are in the range 1 to 4. In the case when there is no change of transformation mechanism value of n_{SRX} is constant and shows no temperature dependence.

Driving force for recrystallization is absorbed strain energy, there was a need for quantification of recrystallization kinetics that takes into account the influence of material and processing parameters. Therefore, equation (3) can be rewritten:

$$X_{SRX} = 1 - \exp\left[-B\left(\frac{t}{t_F}\right)^{n_{SRX}} \right] \qquad (11)$$

where:
X_{SRX} - fraction of recrystallized structure
t – time
t_F – time for recrystallization of fraction
n_{SRX} - Avrami exponent
B – constant calculated from equation (12):

$$B = -\ln(1 - F) \qquad (12)$$

 Usually, this is time for 50% of recrystallized fraction (F=0.5), and equation (11) can be rewritten:

$$X_{SRX} = 1 - \exp\left[-0.693\left(\frac{t}{t_{0.5}}\right)^{n_{SRX}} \right] \qquad (13)$$

Where

$t_{0.5}$ – time for 50% of recrystallization, s - Time for 50% recrystallization is calculated from eq (14) [4,15–25]:

$$t_{0.5} = A_{SRX} \exp\left(\frac{Q_{SRX}}{RT}\right) \qquad (14)$$

Where
A_{SRX} – constant
T – absolute temperature
R – universal gas constant
Q_{SRX} – activation energy for static recrystallization

Activation energy for recrystallization is a energetic barrier that must be overlapped, for continuation of recrystallization. Determination of Q_{SRX} requires series of isothermal two-hit tests on different temperatures, using equations (3–14). In the case when there is no change of transformation mechanism value of Q_{SRX} is constant and shows no temperature dependence. If, on the other hand a change in mechanism occurs, different slopes will be observed, leading to two different activation energies.

Values of Q_{SRX} in low carbon and carbon-manganese steels are reported to be between 250 - 280 kJ/mol [15,21,76,77]. Out of this range, some greater values (300kJ/mol [25]), as well as lower values [18,78] are also reported. It is assumed that the difference originates from variations in

chemical composition, basically C and Mn content (0.01<Mn<1.54). Also, different experimental techniques and/or thermal treatments were employed. For example, driving force for recrystallization depends on strain and strain rate in pass prior to recrystallization.

Addition of microalloying elements changes the values of Q_{SRX}. Values of Q_{SRX} for Nb, Nb/V and Nb/Ti steels are in the range od 250 kJ/mol [4]– 2000 kJ/mol [22] and can be devided into two groups:

$\underline{Q_{SRX}\text{ estimated within temperature range over Tnr temperature}}$. In this temperature range Nb is distributed only in solid solution.Values of Q_{SRX} fall usually in range 260-320 [4,15,16,17], inspite some values out of this range are reported [18,79]. These values are close to activation energies for ddiffusion of Nb in austenite (270kJ/mol [80]) and activation energy for self-diffusion of austenite (300kJ/mol [81]).

$\underline{Q_{SRX}\text{ estimated within temperature range below Tnr temperature}}$. In this temperature range Nb is distributed only both in in solid solution and second phase particles, who have major role in inhibitiing brain boundary movement.Values of Q_{SRX} can be as big as 1200kJ/mol. [79].

Influence of chemical composition. According to reported results, it is well accepted that Q_{SRX} depends on chemical composition. One of the first efforts towards quantification of this influence was reported by Medina&Mancilla [19]. They have proposed the following regression equation, for prediction of Q_{SRX} in temperature range over Tnr temperature:

$$Q_{SRX} = 124714 + 28385.68 \cdot (\%Mn) + 64716.68 \cdot (\%Si) + 72775.40 \cdot (\%Mo) +$$
$$+ 76830 \cdot (\%Ti)^{0.123} + 121100.37 \cdot (\%Nb)^{0.100} - kJ/mol \qquad (15)$$

It is clear that model predicts the strongest influences of Nb and Ti. Also, for pure iron model predicts Q_{SRX} of arround 125kJ/mol, which is close to activation energy for pipe diffusion on dislocations.

Table (1) Values of Q$_{SRX}$ (14) for Nb, NbV, Nb−Ti steels

Number	Steel	Chemical Composition	p	q	R	Temperature range, °C	Q$_{SRX}$ kJ/mol	Comment	Ref.
1	Nb	HSLA Steels	2	-4	-	T>1004	325		4
2	Nb	HSLA Steels	2	-4	-	891<T<1004	780		4
3	Nb	Nb	-	-3.81	0.36	800 – 1200	404		15
4	Nb	Nb-B	-	-3.80	0.42	800 – 1200	436		15
5	Nb	Nb-B-Cu	-	-3.55	0.33	800 – 1200	559		15
6	Nb	0.05C 0.35Mn 0.058-0.094Nb	0.88	*	0.28		f(T, X)		16
7	NbTi	Nb-Ti	2	-2.8	-	T>990°C	292.5		17
8	NbTi	Nb-Ti	2	-2.8	-	T<990C	1200 875	def: 15% def: 20%	17
9	NbTi	0.13-0.2Nb 0.01Ti	2	77Nb-4	-	850 – 1000	330		18
10	C-	0.15C-0.77Mn-0.03Nb	1	-1.5		850 – 1000	250		79
11	Nb	0.082C 0.048Mn 0.036Nb 0.0054N		-2			338	n=0.5	21
12	Nb	0.105C 1.23Mn 0.042Nb 0.0112N		-1.96	0.44	T>Tnr T<Tnr	262 400-2200		22
13	NbTi	0,07C 0,62Mn 0,034Nb 0,067Ti	0,77	-2		T>Tnr	308		82
14	Nb	0.11C 1.3Mn 0.093Nb 0.0119N				T>Tnr T<Tnr	272 300-1100		19
15	NbCu	0.055C 1.40Mn 0.019Nb 0.0075N 1%Cu	2	-2.3	-	T>980°C T<980°C T<980°C	310 830 940	ε=20-60% ε=20% ε=40%	24

- p=f(d,%Nb)

2.1.4 Grain growth

When primary recrystallization is complete, the metal can lower its energy further by reducing its total area of grain surface. With extensive annealing it is often found that grain boundaries straighten, small grain shrink and larger ones grow. The general phenomenon is known as grain growth, and the most important factor governing the process is the surface tension of the grain boundaries [10] .

For a grain boundary migrating, the driving force is $2\gamma/R$, where γ is the specific interfacial energy of the boundary, R is the minimum radius of curvature and as the grain grow, R increases and the driving force decreases until it is balanced by the particle –drag when growth stop [10] .

For completely recrystallized metal the driving force for grain growth lies in the surface energy of the grain boundaries. As the grains grow in size and their numbers decrease, the grain boundary area diminishes and the total surface energy is lowered accordingly [2].

The impurity atoms in the form of second –phase inclusions or particles can inhibit grain growth in metals, grain –boundary atmospheres can effectively hinder the motion of grain boundaries [2] .The experimental results indicate that the most important role of pinning particles is to prevent γ grain growth between consecutive deformations during hot working and during cooling between the last deformation and phase transformation. For forging steels, this can be achieved through microalloying either with Ti or with Nb [6] .

The temperature also has an effect of grain growth, as shown in figure (11), as annealing temperature increase i.e. the increase the magnitude of grain growth.
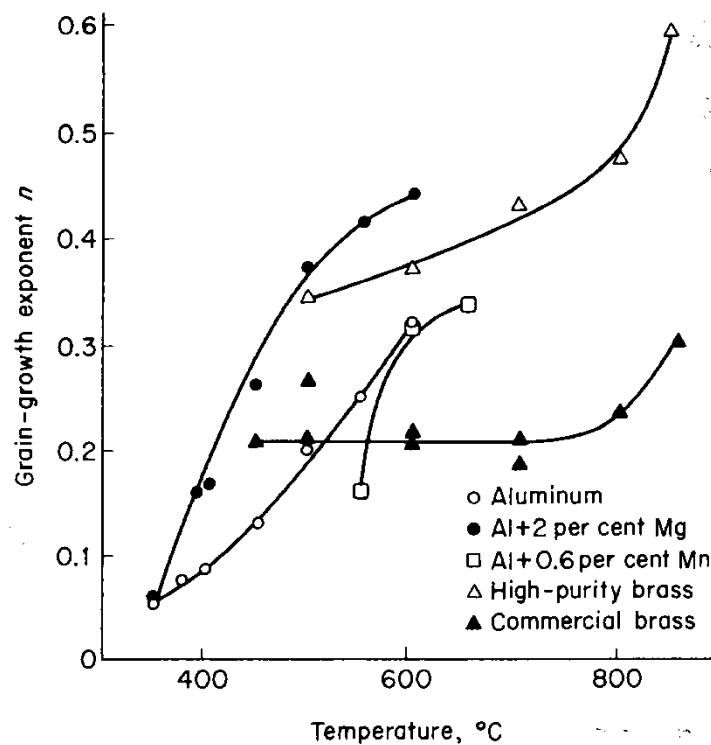

Figure (11) Grain growth exponent as a function of temperature for several metals [2].

This temperature dependence of the grain –growth exponent can be explained by assuming that the grain –boundary solute atmospheres are broken up by thermal vibrations at high temperatures. The

effect of solutes in retarding grain growth varies with the element concerned even as small quantity as 0.01 % of oxygen will effectively retard grain growth in copper [2] .

Impurity atoms in the form of second –phase inclusions or particles can inhibit grain growth in metals, as shown in figure (12), In many cases, second –phase particles tend to dissolve at high temperature. It is also generally true that second –phase particles tend to coalesce at high temperatures and form fewer larger particles. Both of these effects the decrease in amount of the second phase and the tendency to form larger particles remove the retarding effect of the inclusions on grain growth in metals [2] .
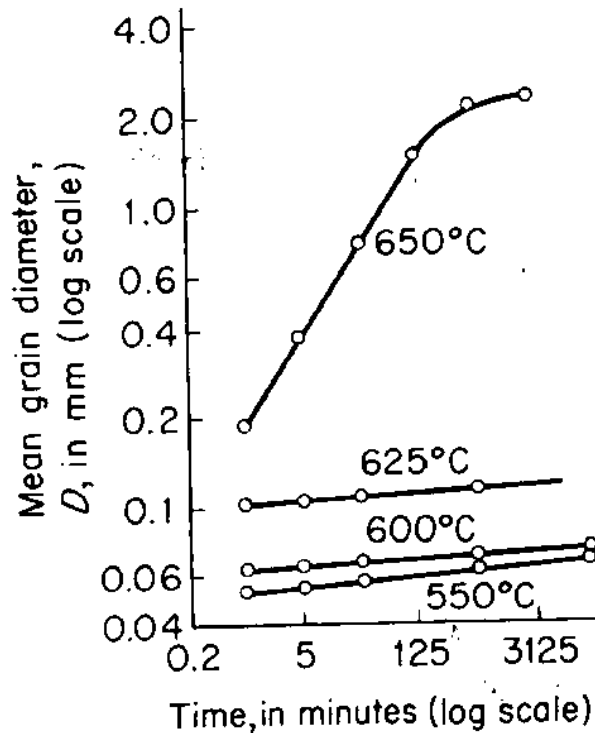
Figure (12) The effect of second phase inclusions on grain growth in Mn − Al alloy [2] .

From figure (12) , when grain size become higher than 1.8 mm , the grain growth retard because of the free surface effect , as the grain become larger , the effect of thermal grooving appear These lead to decrease grain boundary movement i.e. reduce the grain growth rate i.e. as grain size of metal sheet becomes $> (1 / 10 \, t)$, where t is thickness , i.e. lead to reduce the growth rate .For MA steel , current mathematical models for grain growth predict that the rate of grain growth would be extremely rapid for austenite grain size of less than 5 microns [26] .

The specimen geometry may play a part in controlling the rate of grin growth for cylindrical surface, $\Delta\rho = 2\gamma / R$, for spherical surface, $\Delta \rho = 4 \, \gamma / R$ this lead, to the pressure difference for spherical surface > cylindrical surface these the reason for spherical surfaces moves at rate faster than cylindrical surfaces. where γ is surface tension, R is the radius of the curvature.

The grain –boundary grooves are important in grain growth because they tend to anchor the ends of the grain boundaries (where they meet the surface) [2] . The, grain boundary move away from the groove this lead to become free from its groove that is lead to increase the total surface area i.e. (total surface energy) to do it it requires work for these reasons the groove restrains the movement of boundary.

As we know, the presence of inclusions restrains the movement of grain boundary, so at restraining force $= \eta$ These lead to grain boundary not able to pull itself away from its inclusion, where η = force per unit area, γ is the surface tension of grain boundary.

For spherical particles and uniform distribution $R = 4 / 3 \; r / \xi$

20

This, equation show that the ultimate grain size to be expected in the presence of inclusions is directly dependent on the size of the inclusions. where r, ξ is the radius and volume fraction of inclusions respectively [2]

2.2 MICROALLOYED (MA) STEELS

Compared with carbon steels, MA steels offer not only a higher yield strength, which in most cases permits savings in weight or prolonged service life of components and structures, but also favorable working properties, such as improved formability and weldability, and optimized service properties, such as resistance to brittle fracture, to lamellar tearing, and hydrogen−induced or stress corrosion cracking [37]

The typical structural changes occurring during intervals between hot−rolling passes of austenite are static recovery, static recrystallization and strain−induced precipitation. These structural changes play an important role in determining the final microstructure and properties of high strength low alloy (HSLA) steels. To obtain a desirable combination of mechanical properties, a good understanding of the underlying physical metallurgy of static restoration processes is needed, and a proper control of their occurrence is required [28] .

The microalloyed steels are steels in which small addition of alloying elements lead to intensive grain refinement and ∕ or precipitation hardening due to precipitation of stable carbides, nitrides or carbonitrides [29].The major roles of microalloying elements are precipitation hardening (Nb, V and Ti), grain refinement in normalizing and retardation of recrystallization in hot rolling (Nb, Ti) [30] .

Nowadays, these steels are alloyed with Nb and ∕ or V and ∕ or Ti, in total amount of 0.15 %.Ti , Nb, and V form precipitates (TiN, TiC, NbCN, NbC, NbN, VN and VC), whose stability depend on the composition [31]. Chronological development of the use of microalloying elements in steels is given in Fig. (13). ″ Domination ″ of any element can be attributed to price and advantages for thermomechanical processing. The, main motives for developing MA steels were : significant increase in strength, leading to either lowering the construction weight or increase in carrying capacity, and a demand on world market for steels with good weldability for pipelines [29] . Several studies have shown that HAZ grain size can be controlled by Ti addition because the titanium nitride is stable at the high temperatures attained in the fusion boundary region of the HAZ and can prevent grain growth of austenite in this region [32,33,34] .
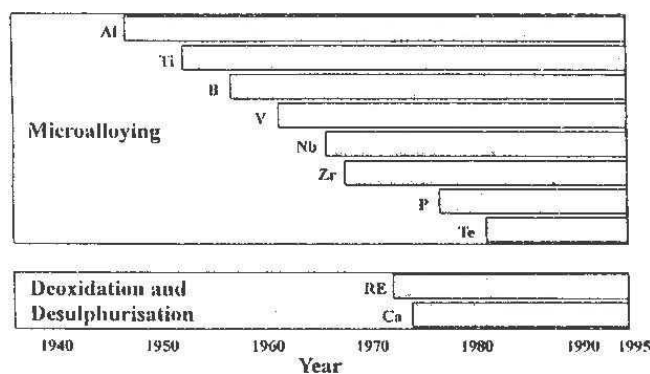

Figure (13) Chronological development of the use of MA elements in steels [29] .

Improved toughness (lower the transition temperature) of the HAZ of welds is obtained through refinement of the grain size by particles of TiN which are stable at the welding temperatures and by a ferritic intragranular microstructure produced by the vanadium [35] . The small TiN − particles existing after strand casting of Ti − microalloyed steels, not only engender. The, small TiN − particles existing after strand casting of Ti − microalloyed steels, not only engender effective grain − growth inhibition between rolling passes and during colling following the termination of rolling, but are also useful for restricting HAZ − grain coarsening in association with subsequent welding [36] . The large heat input welding causes coarsening of ferritic or bainitic grains in HAZ, so the toughness of HAZ depends largely on heat input [30] . To suppress this grain coarsening, addition of 0.010 − 0.015 % Ti will provide TiN precipitation on grain boundaries [29] . For the lower heat input (1.7 kJ ∕ mm), a total of the titanium and nitrogen (Ti∕N) contents of 0.005 to 0.01 is optimum, whereas the high−heat input (3.3 KJ ∕ mm) requires higher levels of Ti ∕ N (0.015 to 0.02) to prevent complete dissolution of the precipitates [37] , for high−heat input condition the stoichiometric ratio of Ti : N in TiN, which occurs between 0.019 and 0.020 wt. % Ti. The maximum level of fine TiN precipitation from supersaturated solid solution occurs when the levels of Ti and N in the steel are at the stoichiometric ratio [38] i.e the increasing levels of TiN precipitation with increasing Ti in the steel, only a part of this precipitation is fine enough to be effective in controlling grain size i.e. the use of Ti−based micro alloy precipitates reveals an attractive means of controlling the coarse grain size in high heat input welding application [38] . The minimum austenite grain size around the Ti ∕ N stoichiometric ratio. However, the HAZ austenite grain size increases abruptly when the Ti contents beyond the Ti∕N stoichiometric ratio [39] .The lower carbon contents in MA steels also led to improved weldability and weldment properties. Graville has shown that the susceptibility to under bead or cold cracking of the weld HAZ is directly related to the composition of the base plate, Fig (14).

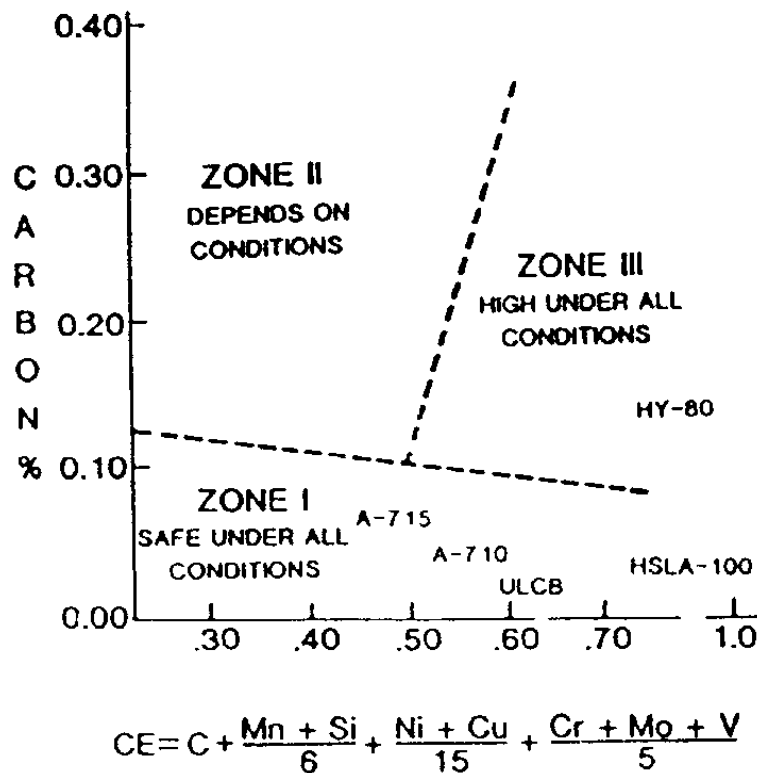$$CE = C + \frac{Mn + Si}{6} + \frac{Ni + Cu}{15} + \frac{Cr + Mo + V}{5}$$

Figure (14) Influence of steel composition on the susceptibility of the heat affected zone to cold cracking. Carbon concentration and carbon equivalent (CE) values are represented by weight % [40]

Clearly, the ability to achieve high strengths in the base plate without relying on high carbon contents can lead to impressive improvements in both weldability and weldment toughness [40] . One, common criteria of weldability is the carbon equivalent (CE) which gives information of the risk for hydrogen induced cracking in heat affected zone (HAZ). If (CE) ≤ 0.41 the risk of cracking is negligible for the sheet thickness of interest (3–8 mm) [41] . The strengthening due to grain refinement and precipitation hardening by microalloying permits a reduction in (CE) to the result that the net effect is an improvement in cold cracking susceptibility [30] .

The microalloying steels with small amounts of strong carbide and nitride forming elements such as Nb, Ti and V have achieved a great improvement in their mechanical properties. These improvements in mechanical properties are a result of many factors. The most important of which are [42] :

(1) Refinement of the ferrite grain size by the formation of a fine sub grain structure.

(2) Strain – induced precipitation of the carbides and nitrides of the strong carbide and nitride forming elements.

(3) Precipitation strengthening of the ferrite

2.2.1 Precipitation in MA steels

The steels are soaked i.e. preheated at high temperatures to dissolve the carbonitrides during hot rolling, as the temperature decreases i.e. the carbonitrides precipitate out the austenite.

During the first stage which takes place at high temperatures (above 1000 °C), The coarse austenite grains which are produced in this stage are decreased in size by recrystallization.

The carbonitrides particles which are induced by the deformation reduce the size of the recrystallized grains by (pinning) the grain boundaries [42] . Precipitates which can exist at high temperatures above the recrystallization temperature of austenite while steel is being rolled or gorged may pin grain boundaries and ensure a fine grain size at transformation and hence a relatively fine ferrite grain size in the finished steel [33] .

Nb, C and N are in solution of austenite at temperature below the start of precipitation. The precipitation of Nb (CN) occurs when the temperature is lowered during deformation process i.e retarding recrystallization due to higher pinning force (F_{PIN}). The higher number of fine precipitates with small interparticle spacings would lead to a higher F_{PIN} [11] . An extensive metallographic study using TEM has shown that the Nb CN particles were located in highly specific sites in the beginning of precipitation. These sites are known to be prior austenite grain boundaries, deformation bands and sub grain boundaries [28] .

Generally, the precipitation effects markedly increase the strength but lower the impact resistance. Recent development has combined precipitation hardening with grain refinement, by the use of niobium, vanadium or titanium. The effectiveness of these elements depends on their solubility in austenite, which controls how much can be dissolved and is thus available for precipitation [43] . The solubility data are available in table (2).

Table 2. Solubility products for Nb − C, Nb − N and Nb − C − N systems in austenite [11]

System	Product	Reference
Nb – C	Log [Nb] [C] = 2.9 − 7500∕ T	44
"	Log [Nb] [C] = 3.04 − 7290∕ T	44
"	Log [Nb] [C] = 3.7 − 9100∕ T	44
"	Log [Nb] [C] = 3.42 − 7900∕ T	46
"	Log[Nb] [C] = 4.37 − 9290∕ T	47

"	$Log [Nb] [C]^{0.87} = 3.18 - 7700/T$	48
"	$Log [Nb] [C]^{0.87} = 3.11 - 7520/T$	44
"	$Log [Nb] [C] = 2.96 - 7510/T$	44
"	$Log [Nb] [C]^{0.87} = 3.4 - 7200/T$	44
"	$Log [Nb] [C] = 3.31 - 7970/T + [Mn] (1371/T - 0.9) - [Mn]^2 (75/T - 0.0504)$	49
"	$Log [Nb] [C]^{0.87} = 2.81 - 7019.5/T$	50
"	$Log [Nb] [C]^{0.87} = 3.4 - 7920/T$	51
"	$Log [Nb] [C] = 1.18 - 4880/T$	52
"	$Log [Nb] [C] = 3.89 - 8030/T$	52
Nb – N	$Log[Nb][N] = 4.04 - 10230/T$	53
"	$Log [Nb] [N] = 3.79 - 10150/T$	48
"	$Log [Nb] [N] = 2.8 - 8500/T$	46
"	$Log [Nb] [N] = 3.7 - 10800/T$	54
"	$Log [Nb] [N]^{0.87} = 2.86 - 7927/T$	50
"	$Log [Nb] [N] = 4.2 - 10000/T$	52
Nb–C–N	$Log [Nb] [C]^{0.24} [N]^{0.65} = 4.09 - 10500/T$	44
"	$Log [Nb] [C 12/14N] = 3.97 - 8800/T$	55
"	$Log [Nb] [C + N] = 1.54 - 5860/T$	44
"	$Log [Nb] [C]^{0.83} [N]^{0.14} = 4.46 - 9800/T$	56
"	$Log [Nb] [C + 12/14 N] = 2.26 - 6770/T$	56

Where [Nb] , [C] , and [N] are the concentrations in weight percent, and T is the absolute temperature.

If we take, for example: –

$$Log [Nb] [C + 12/14 N] = 2.26 - 6770/T \qquad (16)$$

(which is most commonly used equation), if the both sides are equal, the precipitation start, clearly we can calculate the precipitate dissolution temperature from the solubility products which is shown in table (2). During cooling Nb (CN) precipitates at the ferrite – austenite interface during the transformation[43] .

Niobium addition to plain carbon steels is used to refine the ferrite grain size and also to impart precipitation strengthening. The precipitation strengthening is due to the precipitation of Nb (CN) in the ferrite formed from transformation of the austenite present at the finish–rolling temperature. The maximum precipitation strengthening occurs at the stoichiometric Nb : (C + N) ratio in the steel [57] .The effect of Nb:C $_{Eq}$ ratio on the precipitation strengthening is shown in fig (15).
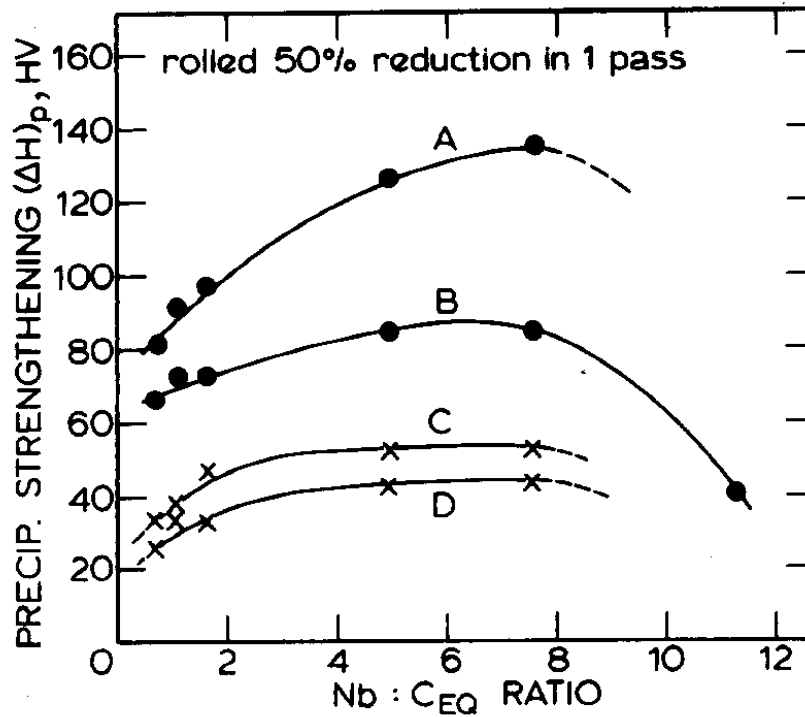
24

Fig. (15) Effect of Nb : C $_{Eq}$ ratio on precipitation strengthening (ΔH) $_P$ [57] .

In the final stages of hot rolling, these precipitates retard recrystallization because they prevent the substructure from changing by the processes of dislocation and sub grain boundary migration. The net effect of these processes is to progressively flatten the austenitic grains so that a (pan–cake) structure is produced which has a higher austenitic grain boundary area per unit volume than normally would be obtained. Since the ferrite nucleates mainly in the austenitic grain boundaries, the increased grain boundary area will provide more nuclei for ferrite and hence lead to a finer ferrite grain size. Finally, any microalloying element left unprecipitated during hot rolling will precipitate in the ferrite either during cooling to room temperature (plate steels) or during the coiling operation (strip steels). The precipitation in the ferrite will provide additional strength to the micro alloyed steels [42]. A small addition of microalloying elements, MAE (0.1 %), such as Nb, V, and Ti, can provide sufficient microstructure control, that produces a fine –grained steel with good combination of strength and toughness, thus post–process heat treatment is not necessary. The elimination of heat treatment is cost reduction factor that provides the driving force for the development of MA steel for forgings [6] .

The microalloying elements (MAE) Nb, Ti and V are widely appreciated and exploited for their ability to increase the strength and toughness of structural steel. The MAE are known to impede the motion of crystalline defects such as grain boundaries, recrystallization boundaries and dislocations when the MAE are present either as solute (weak pinning) or as precipitate (strong pinning). Hence, the MAE can suppress grain coarsening, static recrystallization and the motion of dislocations [40] .

The strain inducement of precipitation during thermomechanical treatment will depend on the strain, strain rate, time, and temperature parameters involved in the treatment [57] .

2.2.2 Static recrystallization in MA steels

In order to estimate the kinetics of static recrystallization taking place after meta dynamic recrystallization, further experiments were carried out in which the strain rate and temperature were held constant, and only the effect of strain on the rate of softening was explored [14]. From the

softening curves, an expression for the time of 50 % softening by static recrystallization was derived as a function of strain, strain rate and temperature based on the equation proposed by Sellars [14] .

$$t_{50} = B\, Z^r \exp\left(Q_{rex}/R\,T\right) \tag{17}$$

Where B and r, are constants, Z is the Zener–Hollomon parameter, Q_{rex} the activation energy for recrystallization and T the temperature as shown in table below. Table (3) is a compilation of the equations employed by the different research groups to develop models to predict microstructural evolution during hot rolling of steel strip for plain C – Mn steels. During hot rolling, the first metallurgical phenomenon that must be accounted for is dynamic recrystallization, since it occurs during the course of deformation. The lack of increase in flow stress with decreasing temperature indicates that dynamic recrystallization is taking place during deformation, followed by meta dynamic recrystallization [58] . As can be seen from figure (16) there is an accumulation of work hardening from the first finishing pass to the second, but after that, the maximum flow stress remains about the same. To confirm that dynamic recrystallization occurred during the finishing passes, a test was performed in which all the finishing passes were executed isothermally at 930 C° (Fig. 16). Dynamic recrystallization leads to somewhat lower rolling loads than austenite pancaking, but to considerably higher loads than static recrystallization. This, is because dynamic recrystallization does not remove dislocations as effectively as static recrystallization, but still reduces the density below the levels present in fully work hardened (i.e. pancaked) austenite [58] When the dislocation substructure due to hot deformation becomes dense and inhomogeneous, new recrystallized grains may be nucleated. The mechanism of nucleation of recrystallized grains depends on the strain rate for a particular temperature. At a low strain rate, nucleation occurs by bulging of existing grain boundaries, while at high strain rates, a cellular substructure of tangled dislocations develops throughout the grain giving rise to nuclei.[59] . Dynamic recrystallization initiates at a critical strain, ε_c, which has been found to be slightly less than the peak strain. Sellars and Saito et al. have employed a relationship relating the critical strain to the Zener – Holloman parameter and the initial grain size (d_0) to determine the onset of dynamic recrystallization, as can be seen in Table (3). Through a series of measurements, Senuma and Yada have found the critical strain to be independent of both the initial grain size and the strain rate, the relationship employed in their model is also given in Table (3). The dynamic recrystallization kinetics for single – peak flow curves can be represented by an Av rami expression.
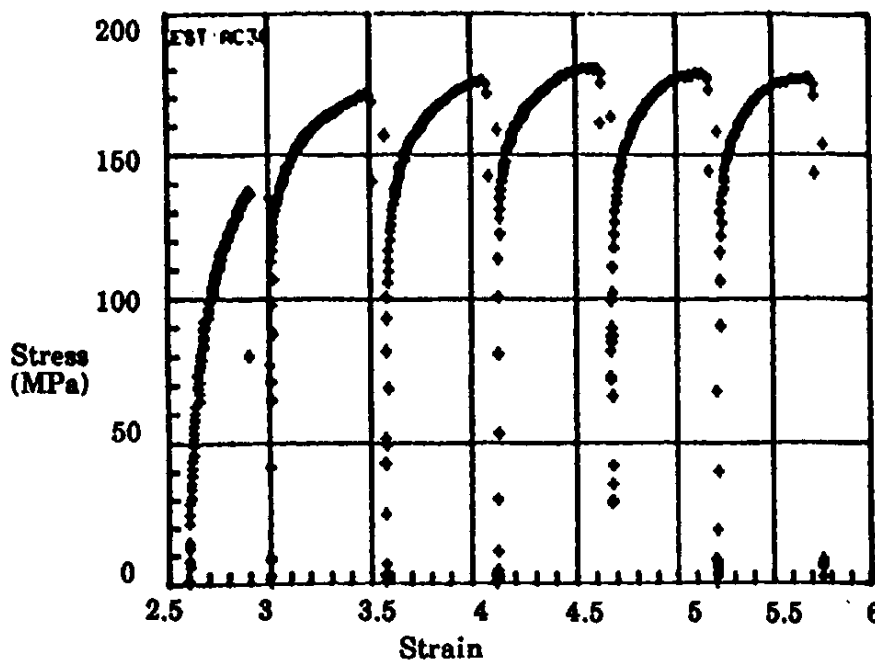

Fig. (16) Finishing flow curves for Nb–steel (0.056 wt. %) [58] .

26

Table (3) Summary of some Reported Recrystallization and Grain Growth Relationships [59] .

University of Sheffield Sellars and Co–Workers	Nippon Ste Yada Et al.	Kawasaki Steel Saito et al.	IRSID Laboratories Perdrix
	Dynamic Recrystallization		
$\varepsilon_p = 4.9 . 10^{-4} d_0^{1/2} Z^{0.15}$	$\varepsilon_c = 4.76 . 10^{-4} \exp(8000/T)$	$\varepsilon_c = 3.68 . 10^{-4} Z^{0.19} d_0^{0.44}$	not incorporated
$\varepsilon_C = a \varepsilon_p$	$d_{dyn} = 22,600 Z^{-0.27}$	$d_{dyn} = 2.82 . 10^4 Z^{-0.24}$	
$Z = \varepsilon \exp^{Q/RT}$	$Z = \dot{\varepsilon} \exp Q/RT$	$Z = \dot{\varepsilon} \exp Q/RT$	
$Q = 312$ k J/mol	$Q = 267.1$ KJ/mol	$Q = 312$ KJ/mol	
(metadynamic)	$X_{dyn} = 1 - \exp(-0.693(\varepsilon - \varepsilon_c/\varepsilon_{0.5})$		
	$\varepsilon_{0.5} = 1.44 . 10^{-5} d_0^{0.28} \varepsilon^{0.05} \exp(6420/T)$		
$X = 1 - \exp(-0.693(t/t_{0.5}))$			
	Static Recrystallization		
$X = 1 - \exp(-0.693(t/t_{0.5})^2)$	$X = 1 - \exp(-0.693(t/t_{0.5})^2)$	$X = 1 - \exp(-0.693(t/t_{0.5})^2)$	$X = 1 - \exp(-0.693(t/t_{0.5})^{nr})$
$\varepsilon < 0.8 \varepsilon_p$			
$t_{0.5} = 2.5 . 10^{-19} \varepsilon^{-4} d_0^2 \exp(Q/RT)$	$t_{0.5} = 2.2 \, 10^{-12} S_v^{-0.5} \dot{\varepsilon}^{-0.2} \varepsilon^{-2} \exp(30,000/T)$	$t_{0.5} = 2.5 . 10^{-19} \dot{\varepsilon}^{-4} d_0^2 \exp(Q_s/RT)$	$t_{0.5} = 3.67 . 10^{-14} \varepsilon^p \dot{\varepsilon}^{-0.28} . d_0^{0.14} \exp(Q_s/RT)$
$\varepsilon > 0.8 \varepsilon_p$	$d_{rex} = 5/S_v^{0.6}$	$Q_s = 300$ KJ/mol	
	$S_v = 24/\pi d_0(0.491 e^\varepsilon$	$d_{rex} = 0.5 d_0^{0.67} \varepsilon^{-1}$	
$t_{0.5} = 1.06 . 10^{-5} Z^{-0.6} \exp(Q_s/RT)$	$+ 0.1433 e^{-3\varepsilon})$		$n_r = 272 d_0^{-0.155} \varepsilon^{-0.5} . \exp(-37,492/RT)$
$Q_s = 300$ KJ/mol			$d_{rex} = 18.51 \ln(T/973) . d_0^{0.374} \varepsilon^U \dot{\varepsilon}^{-0.1}$
$D_{rex} = 0.5 d_0^{0.67} \varepsilon^{-1}$			
$(\varepsilon < \varepsilon^*)$			$u = -0.5 d_0^{0.267}(973/T)^{3.933}$
$d_{rex} = 1.8 . 10^3 Z^{0.15}$			
$(\varepsilon > \varepsilon^*)$		$P'' = -0.86 d_0^{0.24}$	
$\varepsilon^* = 0.57 d_0^{0.17} \varepsilon_p$		$Q_s = 301$ KJ/mol	
	Grain Growth		
$d^{10} = d_0^{10} + At \exp(-Q_{gg}/RT)$	$d^2 = d_0 + At \exp(-Q_{gg}/RT)$	$d^{10} = d_0^{10} + At \exp(-Q_{gg}/RT)$	$d = d_{rex}(1 + \alpha \ln t/t_{rex})$
$T > 1100$ C°	$A = 1.44 . 10^{12} Q_{gg}/R = 32,100$	$T > 1100$ C°	$\alpha = 0.195$
$A = 3.87 . 10^{32}$		$A = 3.87 . 10^{32}$	(C–Mn–Al steels)
$Q_{gg} = 400$ KJ/mol		$Q_{gg} = 400$ KJ/mol	$\alpha = 0.098$
$T < 1100$ C°		$T < 1100$ C°	(Nb grades)
$A = 1.31 . 10^{52}$		$A = 1.31 . 10^{52}$	
$Q_{gg} = 914$ KJ/mol		$Q_{gg} = 914$ KJ/mol	

The static recrystallization on the other hand, is a process by which a large number of dislocations are simultaneously annihilated. The recrystallization kinetics are well described by the Avrami equation, as indicated in the models summarized in Table (3). The basic static recrystallization behavior of C – Mn steels shows that the time to a given level of recrystallization decreases with increasing strain, ε, increasing temperature, T, and decreasing initial grain size, d_0 [60] . Partial recrystallization can occur if there is insufficient time at temperature or if the strain level at given temperature is inadequate to promote full recrystallization. More work is clearly required to understand the behavior of partially recrystallized structures [59] .

The meta dynamic recrystallization kinetics have been defined by Sellars to have a form similar to that for static recrystallization with a time exponent equal to 1 and $t_{0.5}$ corresponding to a strain greater than

0.8 ε_p, as shown in Table (3). The, static recrystallization of austenite at moderate rolling temperatures is used to engender fine as hot rolled ferrite grain sizes. As shown by Sah et al, Sakui et al, and Roberts et al [4] increase in grain size

(d_0) leads to an increase in ε_p and their data indicate a relationship of the form

$$\varepsilon_p \alpha d_0^{1/2} \tag{18}$$

The kinetics of recrystallization or restoration have been determined for a range of niobium treated steels after deformation by rolling, in tension or in torsion. The results are shown in terms of strain and grain size compensated time to 50 % recrystallization or restoration as a function of temperature There are few data on Nb – steels to determine the strain dependence of recrystallization [4] .(all the observations were made on materials reheated to sufficiently high temperatures for complete dissolution of NbC to take place). For the Nb–treated steel, the results show that austenite grain refinement by static recrystallization is most effective when the initial austenite grains is relatively large (137 μm) and the one–hit deformation is equal to or larger than 0.2 true strain. Little or no grain refinement can be achieved when either the initial grain size is on the order of 20 μm or the applied strain is less than 10% [6].

Whittaker et al. suggest that recrystallization times increase with increasing carbon and manganese content, no systematic effect were observed by Irvine et al [4]. The extent of recrystallization and grain growth between rolling passes and after the termination of processing is, of course, strongly dependent on various variables which are together called the rolling schedule. In this context, the principal variables are :

1) the vector of pass reduction (N elements for N passes),
2) the vector of pass temperatures (N elements),
3) the vector of inter – pass times ((N – 1) elements), and
4) parameters defining the cooling of the stock between FRT and Ar₃ which in turn depend on the plate or strip thickness, application of accelerated cooling etc. [36]

The static recrystallization is a thermally activated process, a plot of the characteristic recrystallization time $t_{0.5}$ vs the inverse absolute temperature leads to estimates of the activation energy for recrystallization i.e. $t_{0.5}$ was found to very linearly with inverse temperature in all of the steels [15] .

2.2.2.1 Influence of strain

The dependence on strain of the characteristic time $t_{0.5}$, measured by either metallographic or restoration methods, is shown for several steels in Figure (17). All the curves show a steep dependence on strain for strains up to ~ 0.8ε_p[4], which fits a relationship

$$t_{0.5} \alpha \varepsilon^{-m} \tag{19}$$

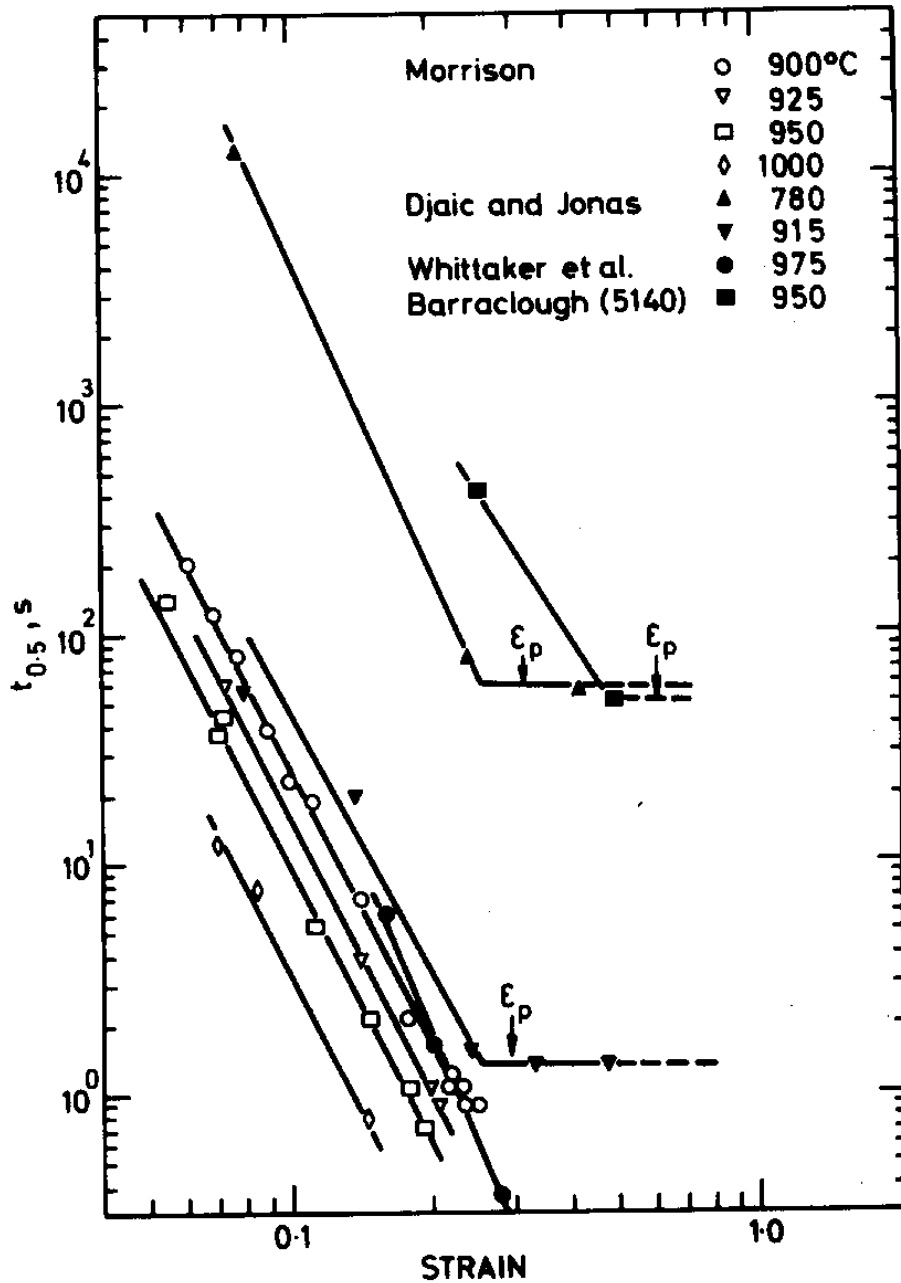28

Where the mean value of m = 4.

Fig. (17) Dependence of time for 50 % recrystallization or restoration on strain for C – Mn and Low alloy steel [4] .

The observations of Djaic and Jonas [4] indicate that an abrupt change takes place from strain dependence to independence at a strain ~ 0.8 ε_p, as illustrated in figure (17). because preexisting recrystallization nuclei are always present in the deformed structure at strains greater than ε_c. During steady state deformation the dynamically recrystallized grain size depends only on Z, independent of strain and original grain size [4] .

2.2.2.2 Influence of Reheating Temperature

The effect of austenitizing temperature on the as reheated γ grain size is given in figure (18), so grain refinement depends on the as–reheated grain size of austenite, niobium is an effective grain refining element [6,30] . The effect of reheating temperature on the recrystallization curves is illustrated in Figure

(19) for the Nb–B steel. When this temperature is increased from 1100 C° to 1200 C° , the recrystallization kinetics are slightly delayed due to the somewhat larger initial grain size (table 4) and also because of the increase in the amount of niobium in solution. In, the Cu–Nb–B steel, no effect of reheating temperature on the recrystallize kinetics was observed between 1000 C° and 1200 C° . Table (4) shows that the initial grain size remains almost constant as the reheating temperature is raised from 1000 C°to 1250 C° . Since the initial grain size affects the density of nucleation sites [15] .
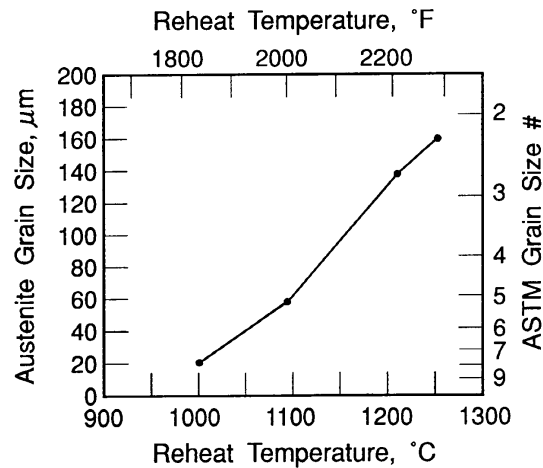
Fig. (18) Austenite grain size as a function of austenitizing temperature for the Nb treated steel (holding time at the temperature was 5 min) [6]

Table 4. Dependence of the Austenite Grain Size on Reheating Temperature in the Boron − Containing Steels [15]

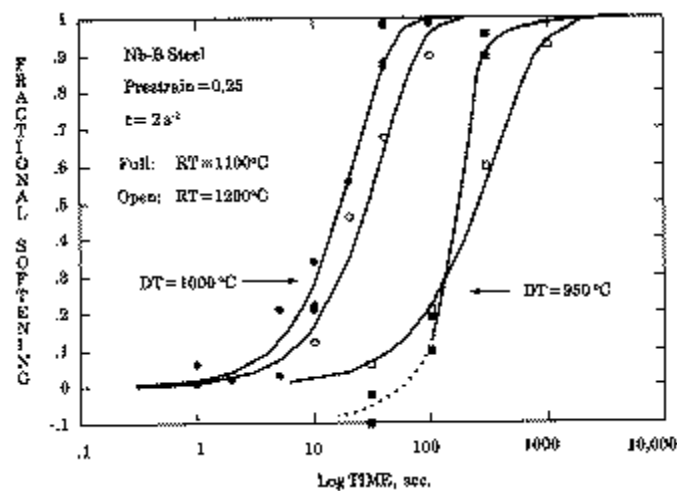| RT (C°)	$d_{0\gamma}$ Nb –B (μ m)	$d_{0\gamma}$ Cu –Nb – B (μ m)
1000	—	16
1050	33	—
1100	38	17
1150	45	—
1200	—	20
1250	52	23

Fig. (19) Effect of reheating temperature (RT) on the softening rate for Nb−B steel [15] .

In the Cu − Nb − B steel, practically no effect of reheating temperature on the recrystallization kinetics was observed between 1000 C ° and 1200 °C.

2.2.2.3 Effect of Deformation Temperature

The effect of temperature on the recrystallization kinetics is evident from Figure 20 (a) , where the fractional softening goes from 12 pct at 900 C° to almost 70 pct at 1000 C° within a holding time of 1 second i.e. the fractional softening does not go to completion , even at holding times greater than 100 seconds such incomplete softening at long holding times has been observed in hot deformed polycrystalline nickel by Sakai et al ,who attributed it to the presence of meta dynamically recovered grains . These grains are stable at high temperatures because they have a dislocation density which is below the critical level. so that there is insufficient driving force for nucleation [15] . In the Nb steel figure 20 (b), the deformation temperature has the same effect on fractional softening i.e. the recrystallization kinetics are delayed by more than an order of magnitude in time when the temperature is decreased from 1000 C ° to 900 C ° . Similar trends are displayed by the Nb − B and Cu − Nb − B steel. In Figures 21 (a) and (b), the effect of strain prior to holding is illustrated for the base and Nb − B steel, respectively. Here, also, a reduction in the pre strain results in the strong retardation of recrystallization [15] .
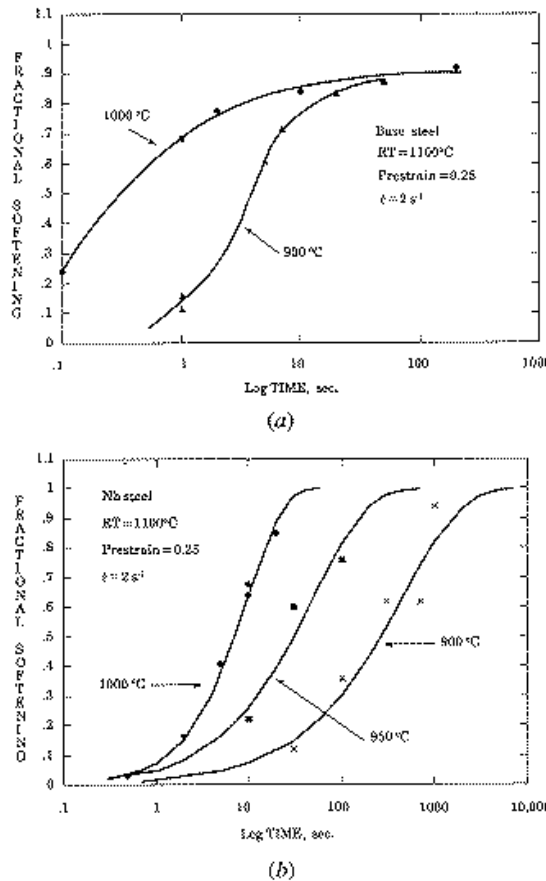

Fig. (20) Effect of temperature on softening (a) in the base steel pre strained to 0.25 and (b) in the Nb steel pre strained to 0.25 at 2 s $^{-1}$ [15] .
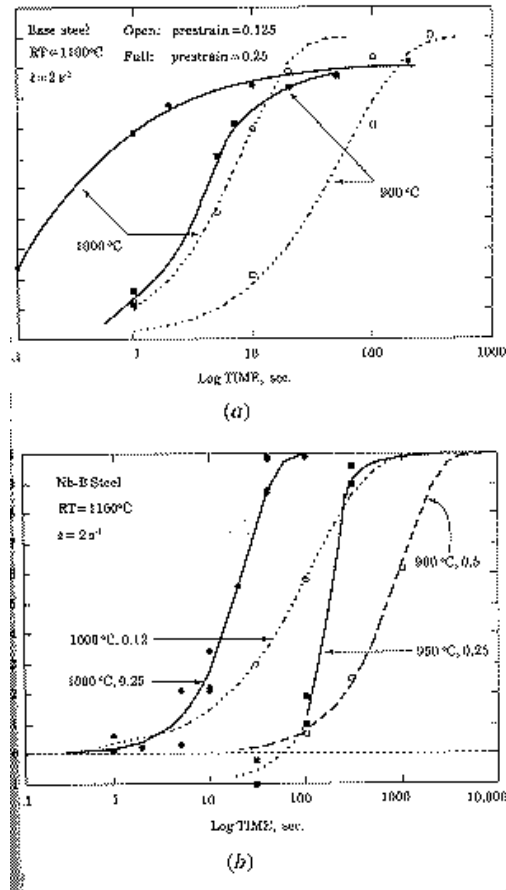
31

Fig. (21) Effect of pre strain on softening (a) in the base steel and (b) in the Nb − B steel [15] .

2.2.2.4 Influence of Strain Rate

The recrystallization kinetics are significantly accelerated when the strain rate is increased [15,28,13,26] . Such behavior is observed in both the base and microalloyed steels and is illustrated in Figures 22(a) and (b). This acceleration in softening rate is due to the decrease in the amount of dynamic recovery and the consequent increase in dislocation density that accompanies the increase in strain rate. The higher dislocation density is associated with higher stored energies i.e. this energy constitutes the driving force for recrystallization [15] .

The strain rate effects the softening kinetics i.e. the softening curves shift to the left with increasing strain rate. For, the plain C−Mn steel (0.043 % C ,0.3 %Mn), at a strain rate of 3 s^{-1}, there is no significant effect of temperature (Fig. 23) . At all temperature, softening is very rapid with 50 % softening occurring within 200 to 300 ms, and completion taking approximately 1 s [26] . However, there is a marked effect of strain rate with an order of magnitude decrease from 3 to 0.03 s^{-1} leading to an equivalent reduction in the softening kinetics (Fig. 24) The kinetics are considered to increase with the applied strain rate because more crystalline defects are produced at higher strain rate i.e. it is generally believed that the grain boundary area is the most favorable nucleation site for precipitation [28].
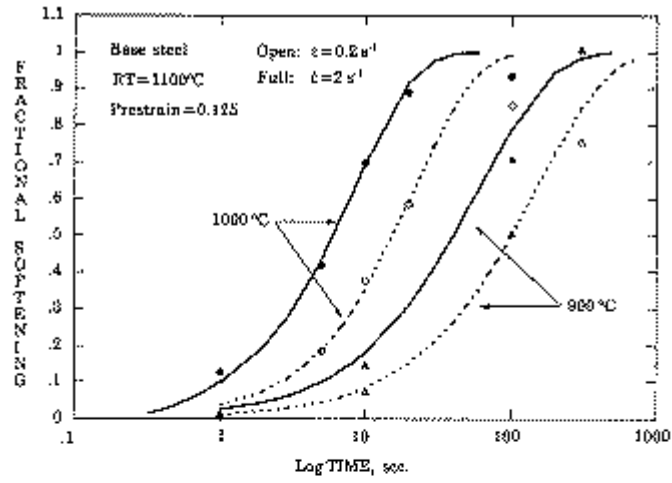
(a)
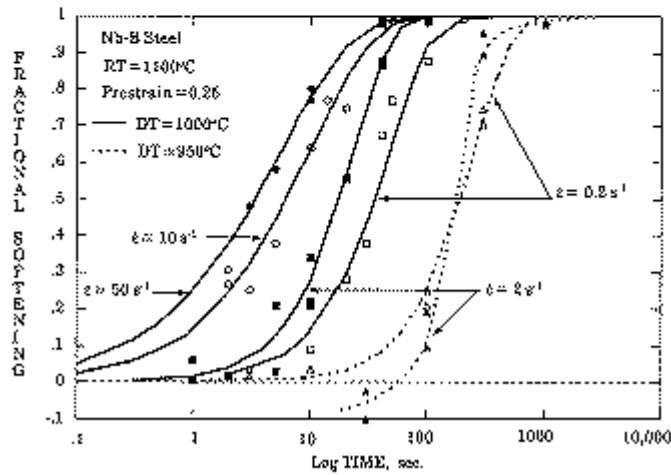
(b)

Fig. (22) Effect of strain rate on softening (a) in the base steel pre strained to 0.125 and (b) in the Nb – B steel pre strained to 0.25 [15] .
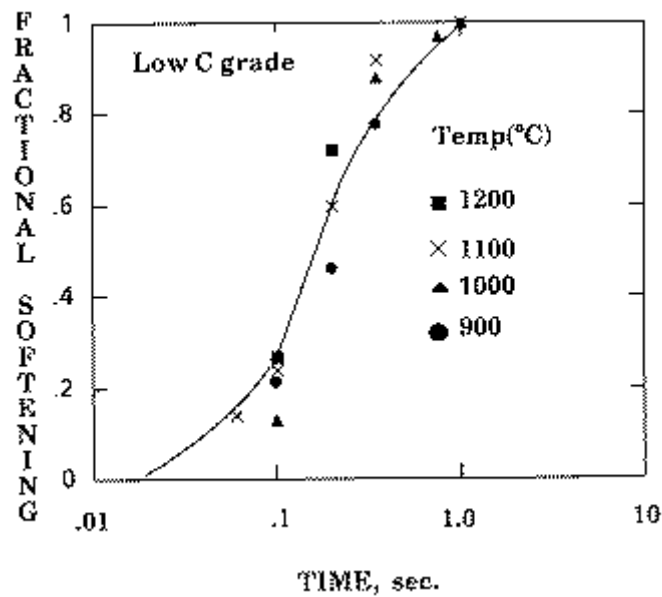

Fig. (23) The post deformation softening kinetics of low C steel are extremely rapid and insensitive to temperature [26] .
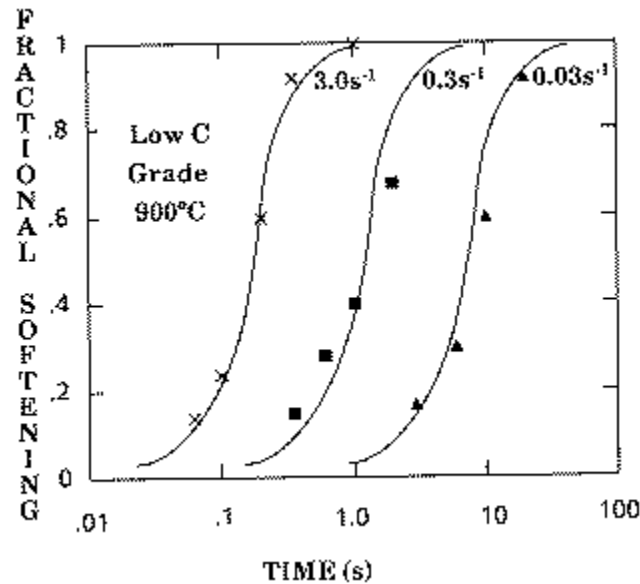
33

Fig. (24) There is a strong effect of strain rate on the post deformation softening kinetics of the low C steel [26] .

2.2.2.5 Influence of chemical composition

In recent decades significant effort has been put into establishing the influence of chemical composition, metallurgical and thermomechanical factors on the static recrystallization kinetics and on the interactions between recrystallization and precipitation in hot deformed microalloyed austenite [62]

The influence of additions of niobium, molybdenum, titanium, and vanadium on the retardation of both static recovery and recrystallization was investigated by measuring the amount of softening taking place during an interval following deformation at an elevated temperature [63] . The studies confirmed that a small addition of Nb, Ti or V retards the progress of static recovery and recrystallization of austenite in HSLA steel. This retarding effect may be attributed to either solute–drag of dissolved alloying elements or precipitation pinning [28] . Whether the main portion of the retardation is due to solute– drag or precipitation has been a subject of controversy and argument. However, most studies have shown that the static softening can be more effectively retarded by extensive, fine matrix precipitation [28] . There are few observations on vanadium and titanium treated MA steels compared with those for the niobium steels. Irvine et al found little or no effect of additions of 0.15 % or 0.03 % Ti on recrystallization kinetic, although they retarded grain growth after recrystallization [4] .

Cordea and Hook There are few observations on vanadium and titanium treated MA steels compared with those for observed some retardation of recrystallization in a 0.059 % V steel at temperatures below 925 C ° , but the effect was less than with 0.011 % Nb. Korchynsky and Stuart also report that retardation of recrystallization is less in vanadium steel than in a 0.02 % Nb steel. Similarly, Ouchi et al found little retardation of the start of recrystallization in a 0.019 % Ti steel although there was some evidence that the rate of recrystallization decreased [4] .

It is thus clear that vanadium and titanium are much less effective than niobium in retarding recrystallization, but quantitative relationships cannot be put forward at present [4] .

With a large addition of titanium (0.2 %), Korchynsky and Stuart found very marked retardation of recrystallization and observations of retardation in a 0.24 % Ti steel have also been reported by Cordea and Hook [4] .

In recrystallization rolling, the basic philosophy is to make use of the grain refinement accruing from the static recrystallization of austenite at moderate finish rolling temperatures (FRT), typically 900 – 1000 °C. However, in order to maintain the fine recrystallized grain size during cooling between the FRT and

34

the temperature at which the steel starts to transform to ferrite, it is necessary that grain growth be restricted in some way e.g. by particles, TiN is a suitable candidate for such grain growth inhibition [36] . The recrystallization kinetics of the Ti − V steel is very much slower for small pre strains than in the case of C − Mn austenite. The reason for the delayed recrystallization in Ti − V austenite is thought to derive from the drag force on moving grain boundaries due to the presence of TiN − particles [36] .

2.2.3 Austenite to ferrite transformation

One of the major structural parameters affecting the properties of hot rolled products is the ferrite grain size [4,5]. This is shown in Fig (26) i.e. (ferrite grain size increases with austenite grain size). The, requirements for the finest ferrite grain size necessitates a high ferrite nucleation rate during the transformation. As ferrite nucleates predominantly at austenite grain boundaries, the need for a fine austenite grain size is a apparent. The, parameter which has been often used to indicate the nucleation frequency for ferrite is the austenite grain boundary area per unit volume, S_V, which increases with a refinement of the recrystallized austenite grain size and with increasing elongation of uncrystallized austenite grains. As it was shown on Fig. (25), for a given S_V, the ferrite grain size was finer when produced from uncrystallized austenite than recrystallized austenite[61] . The various nucleation sites for ferrite not only austenite boundaries, but also deformation bands, second phase particles (particularly undissolved micro−alloy carbide / nitrides), recovered sub−grain boundaries especially if decorated by precipitates, and even the non−coherent ledges on twin boundaries. Because many of these sites occur particularly in uncrystallized austenite, the finest ferrite grain size will be produced from the finest austenite grain size rolled to a maximum extent below the recrystallization temperature[61] .
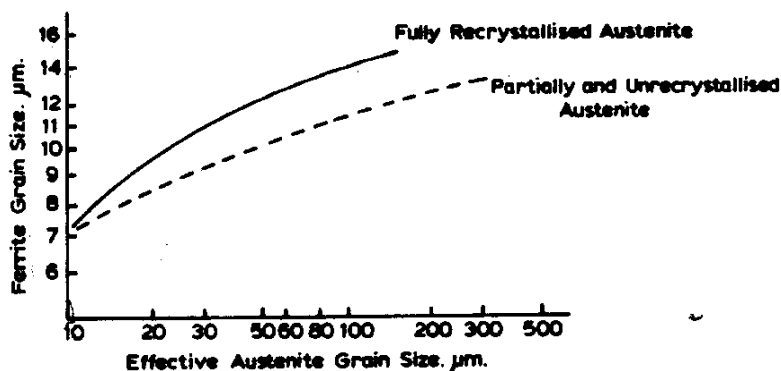

Fig. (25) Effect of state of austenite recrystallization on the relationship between the austenite grain size and the transformed ferrite grain size[61]

As shown in Fig (25), the ferrite grain size can almost equal the austenite grain size if the latter is very fine, but for large austenite grain sizes the ferrite grain size may be less than one tenth of that of the austenite[61]. A useful method of refining the ferrite grain size for a given austenite grain size is to decrease the transformation temperature. This increases the ferrite nucleation rate and the effect may be achieved by alloying (the reason for the high manganese content in MA steels) or by increasing the cooling rate [61] .

The results of Kozasu et al. also emphasize the importance of retained strain in the austenite grains at the time of transformation in niobium treated steel. This has been associated with the development of deformation bands within the elongated austenite grains, which provide additional nucleation sites and result in considerably accelerated transformation kinetics as well as grain refinement, Similar effects of retained strain would be expected in C − Mn steels [4].
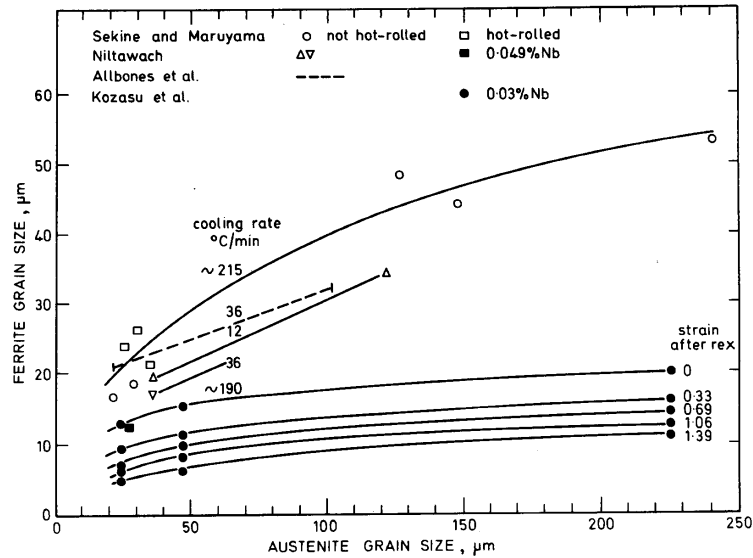
35

Figure (26) Dependence of ferrite grain size after transformation during cooling on austenite grain size and retained strain in austenite grains [4]

In addition to these variables, the cooling rate through transformation is important in determining ferrite grain size [4] . This is shown by the results of Niltawach in Fig (26), and observations by Allbones et al on an experimental low residual C − Mn steel of initial austenite grain sizes 20 − 100 μm closely fit a relationship

$$d_\alpha = 11.7 + 0.14\, d_\gamma + 37.7\, R^{-1/2} \tag{20}$$

When grain sizes are measured in μm and cooling rate R in C°/min (range studied 3.6 − 120 C°/min)

The linear relationship between ferrite and austenite grain sizes shown by equation (20) may not be the true from over a wider range of austenite grain sizes. At larger austenite grain sizes there are difficulties in defining the relationship because of the appearance of Widmanstatten ferrite [4] .

2.2.3.1 Influence of the first finishing pass temperature and strain

The influence of the total finishing strain on the austenite microstructure is shown in figure (27). As can be seen from this figure, increasing the total finishing strain makes the grain size more uniform by enabling dynamic recrystallization to pass more completely through the microstructure. In this way it also decreases the average austenite grain size [58] . The effect of the finishing strain on the ferrite microstructure in 0.06 Ti steel is displayed in figure (28). A gain it is clear that increasing the total finishing strain leads to a finer ferrite grain size [58] . The effect of first finishing pass temperature on the final grain size of 0.06 % Ti steel is illustrated in figure (29). As expected [58], lowering the first finishing pass temperature decreases the ferrite grain size. The ferrite grain sizes of the two steels, (0.056 % Nb and 0.06 %Ti) are plotted against inverse first finishing pass temperature in figure (30). From this diagram, it is evident that, for a given finishing temperature, steel (0.056 % Nb) has a finer ferrite grain size than (0.06 %Ti). This can be related to the stronger solute drag effect of Nb than Ti [58]. Furthermore, TiN and TiC start to precipitate at higher temperatures than NbC and NbN. Thus, the Nb precipitates should be finer and more effective with respect to retarding grain boundary movement than the Ti ones [58]. Also, the first finishing pass temperature influence the mean flow stress as shown in figure (31). This figure shows that an increase in the mean flow stress (MFS) leads to a decrease in the ferrite grain size i.e. (decrease in first finishing pass temperature).
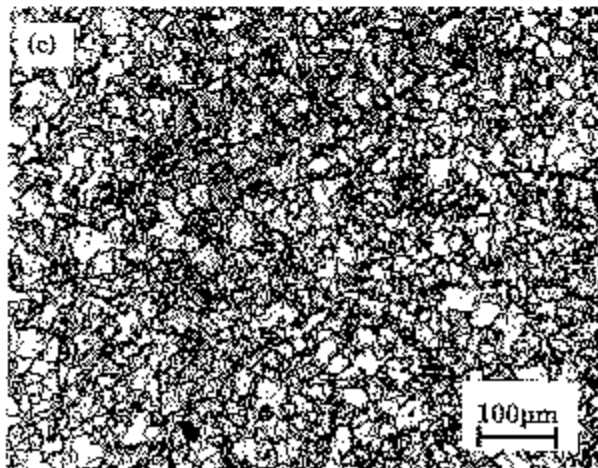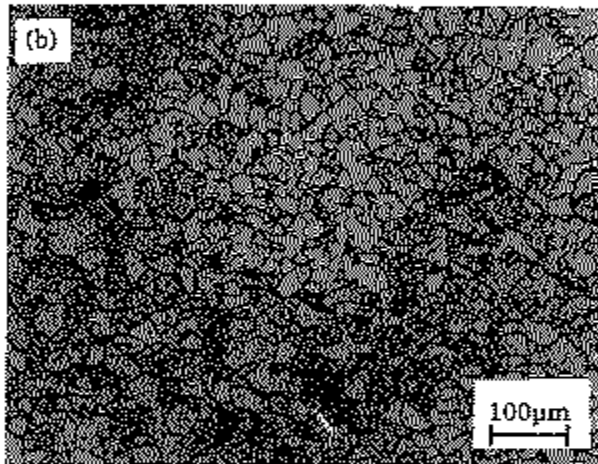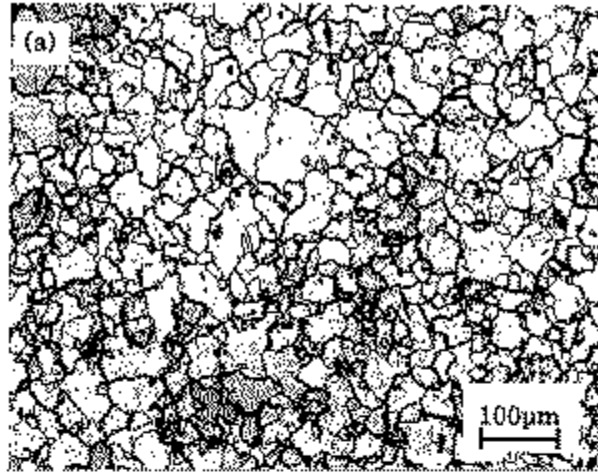
36

Fig. (27) Effect of amount of total finishing strain on the austenite grain size of 0.06% Ti steel (first finishing pass temp. = 990 C°) (a) ε =2.1 (b) ε= 2.6 (c) ε= 3.2 [58]
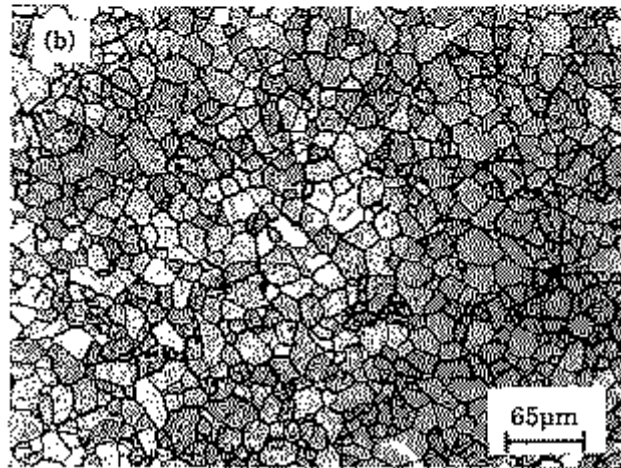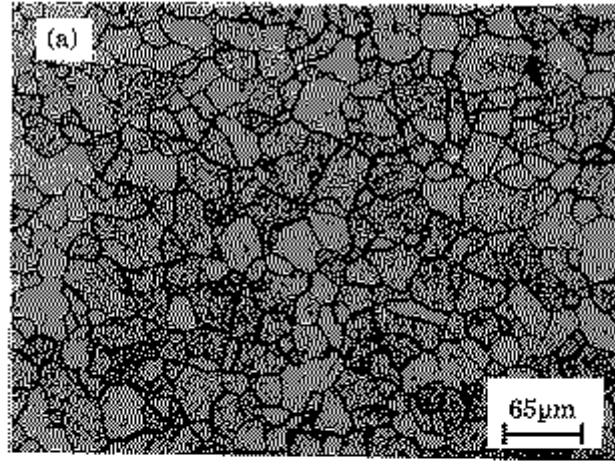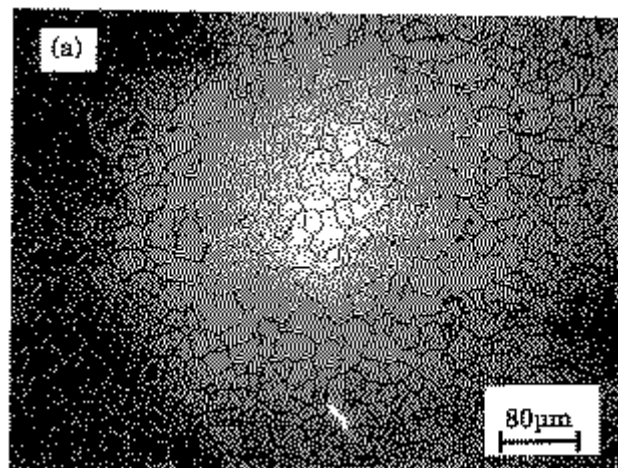
Fig. (28) Effect of total finishing strain on the ferrite grain size of 0.06 %Ti steel (first Finishing pass temp. =960 C°) . Cooling rate of $\cong$ 5 C°∕s (a) ε=2.1 (b) ε=3.2 [58].
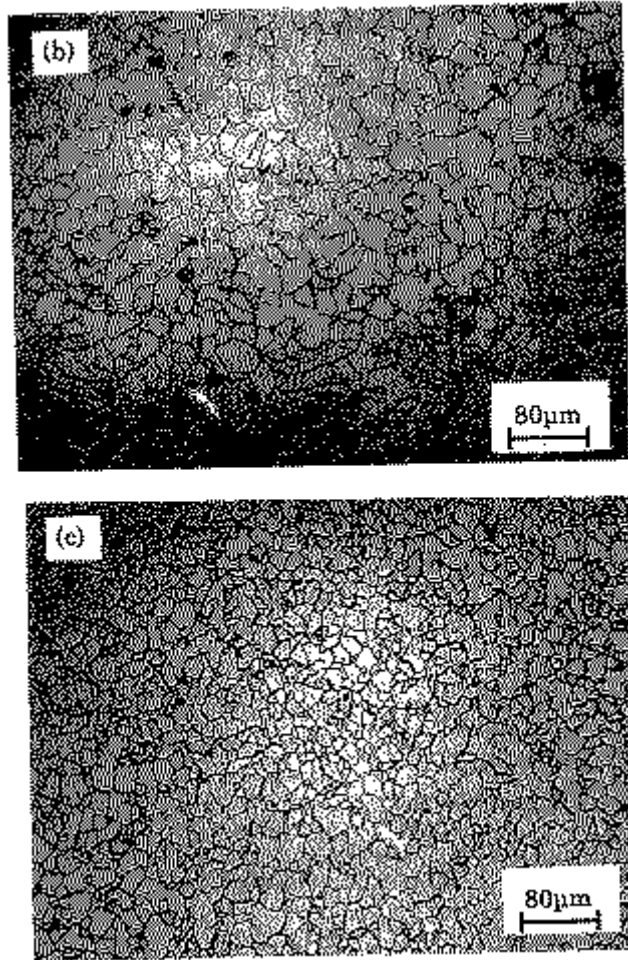
Fig. (29) Dependence of ferrite grain size of 0.06%Ti steel ($\varepsilon = 3.2$) on first Finishing pass temperature (f1). a) f1 =990 C° b) f1 =970C°,c)f1=930C°[58] .
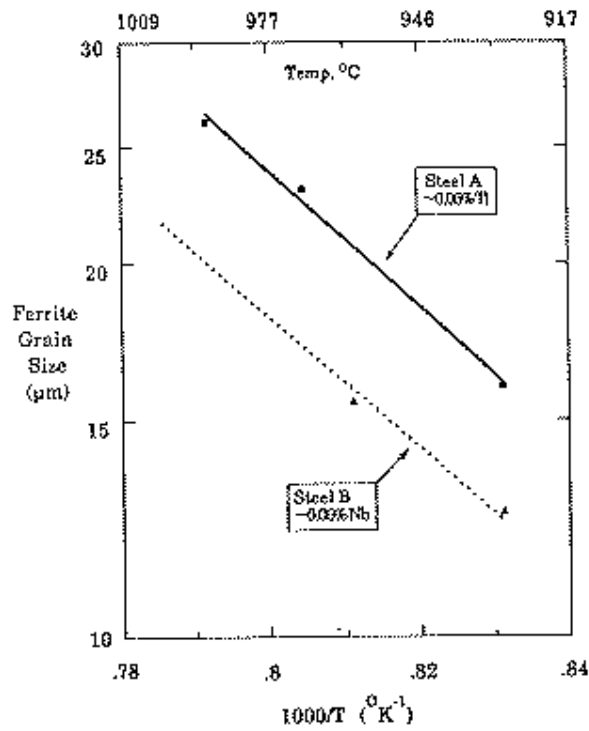

Fig. (30) Influence of first finishing pass temperature on ferrite grain size [58].
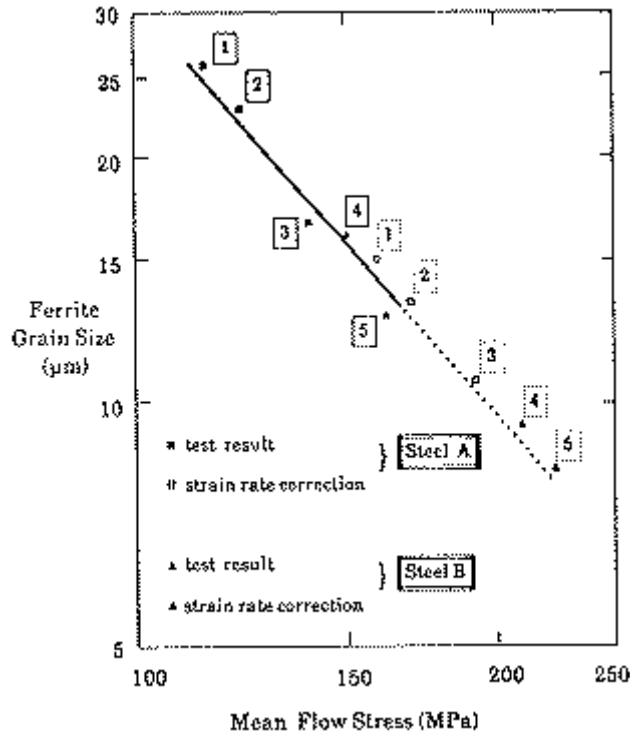
Fig. (31) Relationship between the average flow stress of the last four finishing passes and the ferrite grain size [58] .

2.2.3.2 The effect of cooling rate

In practice the rate at which a steel cools will however determine the actual temperature at which precipitates and transformation occur. The higher the cooling rate the lower the temperature at which the precipitates form. The rate of cooling can in fact determine whether a precipitate forms in austenite or ferrite [33]. Each steel has an optimum cooling rate which produces a maximum precipitation strengthening (σ_{ph} max) as shown in figure (32) i.e. The cooling rate also affects the intensity of precipitation – strengthening by altering the transformation temperature, so if steel slowly cooled, give rise to high transformation temperatures, coarse ferrite grains and poor yield strength and impact properties [43,65] The cooling rate after hot–working, especially between 800 and 600 C°(Ar_3–Ar_1), profoundly affected the mechanical properties of the steel because microstructure and also precipitation strengthening effects change with cooling rate [70] .
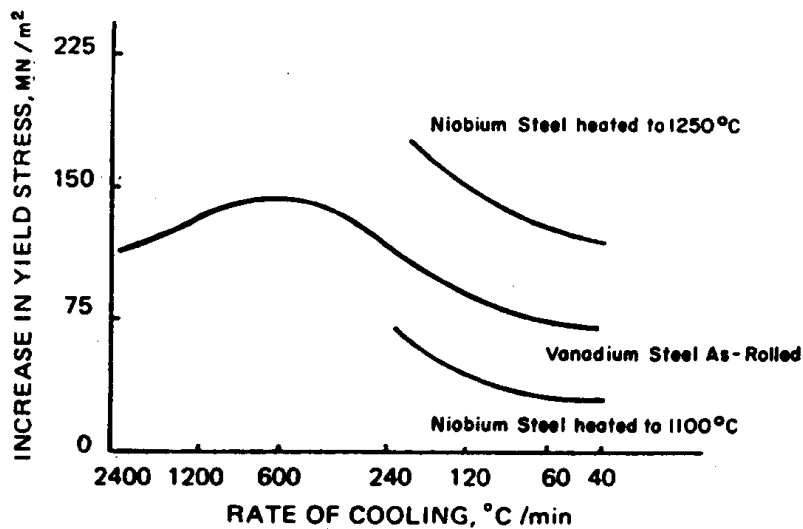

Fig (32) Effect of rate of cooling on the strengthening due to precipitated carbide in niobium and vanadium steels [43].

2.2.4 Determination of recrystallized fraction

2.2.4.1 Fractional softening test

A wide variety of techniques has been used to study the precipitation kinetics, including electrical resistivity, chemical analysis, hardness testing, x–ray diffraction, electron microscopy of thin foils and replica specimens, and flow curve analysis [28] . The kinetics of precipitation have also been determined from the analysis of the softening curves. where the precipitation start times were considered to be the point where a softening curve started to deviate from the simple sigmoidal behavior. This technique has been employed by Andrade et al and Akben et al to estimate the precipitation kinetics without showing any supporting metallographic evidence [28] .

The progress of static recrystallization with time can be directly obtained from metallographic examination. However, this procedure is tedious and time consuming, and in many cases even impossible to use due to low hardenability and / or the complexities in observing the quenched austenite, as is the case with some low and ultralow carbon microalloyed steels. Therefore, a mechanical testing procedure, commonly the double deformation technique, has been used for this purpose. In this method the amount of recrystallization can be indirectly estimated by the degree of softening measured from an interrupted mechanical test (compression, tension or torsion) [14,28,62] . The recrystallization and softening fraction can be usually described by an Avarmi type equation, from which the time for 50 pct of recrystallization ($t_{0.5}$) is determined. The effects of deformation conditions such as initial grain size, temperature, strain and strain rate are incorporated into the normalized parameter $t_{0.5}$. However, the lack of a standardized method to evaluate the softening ratio leads to a wide variation in the experimentally determined constants in $t_{0.5}$ [62] . A typical true stress − true strain curve obtained in this kind of experiment is shown in Figure (33). The degree of softening, X, after an interval of hot working was calculated from the expression :

$$X = \sigma_m - \sigma_r / \sigma_m - \sigma_0 \qquad (21)$$

Where σ_m is the flow stress immediately before unloading and σ_0 and σ_r are the initial flow stresses recorded during pre-straining and reloading, respectively (Figure 33) [63] .
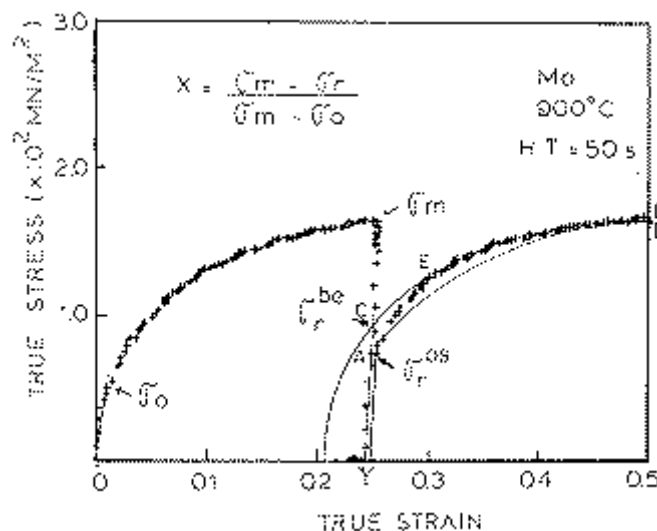
Fig (33) Determination of the reloading flow stress and the degree of softening by the Back Extrapolation (be) and offset (as) methods [63] .

The initial flow stress on reloading, σ_r was determined by two methods :   (1) the conventional offset method .in which σ_r is the flow stress corresponding to a plastic strain of 0.2 pct (σ^{os}_r Figure 33), and (2) the back extrapolation method, which defines σ_r as the stress corresponding to the intersection of the reloading line with the line obtained by superimposing the pre -straining curve on the reloading curve (σ_r^{be} – Figure 33) [63] The fractional softening curves for series of steels are shown in figure (34a) and (34b)

41

. It is evident that static recovery is the most rapid in the plain carbon steel at both 1000 C°and 900 C° . The addition of 0.115 % V, 0.30 % Mo or 0.035 % Nb retard this softening process. At 1000 C° , static recrystallization starts at approximately 0.27 seconds, and is delayed to 0.38, 1.0, and 1.9 seconds by the addition of V, Mo, and Nb, respectively. The recrystallization start time (Rs) are considered to be associated with 10 % fractional softening at this temperature. The recrystallization finish time, R_f (95 % softening) are 7, 9, 27 and 38 seconds, respectively, for these steels [64] .

Fig. 34(a) static recovery and recrystallization in the series of steels at 1000 C. The expected behavior for the Nb–V and Mo–Nb–V steels in the absence of precipitate is indicated by broken lines [64] .

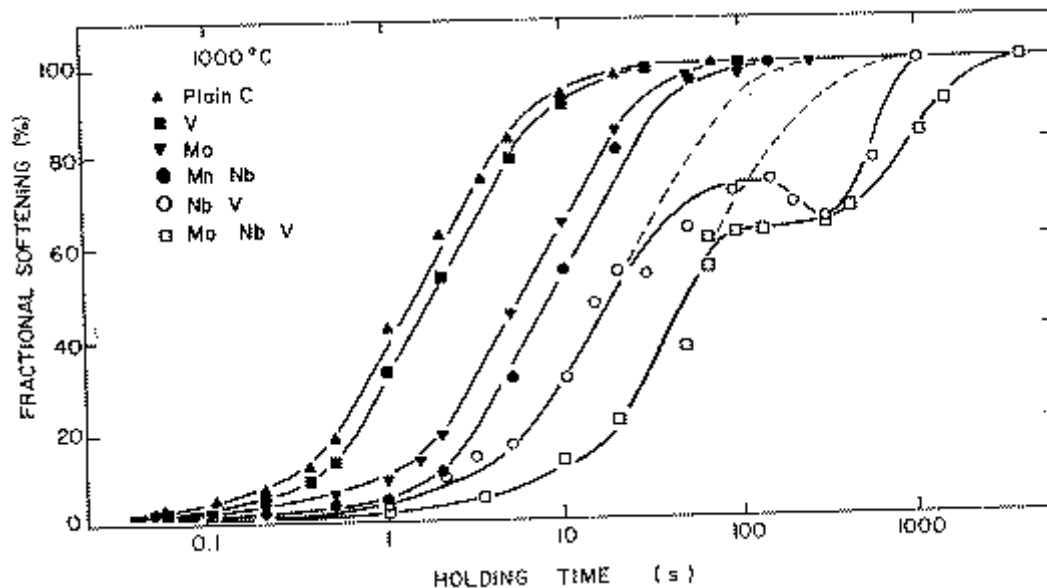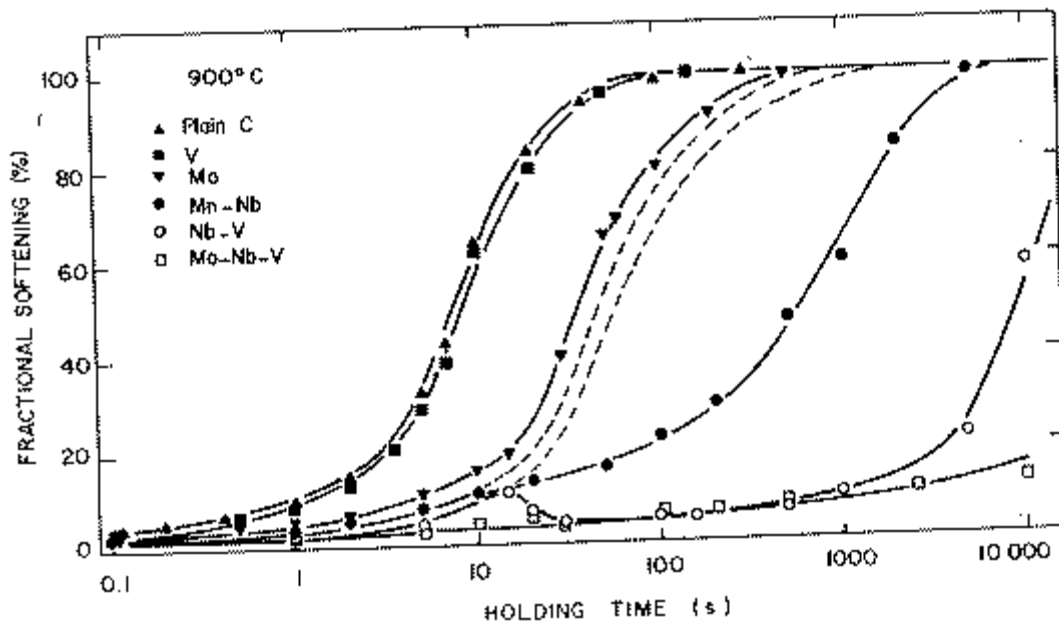
Fig. 34(b) static recovery and recrystallization in the series of steels at 900 C. The expected behavior for the Mn–Nb and Nb–V steel in the absence of precipitate is indicated by broken lines [64] .

2.2.4.2 Mechanical Metallography

The methods were employed to evaluate the degree of softening occurring after an interval of hot working:
(1) back extrapolation (be)
(2) offset methods (os)

(3) area method

OFFSET METHOD. This method is based on double−hit tests. The stress−strain dependence obtained in this test is shown in Figure (35).
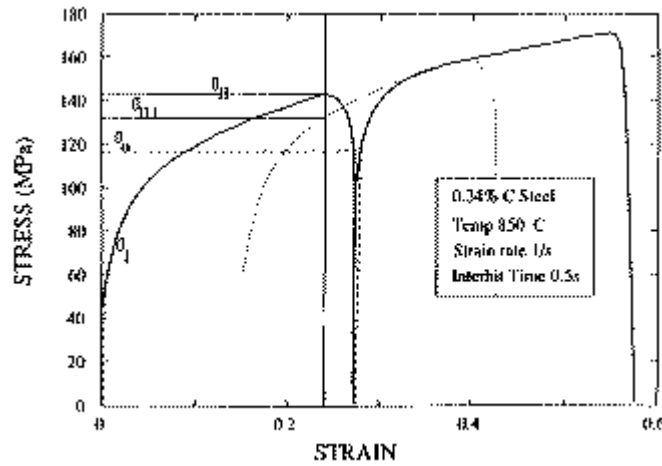

Figure (35) Flow curves obtained by a double−hit test on 0.34 pct carbon steel at 850 C°at an average strain rate of 1 S^{-1} and delay time of 1 S [59]

Strain −− constant = 0.3; Strain rate −−constant = 1.0 s^{-1}; Temperature−−constant = 850 °C; Inter pass time −− variable

The fractional softening (FS) given by the equation

$$FS = \sigma_{II} - \sigma_0 / \sigma_{II} - \sigma_I \tag{28}$$

Where σ_I = yield point of first deformation

σ_{II} = maximum stress in first deformation

σ_0 = yield point of second deformation, after inter pass time.

Values of, of σ_0 and σ_I are determined from flow curves, using offset method, they are determined using 0.2 % criterion in most of the cases [59] .
The advantages of this method are :
(1) easy to determine from the curve.
(2) very quick method
The disadvantages
(1) questionable accuracy.

BACK−EXTRAPOLATION METHOD. The method are also employed to evaluate degree of softening occurring after an interval of hot working. The back−extrapolation method employs the following definition for fractional softening (FS) :

$$FS = \sigma_{II} - \sigma_{III} / \sigma_{II} - \sigma_I \tag{29}$$

Where σ_{III} is defined as the stress corresponding to the intersection of the vertical line with the prestaining curve after it has been superimposed on the reloading curve [15] .

The disadvantages of this method its demand high experience for evaluate the fractional softening.

AREA METHOD. In this method the fractional softening is evaluated based upon the calculated area beneath the flow curves. These techniques are applicable when a distinct difference between elastic and plastic behavior is observed [11] .

$$FS = (A_3 - A_2) / (A_3 - A_1) \tag{30}$$

43

Where A_1 is the area under the flow curve during first straining. A_2 is the area during restraining after some holding time. and A_3 is the area during restraining after an infinitely small holding time as shown in Figure (36) [28] .
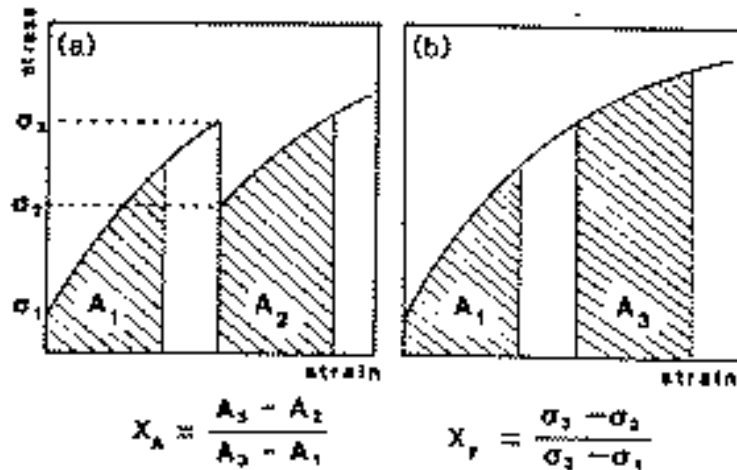

$$X_A = \frac{A_3 - A_2}{A_3 - A_1} \qquad X_r = \frac{\sigma_3 - \sigma_2}{\sigma_3 - \sigma_1}$$

Figure (36) Flow curves of interrupted compression test (A_1, A_2 and A_3 represent the area under the flow curve) (a) After some delay time (b) After infinitely small holding time [28] .

Advantage

The use of the softening parameter based on the area under the flow curve can eliminate problems arising from the use of the softening parameter based solely on the yield strength i.e. this test method is independent of measurement of yield strength for these reason (its more precise measurement) because the measurement of yield strength is extremely difficult at high temperature.

2.2.5 Strengthening in MA steels

The strengthening mechanisms applied in HSLA steels include : –
 Grain refinement;
 Precipitation;
 Dislocation substructure;
 Solid solution strengthening;
 Strain aging.

Grain refinement is the preferred mode of strengthening in ferrite – pearlite HSLA steels because it also improves toughness.

The ferrite grain refinement in these steel is accomplished through restricting the grow of austenite grains during hot rolling and ∕ or by inhibiting the recrystallization of austenite grain during hot rolling so that the $\gamma \rightarrow \alpha$ transformation occurs in uncrystallized austenite .The alloying such as Nb, V, Ti, Al, or Zr (microalloying) with small amounts, generally below 0.10 to 0.15 %, of strong carbide and nitride forming provides dispersion strengthening and helps to produce a fine grain size. In most instances, all Nb, C, and N are in solution at the start of the hot rolling of austenite, but precipitation occurs during the rolling as the temperature of the steel drops. The precipitate particles hinder growth of austenite grains, and at still lower temperatures the particles inhibit recrystallization of the deformed austenite grains [66].

44

As indicated in Fig. 37, the V– carbide has higher solubility in austenite than Ti – carbide and Nb – carbide, so Nb – carbide is most stable at high temperature than other and does not dissolve in austenite, so it will produce more fine ferrite grain than the other (Ti, V).

The yield – strength dependence on grain size is shown in Fig. 38. It is seen that the curve obtained is an extension of that for the plain carbon steel. The effect of the Nb addition is the formation of Nb (CN) at the austenitizing temperature, which retard the growth of the austenite grains much more than without the Nb. If, the Nb – containing steel is austenitized at a higher temperature (for instance, 1250 C°) some of the carbonitrides go into solution in the austenite, and there is less precipitate present to inhibit grain growth. However, the yield strength is considerably higher than for the plain – carbon steel due to the precipitation hardening of the ferrite during cooling [66] .
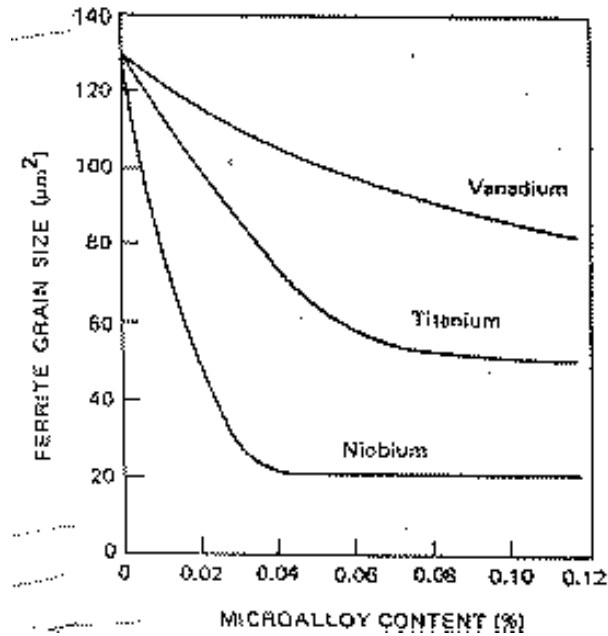

Fig. (37) Effect of microalloying content (Nb, V or Ti) on the ferrite grain size of as hot rolled low – carbon steel strip [66].
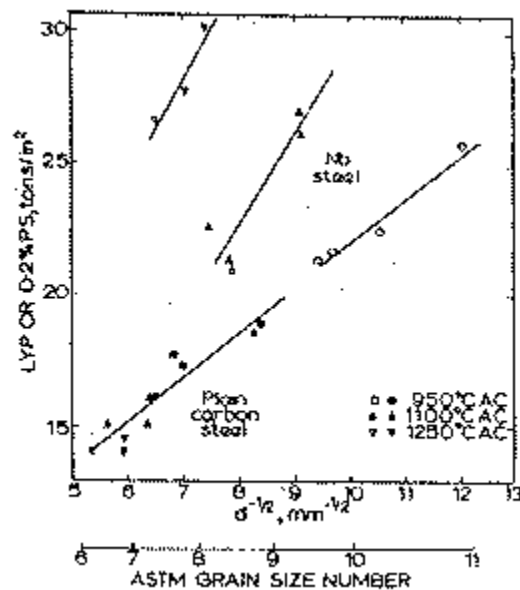

Fig. (38) Effect of austenitizing temperature on the strength – grain size relationship on Nb–Containing steel [66]

45

The yield strength is expressed by the Hall $-$ Petch relation : $-$

$$\sigma_y = \sigma_0 + K_y d^{-1/2} = (\sigma_{LH} + \sigma_{Sh} + \sigma_{dh} + \sigma_{ph} + \sigma_{th}) + K_y d^{-1/2} \qquad (22)$$

where $\quad \sigma_{Lh}$ = intrinsic lattice hardening,

$\quad \sigma_{sh}$ = solid solution hardening,

$\quad \sigma_{dh}$ = dislocation hardening,

$\quad \sigma_{ph}$ = precipitation hardening,

$\quad \sigma_{th}$ = texture hardening and

$K_y d^{-1/2}$ = hardening due to grain refinement.

Considering only the increase in yield stress ($\Delta \sigma_y$) caused by third $-$ stage deformation (below Ar₃) i.e below the austenite to ferrite transformation temperature, then this equation can be changed into :

$$\Delta \sigma_y = \Delta\sigma_{dh} + \Delta\sigma_{ph} + \Delta\sigma_{th} + \Delta(K_y d^{-1/2}) \qquad (23)$$

because the increments, σ_{1h} and σ_{sh} are independent of deformation [67] .

2.2.5.1 Dislocation hardening, $\Delta\sigma_{dh}$

When deformation is completed in the austenite region, the dislocation density in ferrite grains is relatively low. When deformation is extended to the austenite $-$ ferrite two $-$ phase region, however, the dislocation density in deformed $-$ ferrite grains is fairly high i.e. ρ dependence on finish rolling temperature (FRT) as shown in figure 39 [1,67] . The contribution to strength from dislocations was evaluated from the standard relationship [1] :

$$\sigma_{dh} = \alpha G b \sqrt{\rho} \qquad (24)$$

$$= 14.4 \times 10^{-4} \sqrt{\rho}$$

where α is a numerical factor dependent on crystal structure, G the shear modulus, b the Burgers vector, and ρ the dislocation density (lines$/$cm^2)

In general, decreasing the transformation temperature by either alloying or increasing the cooling rate, both refines the grain and increases the dislocation density. This increased dislocation density increases the yield stress [43] .
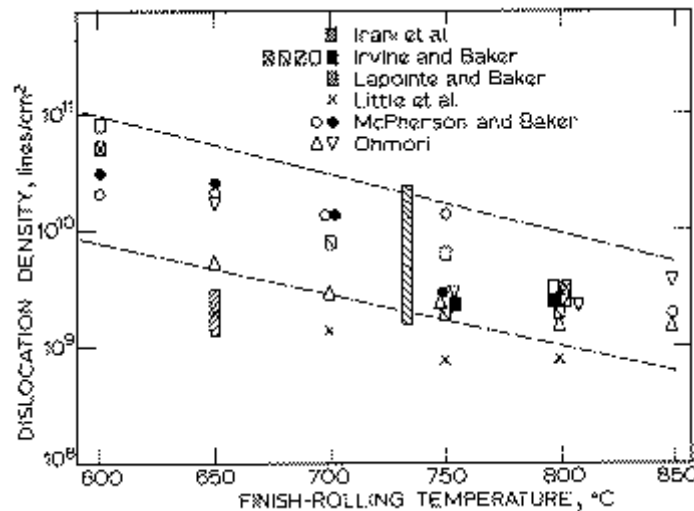

Fig. (39) Variation of dislocation density with finish$-$rolling temperature for microalloyed and low$-$carbon steels [1] .

2.2.5.2 Precipitation hardening, $\Delta\sigma_{ph}$:

The increase in yield stress ($\Delta\sigma_y$) in columbium steel results from deformation and precipitation hardening due to columbium and vanadium, while $\Delta\sigma_y$ in plain−carbon steel results from deformation only, the difference in $\Delta\sigma_y$ between the two steels is due to the precipitation hardening [67] .The value of ($\Delta\sigma_{ph}$) for any given rolling condition increased with increasing reheating temperature up to the stoichiometric Nb : C_{Eq} ratio. The increase in ($\Delta\sigma_{ph}$) with increasing reheating temperature was due to the increaserd solubility of Nb (CN) [57] . The value σ_{ph} was taken from the work of Irvine [1]

$$\sigma_{ph}(N/mm^2) = 0.3\ G\ b\ \sqrt{f}/\ \xi * \ln(\ \xi/2b) \qquad (25)$$

where f is the volume fraction calculated from composition, assuming a stoichiometric composition, and ξ is the mean planar −intercept diameter of the precipitate, in mm (mean diameter of second phase particles) i.e. $\xi = 2\ \sqrt{f^*}/\pi\ N$, where ($f^*$ is fraction of surface area of particles, N is the number of particles per unit area)

2.2.5.3 Texture hardening, $\Delta\sigma_{th}$:

Since 10 % deformation produced a weak texture ($\Delta\sigma_{dh}$ and $\Delta\sigma_{th}$ are negligibly small) The ferrite −grain structure produced by 10 % reduction was quite similar to the structure with no deformation observations by optical microscope at 10 % reduction is the same as that of no deformation [67] . Since there is no decrease in grain size (very little change), the increase in the yield stress must be interpreted in terms of structural features other than grain size. When deformed 30 % or more, the microstructure consisted of polygonal grains and elongated ”cold−worked ” grains, the volume fraction of which increased steadily with increasing amounts of deformation. Below 30 % reduction, the intensity of the (200) reflection was weak, resulting in the small number of separations and high absorbed energy. Over 30 % ,the intensity of the (200) reflection became strong, resulting in the occurrence of numerous separations which, in turn, caused a decrease in the transition temperature and the absorbed energy [67] .

2.2.5.4 Grain refinement, $\Delta(K_y\ d^{-1/2})$:

The structure associated with no deformation consists of solely polygonal grains with low density of dislocations. After 10 % deformation, the microstructure is duplex, consisting of polygonal grains interspersed with patches of substructure. The volume fraction of substructure increases with an increase in deformation [57,67] .The effects of increasing the rolling reduction were complex and depended upon the reheating temperature i.e. volume fraction of substructure influenced by reheating temperature [57] .

Refinement of the polygonal grain size increases the yield stress and yet decreases the impact transition temperature,[43] .

With increasing amounts of deformation, ferrite grains are elongated, texture is more strongly developed, and dislocation density becomes highs. All of these factors contribute to the increase in strength. These effects are minor compared with that of substructure, the importance of which increases gradually with deformation [67] The yield strength is increased if a small ferrite grain size ($< 7\ \mu m$) can be retained after cooling to room temperature. Austenite in the form of a fine polygonal grain ($< 20\ \mu m$) or a deformed elongated structure can provide the necessary small ferrite grain size after transformation [1] .

The microalloyed steels are strengthened by a combination of grain refinement, sub grain formation, and precipitation hardening. The amount of strengthening from columbium carbonitride precipitates depends upon the amount of columbium added, finishing rolling temperatures, and amount of deformation [10] .

The strength and transition temperature obtained during the second stage are determined solely by the ferrite–grain size. Since there is no dislocation and texture hardening ($\sigma_{dh} = 0$, $\sigma_{th} = 0$), equation (22) is reduced to :

$$\sigma_y = \sigma_{Lh} + \sigma_{sh} = \sigma_{ph} + K_y d^{-1/2} \tag{26}$$

This indicates that yield stress is determined only by chemical composition (evidenced by solution and precipitation hardening) and grain size. Because of substructure hardening, the strength obtained during the third stage is expressed as :

$$\sigma_y = \sigma_{Lh} + \sigma_{sh} + \sigma_{ph} + K_y d^{-1/2} + \sigma_{substructure} \tag{27}$$

The composition of the steel with respect to the ratio Nb :C, Ti : C or V : C is also important. The maximum temperature–dependence of the solubility of the precipitate occurs at stoichiometric composition [38,39,43] so that, at this composition, the maximum amount of precipitate will be formed. In most structural steels, the ratio Nb : C, Ti :C or V : C is much lower than the stoichiometric ratio, and consequently increasing the metallic alloy addition will increase the strengthening due to precipitation [38,39,43] . Certain steels contain higher (V + N) addition to increase the grain refinement and give more precipitation strengthening resulting in excellent strength and impact properties. On the other hand, niobium markedly retards recrystallization and also the Nb (CN) particles inhibit grain growth, Fig (40) , Possible reasons for the effectiveness of niobium in retarding recrystallization are solute drag and precipitation of NbC on sub–boundaries thus preventing their migration during recrystallization .Also during rolling, some strain–induced precipitation of NbC occurs, which does not cause precipitation strengthening and yet decreases the amount of subsequent precipitation strengthening which can be achieved For a very fine ferrite grain size to be produced, it is essential to have a very fine austenite grain size prior to transformation [43] .
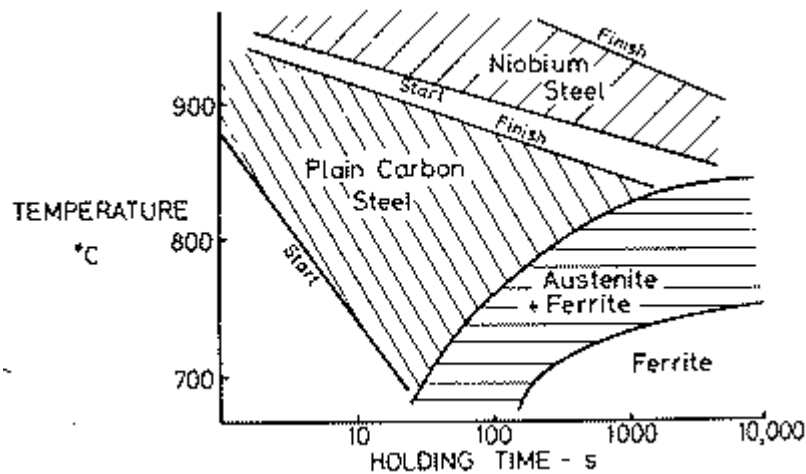
Fig 40 Effect of niobium on the recrystallization of austenite after a reduction of 50 % [43] .

2.2.6 Determination of the three critical temperatures for hot rolling of MA Steels

The three critical temperatures of hot rolling, i.e. the no recrystallization temperature, and the temperature associated with the start and end of the austenite to ferrite transformation (Tnr, Ar3 and Arl, respectively). According to the method of Boratto et al.[58], the critical temperatures for steel can be determined by plotting the mean flow stress (MFS) associated with each pass against inverse absolute temperature, as shown in figure (41) b.

48

Fig. (41) Dependence of mean flow stress on inverse absolute temperature for steel rolled according to the plate schedule [58] .
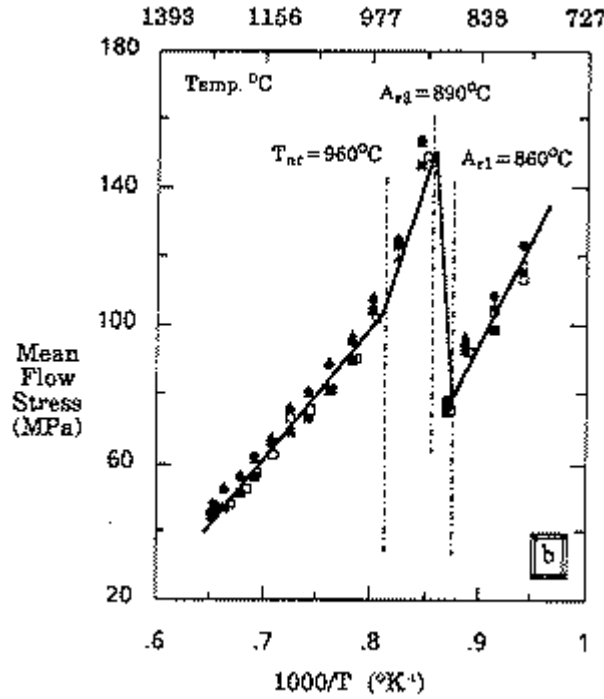
The mean flow stresses (MFS) were calculated from the equivalent stress−strain curves by numerical integration, i.e.

$$\sigma_{eq} = 1/(\varepsilon_b - \varepsilon_a) \int \sigma_{eq} d\varepsilon_{eq} \tag{31}$$

where σ_{eq} is the mean flow stress, σ_{eq} is the equivalent flow stress and $(\varepsilon_a - \varepsilon_b)$ is the equivalent strain of the pass of interest [68,69] . The dependence of the mean flow stresses on the inverse of the absolute temperatures is shown in figure (41). It can be seen that there are clear changes in the rate of increase of the mean flow stress with decreasing temperature at two temperatures (Tnr and Ar $_3$). The validity of the Tnr was further established by observing the austenite microstructure i.e at T > Tnr, the austenite is fully recrystallized, while a partially recrystallized structure is observed at T < Tnr [68]. For $\varepsilon < 0.26$, precipitation is initiated prior to recrystallization, shifting t $_{0.05\ x}$ and t $_{0.95x}$ to longer times, and in these case Tnr = 929 exp 0.0127 / ε , for $\varepsilon \geq 0.26$, in these case recrystallizations is initiated before precipitation, Tnr = 1050 − 314 ε [68] .

2.2.6.1 Prediction of precipitation srart time using the Dutta and Sellars Model

A quantitative model has been developed by Dutta and Sellars [68,70] to predict the strain induced precipitation of niobium during hot rolling and the interaction of this precipitation with the recrystallization behavior. This model is described by equation (32), (33) and (34) :

Time for 5 % precipitation :

$$.t_{0.05} = 3\times10^{-6} [Nb]^{-1} \varepsilon^{-1} Z^{-0.5}\times exp^{270000/R\,T} exp\,((2.5\times10^{10}/T^3(ln\,k_s)) \tag{32}$$

or
$$t_{0.05} = A\,\varepsilon^{-1} \tag{32'}$$

where
$$A = 3\times10^{-6} [Nb]^{-1} Z^{-0.5} \times exp^{270000/R\,T} exp\,((2.5\times10^{10}/T^3(ln\,k_s))$$

(supersaturation ratio) $K_S = (10^{-6770/T_{RH}} + 2.26)/(10^{-6770/T_{PASS}} +2.26)$.

Where T_{RH} and T_{pass} are the reheat and deformation temperature respectively.

49

Time for 5 % recrystallization :

$$.t_{0.05\,x} = 6.75 \times 10^{-20}\, d_0^{\,2}\, \varepsilon^{-4} \times \exp^{300000/R\,T} \exp\{(2.75 \times 10^5/T - 185)[Nb]\} \qquad (33)$$

Time for 95 % recrystallization :

$$.t_{0.95\,x} = 7.64 \times t_{0.05x} \qquad (34)$$

or

$$t_{0.95\,x} = B\, \varepsilon^{-4} \qquad (34\,')$$

where

$$B = 7.64 \times 6.75 \times 10^{-20}\, d_0^{\,2} \times \exp^{300000/R\,T} \exp\{(2.75 \times 10^5/T - 185)[Nb]\}$$
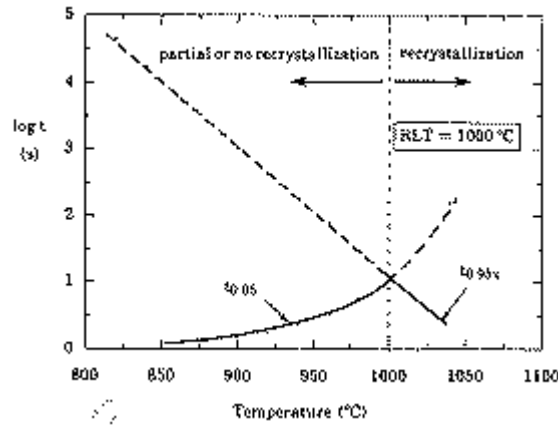

Fig. (42) Interaction of the completion of recrystallization ($t_{0.95\,x}$) and the start of strain induced precipitation ($t_{0.05}$), strain ε=0.2, strain rate =2 s^{-1} and d_0=40 μm [68].

In the above equations, d_0 is the original grain size in μm, and ε is the strain for values less than the critical value for the onset of dynamic recrystallization [68] . Figure (42) an example of the use of these equations to predict the Tnr. The two curves intersect at about 1000°C. Above this temperature full recrystallization occurs. Below 1000C°, 5 % precipitation occurs before 95 % recrystallization can take place. Thus, the RTL is taken as the temperature at which 5 % precipitation takes place before 95 % recrystallization occurs. This can also be taken as definition of the Tnr measured in these tests [68]

2.2.6.2 Effect of Strain Rate on the Tnr

From figure (43), it can be seen that pass stresses increase with increasing strain rate, which is usually rationalized as an increase in strain hardening, which also lead to Tnr increased with increasing strain rate i.e (for $\varepsilon < 0.3$), but for $\varepsilon \geq 0.3$, the Tnr decreased with increasing strain rate [68] . In general, the absence of strain−induced precipitation, increasing the strain rate increases the rate of recrystallization because of the increase in dislocation density i.e (decreases in sub grain size). In the range of temperatures where strain−induced precipitation is likely to occur, both recrystallization and precipitation are accelerated at higher strain rates. At relatively low strain rates, the effect of an increasing strain per pass is to promote precipitation, thereby increasing the Tnr. At relatively high strain rates, increasing strain promote recrystallization over precipitation, and the Tnr continuously decreases. However, the high strain rates of industrial processing will probably always lead to a decreasing Tnr, with increasing pass strains [68] .

Fig. (43) Dependence of the mean flow stress (MFS) on the inverse of the absolute pass temperature for high Nb (0.09 wt %), low C (0.04 wt %) grade steel, pass strain ε = 0.2 [68].

2.2.6.3 Effect of inter pass time on the mean flow stress and Tnr

From figure (44), it can be seen that the Tnr and MFS increases with increasing inter pass time either at small strain (ε= 0.1) or at large strain (ε=0.7). This may be due to an increasing precipitate volume fraction [68] .
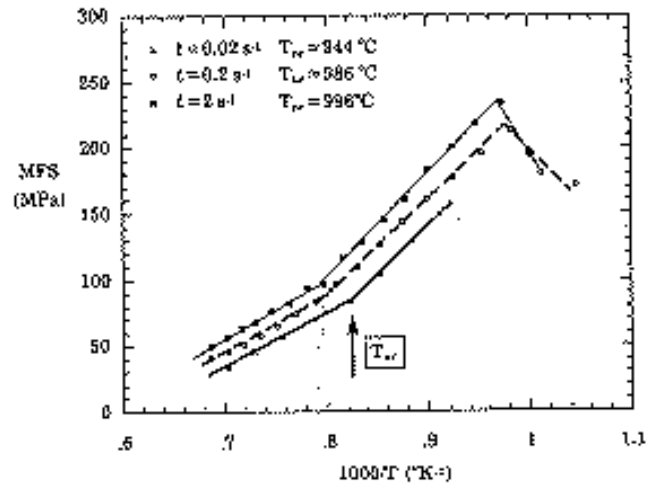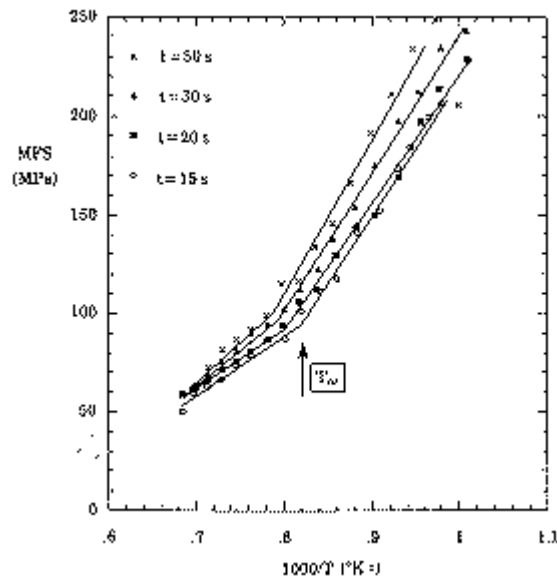

Fig. (44) Dependence of mean flow stress on the inverse of the absolute pass temperature for high Nb (0.09 wt %) , low C (0.04 wt. %) steel, pass strain ε = 0.3, strain rate = 2 s^{-1} [68].

3. EXPERIMENTAL PART

3.1 Material
The steel used in this work was low carbon Nb/Ti microalloyed steel. Chemical composition of tested steel is given in table (5)

Table (5) Chemical composition of steel investigated (in mass %)

C	Mn	Si	P	S	Al	Nb	Ti	N
0.074	1.15	0.21	0.024	0.014	0.068	0.035	0.016	0.009

Steel was produced and continuously casted on vertical continuous caster in Steelworks Sartid (USS). As-casted slabs were hot-rolled in Hot Strip Mill. Specimens were taken from pre-rolled strip (thickness approx. 30mm) in direction parallel to rolling direction. Before machining the specimens, steel was annealed at 1050°C for three hours in protective atmosphere, with aim to remove texture and for homogenization.

Thermo-mechanical treatment
During torsion testing machine and specimen are in contacts. Specimen is fixed on one side, while, other end is connected with a motor which rotates and deforms the specimen. Variables in test are temperature, deformation (angle of twist), stress (turning torque), strain rate, and time. Tests are conducted with constant strain rate, during test, twist, torque and temperature can be measured. Shear stress can be evaluated from torque using Fields & Backofen [72,73] method, equation (35)

$$\tau = \frac{Mu}{2 \cdot \pi \cdot R^3} \cdot (3 + m + n') \cdot 1000 (MPa) \tag{35}$$

where:
τ - shear stress, MPa
Mu – Torqu, Nm
R – radii of the gauge length of the specimen, mm
m – strain rate sensitivity
n′ - stran hardening exponent in torsion testing

Both m and n' are not constants, but their values vary during the test. For example, strain hardening exponent can decrease during the test, and even become lower than zero (cases of dynamic recrystallization or austenite-ferrite transformation). Values of 0.17 and 0.13 for m and n' respectively gives the smallest scatter and were used in this work.

Shear deformation depends on distance from the center of the specimen, and can be calculated using following equation:

$$\gamma = \frac{R \cdot \theta}{Lo} \tag{36}$$

where:
γ - shear deformation
θ - twist angle, rad
R – radii of the gauge length of the specimen, mm
Lo - length of the gauge length of the specimen, mm

To calculate shear stress and strain to stress and strain equivalent to those obtained in tension test, Von Misses' criterions of yielding are used [72,73], equations 37 and 38, respectively.

$$\sigma_{eq} = \tau \cdot \sqrt{3} \tag{37}$$

where:

σ_{eq} – equivalent stress, MPa

τ - shear stress, MPa

$$\varepsilon_{eq} = \frac{\gamma}{\sqrt{3}} \tag{38}$$

where:

ε_{eq} – equivalent strain

γ - shear strain

3.2. High temperature torsion machine

Main purpose of high temperature torsion machine is simulation of hot deformation processes (both single-pass and multi-pass) on high temperatures. Main advantage of this machine in comparison to compression or tensile testing is the ease in obtaining strains that are present in hot rolling practice. Achievable strain in compression or tensile testing is limited to small extent due to appearance of buckling and necking, respectively. Scheme of hot temperature torsion machine is shown in figure(45).

Machine is equiped with low-inertia motor with additional gear, enabling rotation from 1 (one) to 1500 (onethousandfivehundred) turns in minute. Motor is controlled by hronometer, which controlls the time for motor rotation. Induction heater, cooled with water, is connected with optical pyrometer and thermoregulator. Both of latter regulate the power of the heater. For temperature measurement optical pyrometer measures the emmisivity of the specimen surface. Reliable measurements are within temperature range 750-1300°C. To provide good surface quality, specimens are treated in protective atmosphere (usually argon or nitrogen), because emisivity can be wrong if oxidation occurs. If here is a need for quenching the sample, water or some other quenchant can be introduced through glass tube.

1. Specimen
2. Quartz glass tube
3. Induction heater
4. Optical pyrometer
5. Tube for quenching medium
6. Tube for protective gas
7. Dynamometer
8. Data acquisition system
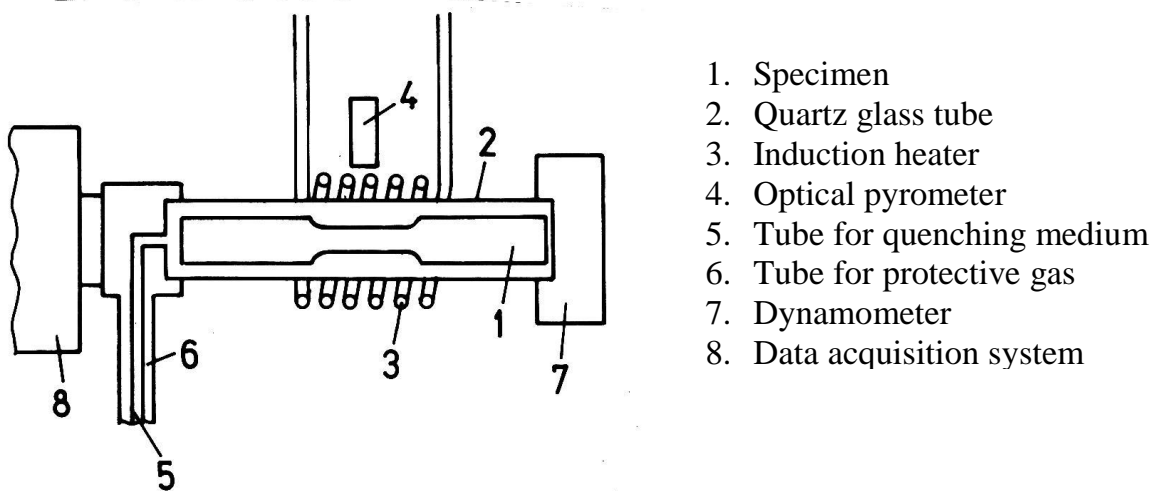
Fig (45) - High temperature torsion machine

For measuring the torque, a dynamometer with range 0-7Nm is used. Measured values are recorded both on photo-paper and in data acquisition system. Data acquisition system provides complete communication with torsion tester goes via PC computer. Resolution of automatic measurements system is 60 measurements for on turn, i.e, on each 6°. Measured values are automatically recorded on PC.

Strain rate in compact specimen with circle in cross-section depends on specimen's geometry and radial speed, equation 39.

53

$$\acute{\varepsilon} = \frac{R \cdot \dot{\Theta}}{Lo} \cdot \frac{1}{\sqrt{3}}, s^{-1} \qquad (39)$$

where:

$\acute{\varepsilon}$ – strain rate, s^{-1}

R – radii of gauge length of specimen, mm

L_0 – gauge length of specimen, mm

Θ – radial speed, rad/s

Radial speed is defined using number of revolutions per minute, using equation 40

$$\dot{\Theta} = \frac{2 \cdot \pi \cdot U}{60}, s^{-1} \qquad (40)$$

where:

Θ – radial speed, rad/s

U – number of revolutions per minute, min^{-1}

Hence, equation 5 can be rewrited:

$$\acute{\varepsilon} = \frac{2 \cdot \pi \cdot U \cdot R}{60 \cdot \sqrt{3} \cdot Lo}, s^{-1} \qquad (41)$$

Strain in torsion tests is defined via equations 42 and 43. The total angle of twist θ is calculated using the total number of turns of the specimen, N.

$$\theta = \frac{2 \cdot \pi \cdot N}{60}, rad \qquad (42)$$

where:

θ the total angle of twist, rad

N – total numbe`r of turns of specimen

$$\varepsilon = \frac{2 \cdot \pi \cdot R}{\sqrt{3} \cdot Lo} \cdot N \qquad (43)$$

where:

ε = equivalent strain

N – total number of turns

R – radii of gauge length of specimen, mm

L_0 – gauge length of specimen, mm

Before conducting the testing, following parameters must be defined, both for single and multipass tests:

- Heating regime up to reheating temperature, time on reheating temperature and cooling time up to deformation temperature
- Temperature, strain, strain rate for each pass
- Total number of passes and each interval time
- Definition of listed parameters is directly via PC, by answering the question in the program

Thermomechanical processing parameters are defined by forming an array of data for each pass.

- X   number of pass for which parameters are defined
- XX   time between two passes (before next), ms
- XXX   number of measurements of torque

- XXXX   number of rotations of the motor, rev ∕ min
- XXXXX   time for rotation of motor, ms
- XXXXXX   test temperature, °C

An example is given. It is a second pass on 1050°C, which will be conducted 5 seconds after previous pass, strain rate is 1.5 s^{-1}, strain 0.35. Gauge length is 50mm, and radii of the gauge length is 3mm. The array with data is given in next paragraph, and complete calculations in appendix to this Chapter.

2.00
5000
106
413.5
293
1050

In the first row number 2.00 indicates that it is a second pass in the multiple test.

In the second row number 5000 indicates that the interpass time that is preceding this pass is 5 seconds (5000 ms).

In the third row number 106 is related to number of measurements that have to be done by data acquisition system, in accordanceto equation 43. For strain of 0.35, total number of turns is 1.606. Therefore, number of measurements is 1.606·60=96. By experience, this number is always increased up to 10%, to take into account possible scatter. As a conclusion, total number of 106 is defined.

In the fourth row, number 413.5 indicates number of turns per minute for motor. For this specimen, following equation (41), 413.5 revolutions per minute will provide strain rate $\acute{\varepsilon}$=1.5 s^{-1}.

In the fifth row number 293 indicates the total time for deformation, in miliseconds.This time is defined by the ratio between strain (ε=0.35) and strain rate ($\acute{\varepsilon}$=1.5s^{-1}), which is 233miliseconds in this case. Anyway, experience has showed that this time must be increased for inertia time of motor which is in range 20-100ms, dependimg on the number of revolutions per minute. For this particular case, time of 60ms, based on experience of stuff, is choosen. Therefore, the total time is 233+60=293 ms

In the last row, number 1050 indicates the pass temperature of 1050°C.

Finally, if a continuous test should be carried on, data array (matrice) content only one column, otherwise, if multipass test is in case, one column for each pass is required.

Also, before testing, with aim to provide reliability of temperature measerement, optical pyrometer must be calibrated

3.3. Test specimen

Figure (46) shows specimens used in testing on high temperature torsion machine. Diameter and gauge length of specimen are 6 and 50mm respectively. Advantage of this method can be seen from equation 43, which is showing that strain and strain rate depend on gauge length, i.e. for higher strain rates gauge length can be reduced up to 5 mm!
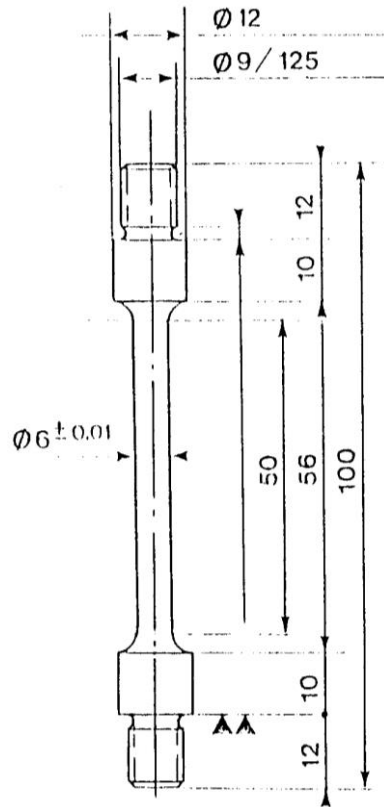
Figure (46). Specimen for torsion testing[74] .

3.4. Two-hit isothermal tests

To obtain data necessary for determination of static recrystallization kinetics a set of two-hit isothermal at different temperatures was performed. In previous work [83] , Tnr of 937°C was obtained, so that temperature range in which Nb is still in solid solution is over this temperature. Scheme of isothermal testing is shown in figure (47).
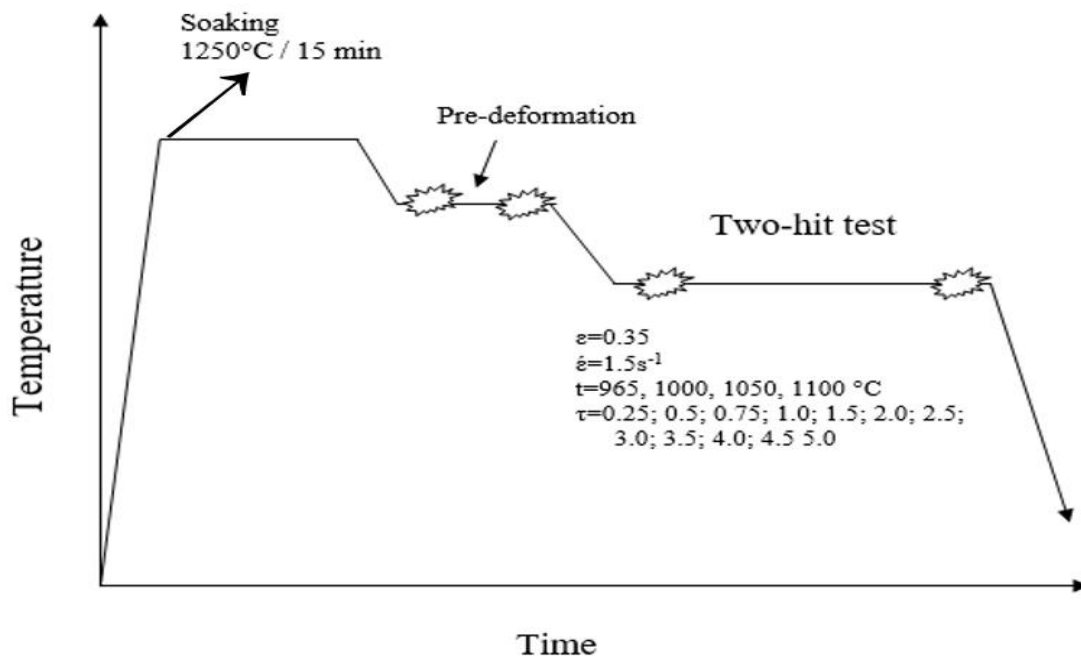

Figure (47) Scheme of isothermal testing

Table (6). Two-hit sothermal test experimental details

Temperature, °C	965, 1000, 1050, 1100
Strain per pass	0.35
Strain rate, s^{-1}	1.5
Interpass time,s	0.5; 0.75; 1.0; 1.5; 2.0; 2.5; 3.0; 3.5; 4.0; 4.5; 5.0

Specimen was mounted to only one side (close to motor), otherwise, thermal treatment before first pass would buckle the specimen. Next step is mounting the glass tube and introduction of argon as protective atmosphere. At this moment, program for testing can be started. First step is definition of input data array, described in previous section. As a next part of program, heating time to reheating temperature in minutes, reheating temperature in °C, reheating time in minutes and cooling time to pre-deformation stage in minutes must be typed directly. After confirmation of all data, thermal part is started and specimem starts to be heated.

Heating time to reheating temperature comes from experience and usually is 5-7 minutes. Reheating has the aim to dissolve all NB containing particles and provide presence of all niobium in solid solution. This temperature was established after solubility product defined by Irvine et al [75] for NbCN in steel. Once when this temperature is attained, sound signal wil be turned on. After defined reheating time, system will cool down the specimen to first pass in pre-deformation regime. When temperature of pre-deformation is achieved, sound could be heard. At this moment, specimen must be mounted into second end (dynamometer side). After this mounting, specimen is prepared for testing. After the end of deformation part, specimen can be quenched by water or helium, if necessary. At that moment, computer will close the acquired data and test is finished. As a final result, set of measured values for torque is obtained.

In all tests, it is usual to perform pre-deformation stage, with aim to refine grain size that may increase during reheating and to provide simillar grain size in all tests, i.e. to eliminate possible influence of grain size. Based on literature data, two deformations followed by two static recrystallizations are sufficient to refine grains.

All data relevant for thermal cycle and pre-deformation are given in tables (7) and (8)

Table (7)Heating, reheating and cooling parameters, up to pre-deformation stage

Heating time to reheating temperature, min	5
Reheating temperature, °C	1250
Reheating time, min	15
Cooling time to pre-deformation stage, min	2

Table (8). Pre-deformation parameters

Number of passes	2
Temperature, °C	1100
Strain per pass	0.3
Strain rate, s^{-1}	0.15
Interpass time,s	10

3.5 Correlation between programmed and obtained torsion schedule

Before testing, a calibration of optical pyrometer was performed, using Pt-PtRh6 thermocouple. Obtained calibration diagram is shown n figure (48).
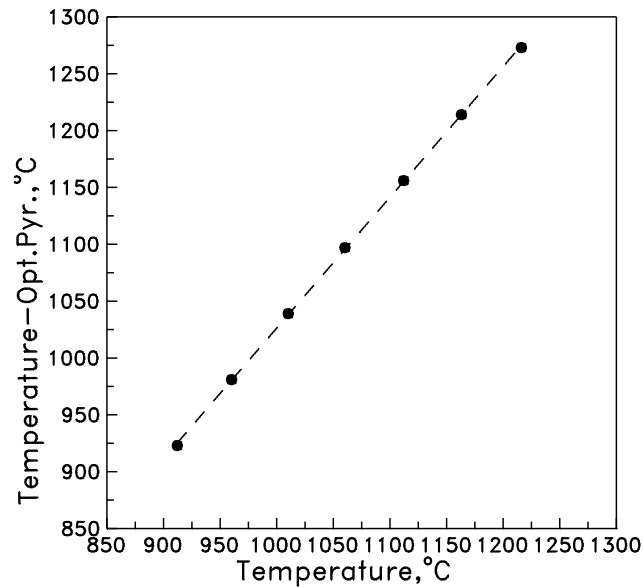

Fig. (48) Calibration diagram

Correlation between real temperature and value registered by optical pyrometer can be described with following equation;

$$T(C°) = (T_{pyr} + 123.36) / 1.1498 \qquad (44)$$

Where :

T – real temperature, °C,

Tpyr – temperature recorded on pyrometer, °C

General impression on performed tests in comparison with programmed one:

– In some test, abnormal heating had occurred, nearly to melting point. It was clear that in all those cases optical pyrometer had recorded lower temperature of the specimen than real one. The reason was that surface was oxidized. This had, in turn, implied the increase in power of heating system, leading to overheating. Oxidation could have origin from humidity in protective gas, unproper cleaning of sample (residual machining oil) or even some darkness on glass tube;

– Temperature of first pass was always accurate, except in cases when surface was oxidized;

– Obtained strain per pass was in order 0.34-0.36, what is considered to be acceptable;

– Inter pass times were accurate.

APPENDIX TO EXPERIMENTAL PART
Input Data for experiment.
Number of deformation increments (C), the one increment is equal 6 °

(i)   Total angle of twist (θ) :

$$\theta = 2 \pi N / 60 \text{ , rad, where N is the total number of rotations}$$

$$\varepsilon = (2 \pi R) / (\sqrt{3} L_0) * N$$

Where :

ε is the equivalent strain,

R is the radius of the specimen (mm)

L_0 is the length of the measuring part of specimen (mm)

58

For $\varepsilon = 1 \Rightarrow 60$ increments

Number (C) = (60 N) × 1.1

Number (C) = 1.10 (60 N)

The 1.10 i.e 10 % is usually given , just to provide enough space for data acquisition .

Example : $\varepsilon = 0.35$, R = 3 mm, $L_0 = 50$ mm

$$N = (\varepsilon \sqrt{3} L_0)/(2 \pi R)$$

$$= (0.35 . 1.73 . 50)/(2 . 3.14 . 3) = 1.6069 \text{ Twists (Rotations)}$$

Number   C = 1.1 (60 × N) = 1.1 . (60 . 1.6069) = 106 i.e. the number C is equal 106 increments

3.3 Number of rotations in minute

$$\dot{\varepsilon} = (2 . \pi . U . R)/(60 . \sqrt{3} . L_0)$$
$$U = (60 . \sqrt{3} . L_0 . \dot{\varepsilon})/(2 . \pi . R)$$
$$= (60 . \sqrt{3} . 50 . 1.5)/(2 . \pi . 3)$$
$$= 413.5 \text{ revolutions}/\text{min}$$

4. RESULTS

4.1 Flow curves.

The representative sets of two hit flow curves are shown in Figure 49(a-i) In the first pass, there is a continuous increase in flow stress. Flow curve is characterized by both low yield strength and a high strain-hardening rate. This kind of behavior was recorded in all tests. In the second pass, depending on inter pass time, flow curve can have different shapes. In the case of longer inter pass times or higher temperatures, shape of the curve is similar to flow curve in the first pass, i.e. low yield point and high strain rate. On the other hand, in some cases, fig.49 (i), shape of flow curve in second pass exhibits much higher yield point, and subsequent low strain hardening rate.
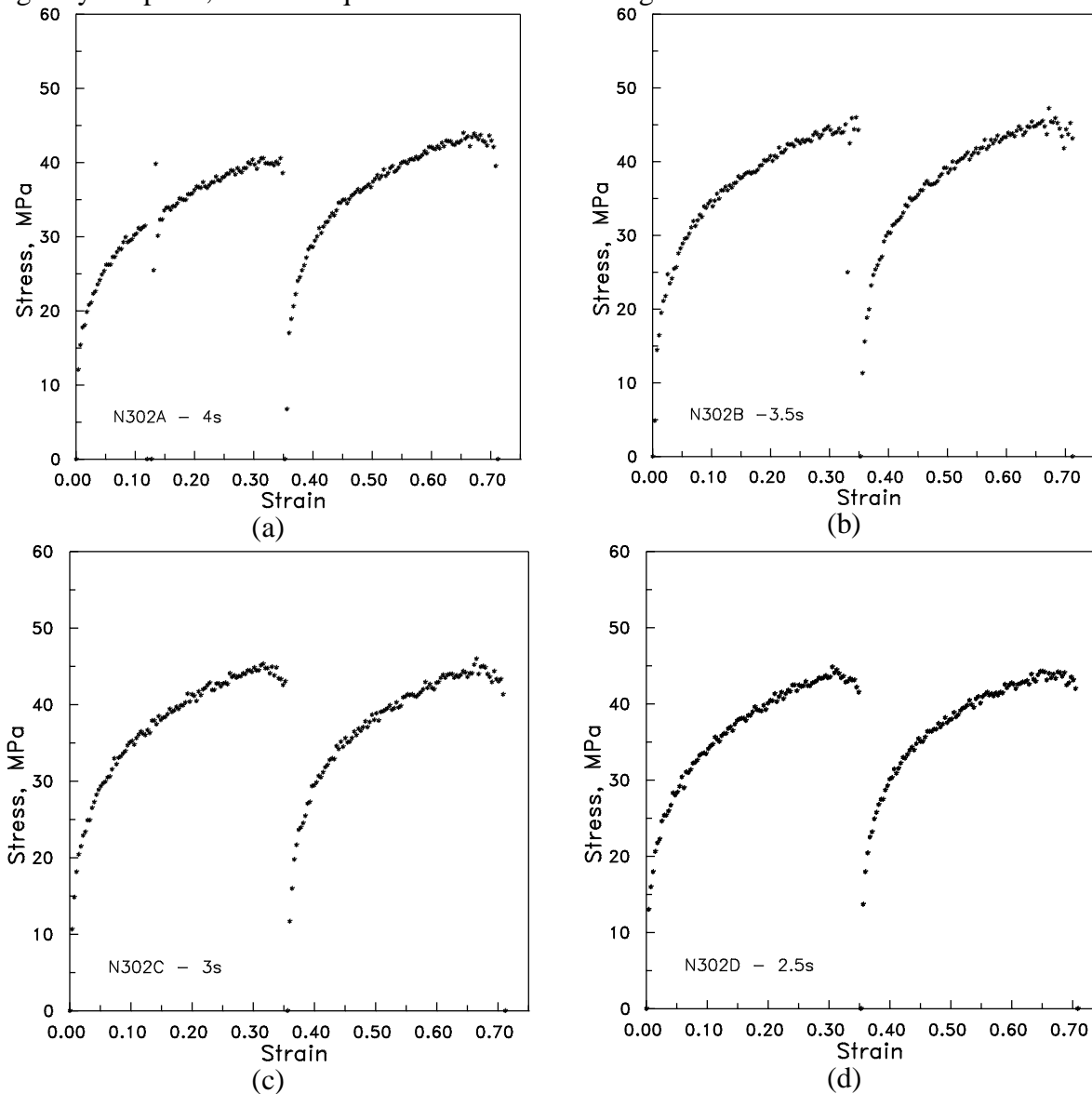

(a)

(b)

(c)

(d)

Figure (49). Stress-Strain curves obtained in two hit torsion tests ($\varepsilon_i = 0.35$; $\dot{\varepsilon}_i = 1.5s^{-1}$; t=1000°C) with different delay times (times indicated in each figure)

Figure 49 (continued). Stress-Strain curves obtained in two hit torsion tests ($\varepsilon_i = 0.35$; $\dot{\varepsilon}_i = 1.5s^{-1}$; t=1000°C) with different delay times (times indicated in each figure)
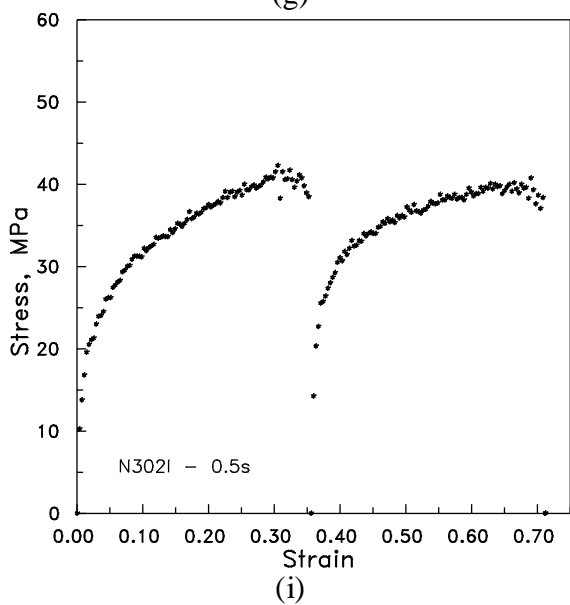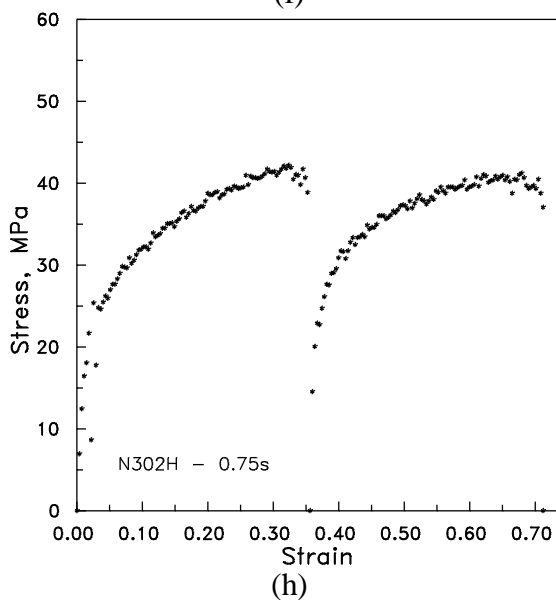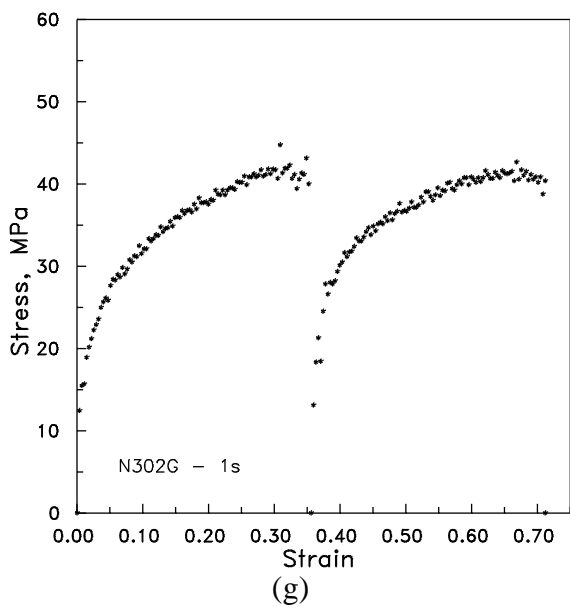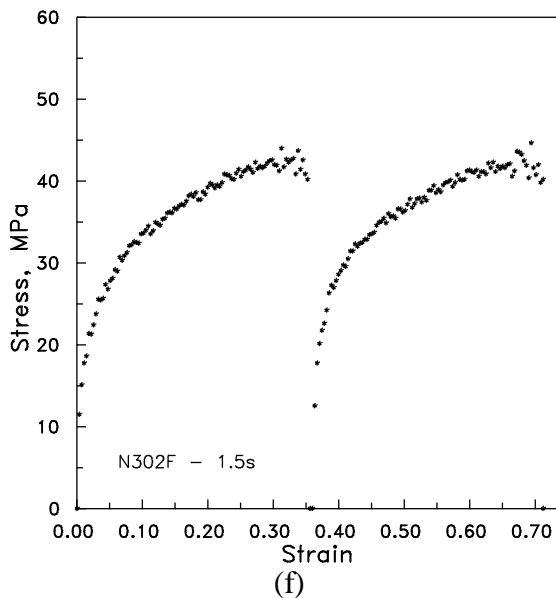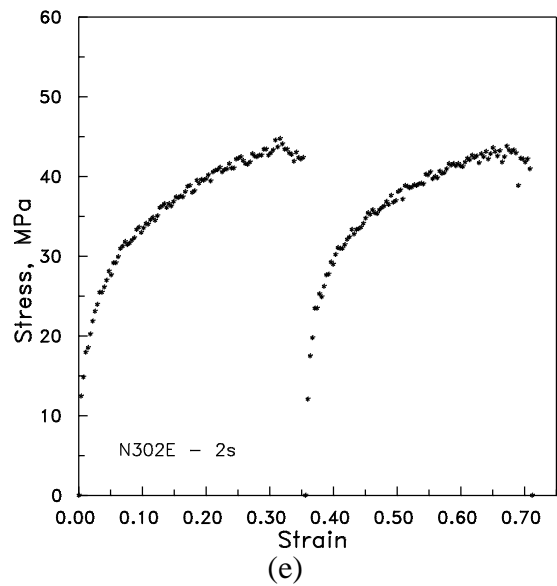
61

4.2 Fractional Softening (FS)

The, an isothermal inter pass softening is calculated for each test, in the manner proposed by [3], using 0.1% offset method. Typical dependence of fractional softening on delay time between passes is shown in figure (50). It is clear that with increase of inter pass time fractional softening increases. This increase is not linear, but has the "S" shape, on log dependence.
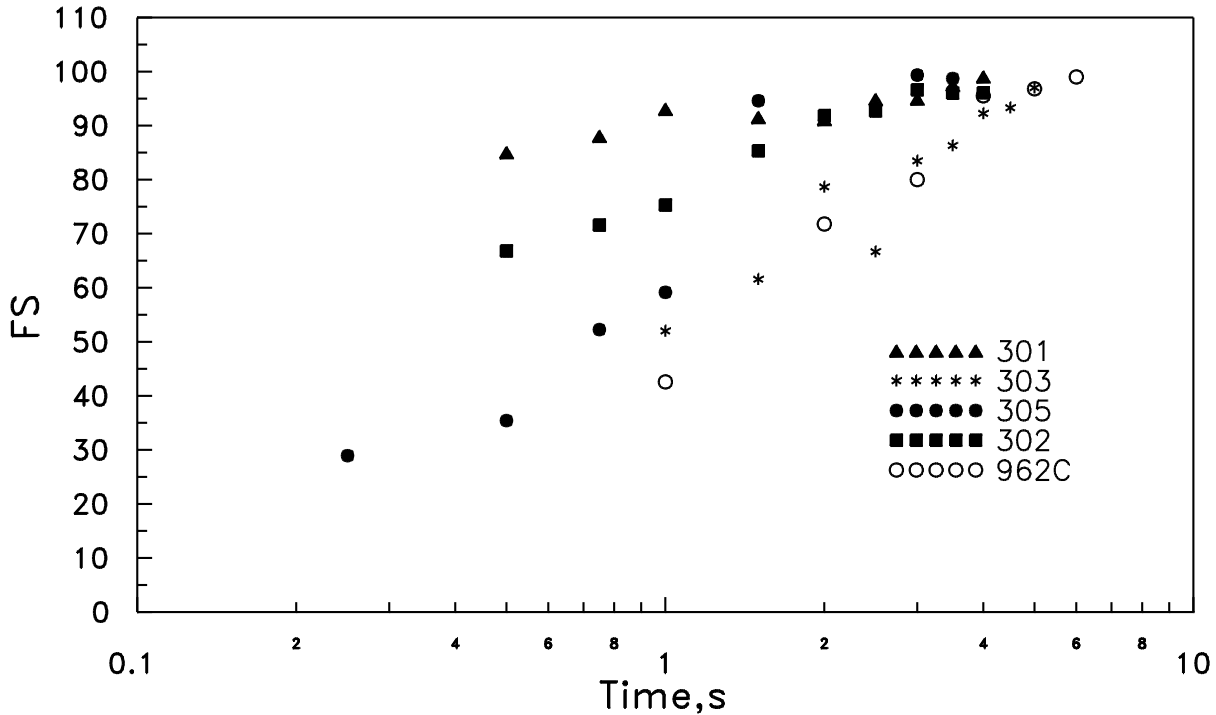
Figure (50) Fractional softening dependence on time (for different test temperatures)

Influence of temperature on fraction softening is shown on figure 50. Increase of testing temperature leads to decrease in time required for full softening i.e. softening rate is higher for the constant delay time. Also, it is worth noting that shape of each curve is very similar, only shifted to shorter times. From this diagram, times for 50% of recrystallization were estimated and given in table (9).

Table 9. Time for 50% recrystallization derived from fig. 50

Temperature, °C	$t_{50\%}$, s
1100	0.1
1050	0.3
1000	0.75
965	1.5

4.3 Avrami kinetics

Avrami exponent (n_{srx}) was calculated using following equation (10)

$$\ln \ln \frac{1}{1-f} = \ln k + n_{SRX} \cdot \ln t$$

In figure (51) is shown a fractional softening vs. time dependence. From this diagram, slope is indicating the Avrami exponent.
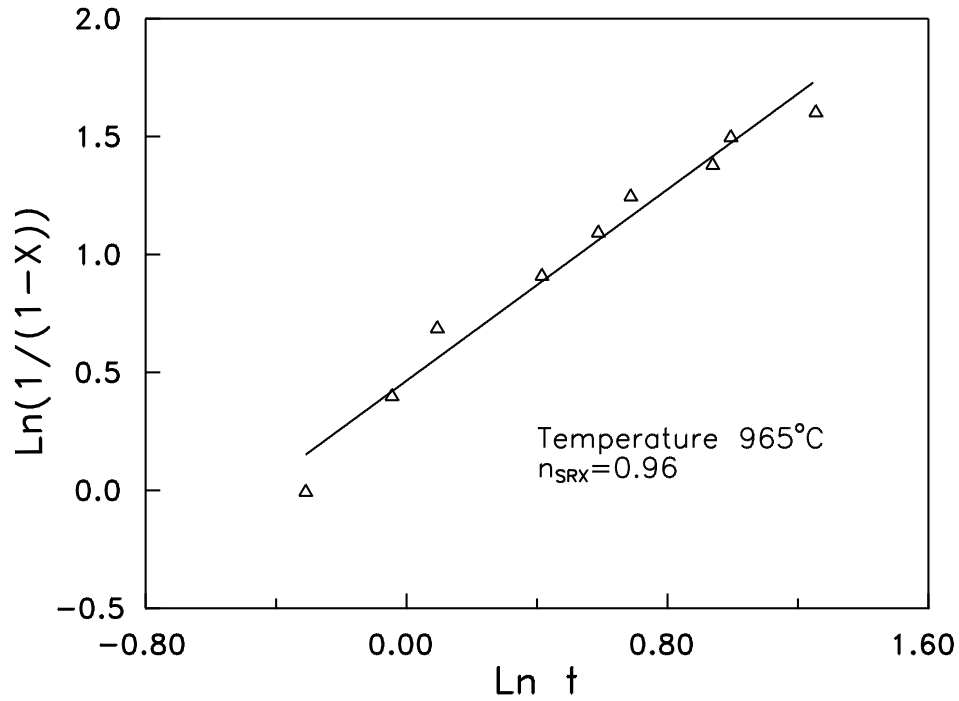
Fig. (51) Fractional softening vs. time dependence

In all cases lines are straight, showing single slope. Results obtained on all temperatures are given in table (10).

Table 10. Avrami exponent calculated on different temperatures

Temperature, °C	n_{SRX}
1100	1.03
1050	1.01
1000	1.02
965	0.96
Average value	1.00±0.03

Activation energy for static recrystallization was calculated using rearranged equation (14).

$$Lnt_{0.5} = \ln A_{SRX} + \frac{Q_{SRX}}{R} \cdot \frac{1}{T} \tag{45}$$

ln t vs. 1/T dependence is shown in figure (52), based on data from table (9). The slope on this figure determines the activation energy, and the intercept is equal to Ln A_{SRX}. Both values are given in table, together with value calculated from Medina model (11). Q_{SRX} obtained in this work has value of 281 kJ/mol, and it is related ONLY to high temperature region.

Fig. 52. Time for 50% of recrystallization dependence on temperature

Table 11. Calculated values for Q_{SRX} (experimental and modeled) and A_{SRX}, in equation (45)

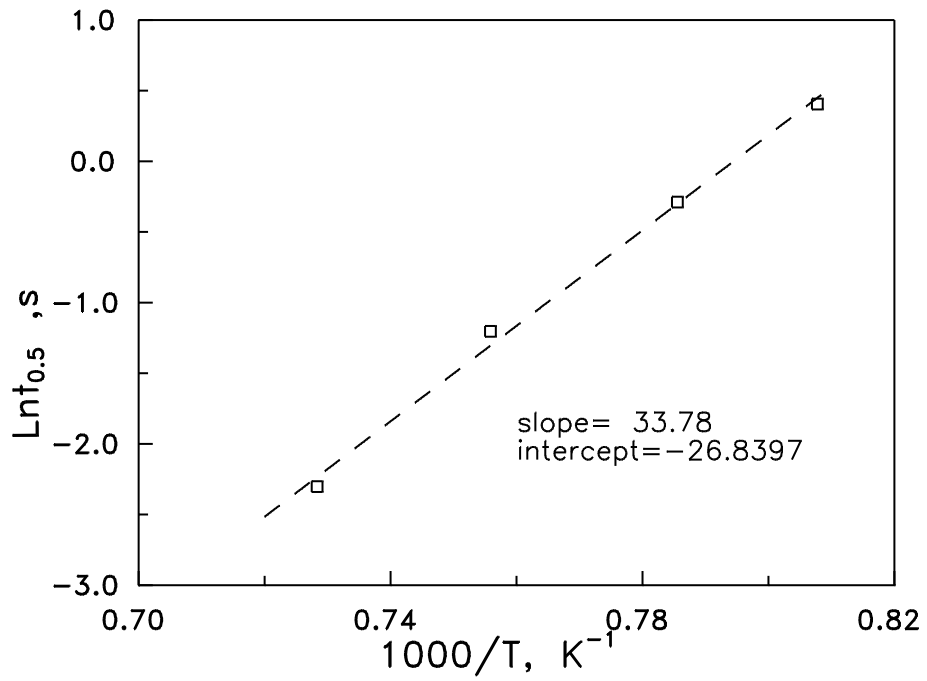| Q_{SRX}, J/mol	A_{SRX}, s	Q_{SRX}, J/mol (Model Medina-Hernandez)
280880.1	$2.21*10^{-12}$	288962.74

5. DISCUSSION

Flow curves. In the first pass, specimen was reheated and with no residual deformation, i.e. microstructure can be assumed to be fully recrystallized. At the begin of the test, during first pass deformation strengthening occurs. Therefore, increase of strain is followed by increase of strength. Since material is "strain free" (dislocation density is very small), strain hardening is very large. During first pass, accumulation of strain will result in certain dislocation density that is greater in comparison to non-deformed specimen. This accumulated strain is the driving force for restoration, that can proceed via recovery (number of dislocations is rather constant) and recrystallization (structure with dislocation density close to non-deformed state). On test temperatures from this work, recrystallization is the most dominant mechanism of restoration [4,5,11,16,40,49]. Since, the first pass was a constant in all tests (strain rate $1.5s^{-1}$; strain $\varepsilon=0.35$) it was assumed that the driving force was constant in all tests [7,10]. Therefore, the extent of recrystallization could have been attributed solely to delay time between passes. In the case of longer inter pass time (fig 49a), there is no significant change in the shape of the second pass, i.e. flow curve of the second pass is characterized by a low yield strength and a high strain hardening rate, implying that full recrystallization takes place during delay time. On the other hand, in the case of short inter pass time (fig 49i), there is a significant change in the shape of the second pass, i.e. flow curve of the second pass is characterized by a high yield strength and a low strain hardening rate, implying that recrystallization is inhibited during short delay time [7,10,79,83].

Fractional softening
To quantify the extent of softening during delay time, the fractional softening was calculated. There are several methods for calculation of fractional softening on the basis of the changes in flow curves (see: chapter two). In this work, a 0.1% offset method has been used. Recrystallization is a process that consists of two steps: nucleation of strain free grains and growth of the nuclei [7,10,11]. Preferential sites for nucleation are grain boundaries, twins, deformation bands etc. [7,10-12]. Also, the transformation is the most intensive on new boundaries between deformed and recrystallized grains. Therefore, the process is auto-catalytical, which is in excellent agreement with the "S" shape of the curve, figure (50). Small increase of softened fraction at early stages is attributed to nucleation of strain free grains, while later acceleration of softening is attributed to growth of stable nuclei [7,10-12]. At this moment, there is no general agreement how to correlate level of softening related to recovery separately to one related to recrystallization [62-64]. In this work, only total amount of softening will be discussed.

The influence of temperature on recrystallization kinetics, fig. (50), is a direct consequence of the thermal activation nature of softening. Therefore, softening on lower temperatures is expected to be shifted to longer times. Also, what is very important, the shape of all curves is similar, indicating that there is no change in reaction mechanism [10-12].

Avrami kinetics
Avrami exponent is very close to one, and shows very good agreement with previously published data [15,20,36,64]. This value indicates the nature of process, i.e. it is related to process that is characterized by nucleation on grain boundaries [15,20,36,64].

Value of 281kJ/mol for activation energy is in very good agreement with previously published data [4,17,19,22,79]. This value is close to the value of activation energy for diffusion of Nb in austenite [4]. Therefore, it is assumed that diffusion of Nb through grain boundary is the controlling step in recrystallization. In growth of stress-free grains, key factor is the mobility of train boundaries. In temperature range tested in this work, Nb and other element were in solid solution, so that solution drag is the most important mechanism of controlling the mobility of grain boundaries.

Activation energy obtained in this work confirms that model for calculation of activation energy for static recrystallization proposed by Medina et al. [19], is valid only in temperature range in which full recrystallization takes place and all Nb is present in solid solution only.

Based on the results of this work, the softening kinetics can be quantified using following equations:

$$X_{SRX} = 1 - \exp\left[-0.693\left(\frac{t}{t_{0.5}}\right)\right]$$

$$t_{0.5} = 2.21 \cdot 10^{-12} \exp(\frac{280880.1}{RT})$$

Or, combining both equations:

$$X_{SRX} = 1 - \exp\left[-0.693\left(\frac{t}{2.21 \cdot 10^{-12} \exp(\frac{280880.1}{RT})}\right)\right]$$

6. CONCLUSION

Low carbon micro-alloyed steel containing Nb and Ti was tested by means of two hit isothermal torsion with the aim to evaluate the inter pass recrystallization data. Testing was performed in temperature range in which full recrystallization take place and all Nb is present in solid solution. The increase in test temperature decreases the time required for full recrystallization. Activation energy for static recrystallization estimated in this work on 281 kJ/mol is in the excellent agreement with previously reported both experimentally and modeled data. It indicates that the diffusion of Nb in austenite is most probably the rate controlling process i.e. presence of niobium in solution delays static recrystallization. The value of Avrami exponent nSRX ~ 1.0 (1.00±0.03), implies that the static recrystallization occurs at interface i.e. on grain boundaries, twins, deformation bands. In this context, the last equation and results obtained in this study will be used for optimization of present model for prediction of roll forces for Hot Strip Mill in SARTID Company for Steel Manufacturing.

7. REFERENCES:

(1) T. N. BAKER, Sub grain and dislocation strengthening in controlled−rolled micro alloyed steels, in Hot working and forming processes, Ed. by C. M. SELLARS and G. J. DAVIES, The Metals Society, London (1980) p32

(2) Robert E Reed hill, physical metallurgy principles, Litton Educational Publishing, Monterey, California, (1973).

(3) K. Hulka and F. Heisterkamp, Physical metallurgy, properties and weldability of pipe line steels with various niobium contents, in HSLA steels technology & application, Ed. Michael Korchynsky, American Society for Metals, Pennsylvania (1984), p 915.

(4) C M Sellars, the physical metallurgy of hot working, in Hot working and forming processes, Ed. C.M. SELLARS and G. J. DAVIES, The Metals Society, London, (1980) p. 3

(5) C M Sellars and J A. Whiteman, recrystallization and grain growth in hot rolling, Metal Science, March−April (1979), P 187.

(6) Roman M. Kuziak and Yi −Wen Cheng, Microstructural Evolution In Micro alloyed Medium −Carbon Forging steels During Thermomechanical Processing, international conference on processing, microstructure and properties of micro alloyed and other modern high strength low alloy steel, Ed by A. .J .De Ardo , The iron and steel society , Pittsburgh (1991) , p51

(7) George E Dieter, mechanical metallurgy, McGraw−Hill, London, (1988).

(8) Richard W Hertzberg, deformation and fracture mechanics of engineering materials, John Wiley & Sons, New York, (1996).

(9) Sidney H Avner, introduction to physical metallurgy, McGraw−Hill, Auckland, (1974).

(10)   R. E. SMALLMAN, Modern Physical Metallurgy, Butterworths, London (1985).

(11) E J Palmiere, C I Garcia and A J Dear do, static recrystallization and precipitation during the hot deformation of austenite, Proceedings of the International Conference on Processing, Microstructure and Properties of Micro alloyed and other Modern High Strength Low Alloy Steels, Ed. by A. J. De Ardo, The IRON AND STEEL SOCIETY, Pittsburgh, (1992) p. 113.

(12) David A Porter, Kenneth E Easterling, phase transformation in metals and alloys, Van Nostrand Reinhold (UK) Co. Ld, Molly Millars Lane, (1981).

(13)B. MIGAUD, Simulation by hot torsion testing of hot strip mill rolling for low −carbon Nb − micro alloyed steels, in Hot working and forming processes, Ed. C. M. SELLARS and G. J. DAVIES, The Metals Society, London, (1980), p 67.

(14) C. Roucoules, P. D. Hodgson, S . Yue and J. J. JONES, Dynamic and post−dynamic recrystallization in a Mo−Ti steel, international conference on processing, microstructure and properties of micro alloyed and other modern high strength low alloy steel, Ed by A. J. De Ardo, The iron and steel society, Pittsburgh (1991), p95.

(15)A. LAASRAOUI and J.J. JONAS, Recrystallization of Austenite after Deformation at High Temperatures and Strain Rates — Analysis and Modeling, METALLURGICAL TRANSACTIONS A ,22 A, (1991) P 151.

(16) P. Choquet et al, Mathematical Modelling of Hot Rolling of Steel, Ed. S. Yue, CIMM, Montreal, Canada (1990), 23 −43

(17) J. Williams, C. R. Kilmore, G. R. Harris, Physical Metallurgy of Thermomechanical Processing of Steels and Other Metals, (THERMEC88), Ed. I. Tamura, ISIJ, Tokyo (1988), 224 −231

(18) P. D. Hodgson, Materials forum, 17 (1993) 403 −408

(19) S. F. Medina and J. E. Mancilla, ISIJ International ,36 (1996), 1070 − 1076

(20) P. D. Hodgson and R. K. Gibbs, ISI J International, 32 (1992) 1329 − 1338

(21) W. Sun et al, Intl. Conference on Thermomechanical Processing of Steels and Other Materials (THERMEC 97), Eds. T. Chandra et al., TMS, Warrendale, USA (1997), 685 − 691

(22) S. F. Medina and J. E. Mancilla, ISIJ International, 33 (1993), 1257

(23) S. F. Medina, Scripta Metallurgical and Materials, 31 (1994) 315 −320

(24) S. Devaraj, Y. Deke, T. Chandra, International Conference on Recrystallization in Metallic Materials, (Recrystallization 90), Ed. T. Chandra, TMS, Warrendale, USA (1990), 237 – 244

(25) W. Roberts, HSLA Steels: Technology and Applications, Ed. M. Korchynsky, ASM, Metals Park, USA (1984), 67 – 84

(26)P. D Hodgson, J. J. Jonas and S. Yue, Evolution of microstructure in Rod and Bar Rolling, in international conference on processing, microstructure and properties of micro alloyed and other modern high strength low alloy steel, Ed by A. J. De Ardo, The iron and steel society, Pittsburgh (1991), p41.

(27) Rodolf. Hammer, Rolf. W. Slimmon, Metallurgical requirements in the production of HSLA steels, in HSLA steels technology & application, Ed. Michael Korchynsky, American Society for Metals, Pennsylvania (1984), p 359.

(28)O. KWON, A. J. De Ardo, Niobium carbonitride precipitation and static softening in hot–deformed niobium micro alloyed steels, HSLA Steel : Metallurgy and Applications, Ed. J. M. Gray et al, ASM, Metals Park, USA (1984)

(29)Dr Nenad Radovic, prof. dr Dorde Drbnjak, Development of steels for fabrication of welded construction with improved safety, Science –Research–Development, 3 (2001) p 81.

(30) Isao Kozasu, Recent developments of micro alloyed steel plate, in HSLA steels technology & application, Ed. Michael Korchynsky, American Society for Metals, Pennsylvania (1984), p593

(31)A. C. Kneissl, C. I. Garcia, A. J. De Ardo, influence of processing on the nature of the precipitates in a micro alloyed linepipe steel, international conference on processing, microstructure and properties of micro alloyed and other modern high strength low alloy steel, Ed by A. J. De Ardo, The iron and steel society, Pittsburgh (1991), p 145.

(32)A. M. Sage, R. C. Cochrane, the development of a normalized Ti–treated vanadium steel with improved HAZ toughness, international conference on processing, microstructure and properties of micro alloyed and other modern high strength low alloy steel, Ed by A. J. De Ardo, The iron and steel society, Pittsburgh (1991), p 443.

(33)A. M. Sage, an overview of the use of micro alloy in HSLA steels with particular reference to vanadium and titanium, in HSLA steels, processing, properties and applications, Ed by Geoffery Tither and Zhang Shou Hua, The Minerals, Metals & Materials Society, (1992), p51

(34)Ji Yancheng, Song Han, Huo Bingshu, and Cao Yinzhi, Improving the toughness of steels by Microalloying with Ti, in HSLA steels, processing, properties and applications, Ed by Geoffery Tither and Zhang Shou Hua, The Minerals, Metals & Materials Society, (1992), p217

(35)Dr A M Sage, Dr. R. C. Cochrane, D. H Owse, The development of a normalized titrated vanadium steel with improved HAZ toughness, international conference on processing, microstructure and properties of micro alloyed and other modern high strength low alloy steel, Ed by A. J. De Ardo, The iron and steel society, Pittsburgh (1991), p443.

(36)William Roberts, Alf Sandberg, Tadeusz Siwecki, Tommy Werlefors, prediction of microstructure development during recrystallization hot rolling of Ti – V steels, HSLA Steels : Metallurgy and Applications, Ed. J. M. Gray et al, ASM, Metals Park, USA (1986)

(37)L. J. Cuddy, J.S Lally, L. F. Porter, improvement of toughness in the HSLA of high heat input welds in ship steels, in HSLA steels technology & application, Ed. Michael Korchynsky, American Society for Metals, Pennsylvania (1984), p697.

(38)L. R. Link, M. G. Vassilaros, stabilization of coarse grain HAZ of Ti treated ULCB steel, international conference on processing, microstructure and properties of micro alloyed and other modern high strength low alloy steel, Ed by A. J. De Ardo, The iron and steel society, Pittsburgh (1991), p 421.

(39)Shi–Rong Chen, Shi–Chin Wang and Rong–Luan Hsieh, the development of high strength low alloy steel plates suitable for high heat input welding, international conference on processing, microstructure and properties of micro alloyed and other modern high strength low alloy steel, Ed by A J De Ardo, The iron and steel society, Pittsburgh (1991), p 435.

(40)A. J. De Ardo, New developments in the alloy design of micro alloyed and other modern HSLA steels, in HSLA STEELS : Processing, Properties and Applications, Ed. Geoffrey Tither and Zhang Shouhua The, Minerals, Metals & Materials Society, (1992) p 21.

(41)Tony. Nilsson, Formable hot rolled steel with increase strength, in HSLA steels technology & application, Ed. Michael Korchynsky, American Society for Metals, Pennsylvania (1984) p253.

(42)William F. Smith, structure and properties of Eng. alloys, McGraw–Hill, New York, (1981).

(43)F. B. Pickering, physical metallurgy and the design of steels, Applied Science Publishers LTD, London, (1978).

(44) Nordberg, H. and Aronsson, B, Solubility of Niobium Carbide in Austenite, Journal of the Iron and steel Institute, (1968), p. 1263

(45) Smith, R. P, The Solubility of Niobium (Columbium) Carbide in Gamma Iron, Transations of the Metallurgical Society of AIME, Vol. 236, (1966), p. 220

(46) Narita, K, Physical Chemistry of the Groups Iva (Ti, Zr), Va (V, Nb, Ta) and the Rare Earth Elements in Steel, Transitions of the Iron and Steel Institute of Japan, Vol. 15, (1975), p. 145

(47) Johansen, T. H, Christensen, N. and Au gland, B., The Solubility of Niobium (Columbium) Carbide in Gamma Iron, Transactions of the Metallurgical Society of AIME, Vol. 239, (1967), p. 1651

(48) Mori, T., et al, Thermodynamic Properties of Niobium Carbides and Nitrides in Steel, Tetsu –to–Hagane, Vol. 54, (1968), p. 786

(49) Andrade, H. L, Akben, M. G. and Jonas, J. J, Effect of Molybdenum, Niobium, and Vanadium on static Recovery and Recrystallization and on solute Strengthening in Micro alloyed Steels, Metallurgical Transactions, Vol. 14A, (1983), P. 1967

(50) Sharma, R . C , Lakshmann , V . K. and Kirkaldy , J . S . , Solubility of Niobium Carbide and Niobium Carbonitride in Alloyed Austenite and Ferrite , Metallurgical Transactions , Vol . 15A , (1984) , P . 545

(51) Lakshmana , V . K and Kirkaldy , J .S , Solubility Product for Niobium Carbide in Austenite , Metallurgical Transactions , Vol . 15A , (1984) , P . 541

(52) Advances in Phase Transitions , Ontario , October 22–23 , 1987 , J . D . Embury and G . R . Purdy , Eds . , Thermodynamics of Fe–Ti–C and Fe–Nb–C Austenites and Nonstoichiometric Titanium and Niobium Carbides , by K . Balasubramanian and J . S . Kirkaldy (Oxford , UK , Pergamon Press , 1988) , p 37

(53) Smith , R . P. , The Solubility of Niobium (Columbium) Nitride in Gamma Iron , Transactions of the Metallurgical Society of AIME , Vol . 224 , (February , 1962) , p . 190

(54) Microalloying 75 , Washington D . C . , October 1–3 , 1975 , M . Korchynsky , Ed. , Quantifying the Effects of Microalloying Elements on Structures During Processing , by T . M . Hoogendoorn M . J . Spanraft , (New York , NY:Union Carbide Corporation , 1977) , p . 75

(55) Santella , M . L. , Grain Growth and High–Temperature Hot Rolling Behavior of Low–Alloy Steel Austenite , Ph . D . Thesis , University of Pittsburg , (1981) , p . 49

(56) Irvine , K . J. , Pickering , F . B . and Gladman , T. , Grain–refined C–Mn Steels , Journal of the Iron and Steel Institute , (February , 1967) , p. 161.

(57)R . K .AMIN , G . BUTTERWORTH , and F . B PICKERING , Effects of rolling variables and stoichiometry on strain–induced precipitation of Nb(CN) in C–Mn–Nb steels , in Hot working and forming processes , Ed by C. M . SELLARS and G. J. DAVIES , The Metals SOCIETY , London , (1980) p 27 .

(58)A . Najafi –Zadeh and J . J . Jones , effects of composition on the recrystallization behavior of steels during simulated hot strip rolling , international conference on processing , microstructure and properties of micro alloyed and other modern high strength low alloy steel , Ed by A .J .De Ardo, The iron and steel society , Pittsburgh (1991) , p 153 .

(59)C DEVADAS, I. V SAMARASEKERA, and E. B. HAWBOLT, The thermal and metallurgical state of steel strip during hot rolling : part 3 Microstructural Evolution, Metallurgical Transactions A, 22 A, (1991), P 335.

(60)P. D. Hodgson, Models of the recrystallization behavior of C – Mn and Nb micro alloyed steels during hot working processes, Materials Forum ,17 (1993) p 403.

(61)F. B. PICKERING, The spectrum of micro alloyed high strength low alloy steels). in HSLA steels technology & application, Ed. Michael Korchynsky, American Society for Metals, Pennsylvania (1984) p7

(62)A. I. Fernandez, B. Lopez, and J.M. Rodriguez. I babe, Relationship Between the Austenite Recrystallized Fraction and The Softening Measured from The interrupted Torsion Test Technique, Scripta Material a, 40 (1999), p 543

(63)H. L. ANDRADE, M. G. AKBEN, and J. J. JONAS, effect of Molybdenum, Niobium, and Vanadium on static recovery and recrystallization and on solute strengthening in micro alloyed steels, METALLURGICAL TRANSACTIONS A, 14 A (1983), P 1967

(64)M . G . Akben , J . J . Jonas, influence of multiple micro alloy additions on the flow stress and recrystallization behavior of HSLA steels, in HSLA steels technology & application, Ed . Michael Korchynsky , American Society For Metals , Pennsylvania (1984) p 149 .

(65)Su . Hui and Yan Zhenqi , Influence of Ti and cooling rate on precipitation strengthening in V−Ti MA steels , in HSLA steels , processing , properties and applications , Ed by Geoffery Tither and Zhang Shouhua , The Minerals , Metals & Materials Society , (1992) ,p 201

(66)Z . CVIJOVIC , Ferrous Alloys , Course notes , Faculty of Technology and Metallurgy , University of Belgrade (2002)

(67)Tomo Tanaka , Nobuhisa Tabata and Taneo Hatomura and Chiaki Shiga , Three stages of the controlled rolling process , Mcroalloying 75 , Ed . M . Korchynsky , Union Carbide (1977) .

(68)D . Q . Bai , S . Yue , W . P . Sun , and J . J . Jones , effect of test variables on the critical temperatures Tnr and Ar $_3$ of high Nb −low C plate steel , international conference on processing , microstructure and properties of micro alloyed and other modern high strength low alloy steel , Ed by A .J .DeArdo , The iron and steel society , Pittsburgh (1991) , p 165 .

(69)Yang−Zeng Zheng , A . J . De Ardo, Robert M. Fix, Guillermo Fitzsimons , Achieving Grain Refinement Though Recrystallization Controlled Rolling and Cooling in V−Ti−N Microalloyed Steels , in HSLA steels technology & application , Ed . Michael Korchynsky , American Society For Metals , Pennsylvania (1984) p 85 .

(70)Jinxiang . DONG , Fulvio . SICILIANO . Jr , JOHN . J . JONAS , W . J . LIU and Elhachmi . ESSADIQI , ISIJ International , 40 (2000) , p613 .

(71) Zai Xiang yong , Liu Jiangang , Song Fengti , and Hong Xiugin , Machinability and Mechanical properties of free−cutting steel YF$_{45}$V(CaS) in HSLA steels , processing , properties and applications , Ed by Geoffery Tither and Zhang Shouhua , The Minerals , Metals & Materials Society , (1992) , P. 431.

(72) D . S . Fields and W . A . Backofen , Proc. ASTM , 57 (1957) P . 1259

(73) S . L . Semiation , G . D . Lahoti and I . I . Jonas , Metals Handbook 9th Edition , Volume 5 , ASM , Metals Park , OH , USA (1978) , P. 154−184 .

(74) High Temperature Torsion Machine IRSID Licence , prospekt .

(75) K . Irvine , F . Pickering , T . Gladman , Journal Iron and Steel Institute , 205 (1967) , p. 161−182 .

(76) T . Senuma ans H . Yada , Annealing Processes −Recovery , Recrystallization and Grain Growth , Ed . N . Hansen et al . , RISOE Roskilde , Denmark (1986) , 547−552

(77) T . Siwecki , Microalloyed Vanadium Steels , Ed . M . Korchynsky , Akademia Gornieczo−Hutnicza , Krakovie ,Polska (1990), 63−78

(78) E . Ruibal , J .J . Urcola , M . Fuentes , Zeitschrift fuer Metallkunde , 76 (1985) , p 568

(79) P . D . Hodgson and R . K .Gibbs , ISIJ International , 32 (1992) , p . 1329−1338 .

(80) Dutta , C . M . Sellars , Materials Science and Technology , 3 (1987) , p . 197−206 .

(81) F . S . Buffington , Hirano and M . Cohen , Acta Metallurgica , 9 (1961) , p . 434−439 .

(82) A . I . Fernandez et al . , Recrystallization and Related Phenomena , (Recrystallization 99) , Eds T . Sakai and H . G . Suzuki , The Japan Institute of Metals , Tokyo , Japan (1999) , 697−702 .

(83) N . Radovic , Dj . Drobnjak , ISI J International , 39 (1999) 575